Alma Mater Studiorum · Università di Bologna

Scuola di Scienze
Dipartimento di Fisica e Astronomia
Master course in Material Physics and Nanoscience

Electrochemical loading of hydrogen in Mg thin films

Supervisor:
Prof. Luca Pasquini

Cosupervisor:
Prof. Astrid Pundt, Dr. Stefan Wagner.

Presented by:
Giulio Bonelli

Anno Accademico 2019/2020

do thin films dream of electronic electrolytes?

Contents

Abstract

The science and technology of hydrogen production from renewable energy, hydrogen sensing and hydrogen storage are central to the realization of a hydrogen-based society, in which me may be living one day. The focus of my Master thesis will be the solid-state hydrogen storage in nanostructured metallic hydrides. In fact, beside the physical storage of hydrogen through pressurized tanks, it is also possible to store hydrogen in the chemical bonds of the metallic hydrides such as MgH2, LaNi5H6,FeTiH2, just to name a few. The problem is to achieve these goals at temperature and pressure as close as possible to ambient conditions. Knowledge-based design of advanced materials can help to solve issues related to unfavourable kinetics and thermodynamics of hydrogen storage. In particular, size effects and interface engineering in nanomaterials are exciting tools to modify and improving hydrogen sorption properties beyond the current state of the art. This is the subject of the present project.

Introduction

My work at Material Science Department (IAM-WK) in KIT, Karlsruhe, focused on the loading of hydrogen in Mg thin films. I started to get acquainted with the experimental apparatus as soon as I arrived.
The work of thesis required many experimental paths to be taken into accounts. At first the electrolyte solution through which I should have performed electrochemical loading of thin films proved to oxidate the samples, making their loading uncontrollable.
Thin films production through sputter deposition has been many times slowed down by technical problems that affected the sputter machine itself.
For that reason it was decided to prepare other thin films using another technique of physical vapor deposition, the MBE (Molecular Beam Epitaxy), at Nanotechnology Institut at KIT (INT), Campus North.
The problem of the electrolyte was solved by replacing the previous with KOH, which entailed the highest level of safety because of its dangerousness (pH>14).
While the samples from INT didn't provide any valuable results, something was achieved with newly sputtered samples from the newly operating sputter machine, in the early days of December 2020.
Notwithstanding the difficulties encountered, I managed to present some results that will be shown in this work thesis. This written consists of 6 chapters plus a conclusive chapter. More in detail:
In the **First Chapter** the concept of "Hydrogen economy" is introduced. The reader gets then acquainted with the problem of hydrogen storage. In the **Second Chapter** a brief overview of the Metal hydrides is provided, entering the details of interstitial metal hydrides, the main topic of this thesis In the **Third Chapter**, the problems we encounter when we reduce the metal hydrogen system to the nanoscale, by means of thin films, are presented. In the **Fourth Chapter** an overview of the different experimental methods to analyze the main physical dimensions characterizing metal thin films are shown. In the**Fifth Chapter** the experimental data I picked up during my staying in Karlsruhe are presented to the Reader. In the **Sixth Chapter** a the most relevant experimental results are discussed. In the **Conlusions** a brief sum up of the main results achieved, their limits, and the next wishable step to take is presented.

Chapter 1

Hydrogeny as source of clean energy

1.1 Why hydrogen

As we enter deeper and deeper the 21th century, the need for a cleaner economy will get huger and huger. Hydrogen is one of the most promising elements that could become the new main source of energy, substituting the fossil fuels.
In fact, electrochemical energy production is being taken under serious consideration as an alternative energy source. It will be more and more effective in this task as the energy consumption becomes as sustainable as possible.
Of course we do not dispose of any gaseous hydrogen site in which we can directly extract it. Actually hydrogen is an energy's carieer rather an energy source. The hydrogen's economy cycle which is brielfy sketched in Fig. 1.1, like any other energetic economy, relies on 3 pillars:

- Hydrogen production: the best way would be to extract Hydrogen from the splitting of a water molecule which occurs according to:

$$2H_2O + Energy \rightarrow H_2 + \frac{1}{2}O_2 \tag{1.1}$$

  Of course, in an ideal world, the energy required for the water splitting should come from a renewable source of energy. In fact, there should be also the possibility to obtain H_2 from "grey" sources, which produce a CO_2 increase, i.e. from natural bas, bio mass, or long-chained hydrocarbons such as natural oil, but that would be regrettable from an enviromental point of view.
  A fancy and "green" way to achieve 1.1 is through Photocatalyitic water splitting, in which we exploit solar energy of an impinginf photon of energy ($h \ni$) to split the water molecule, hence getting H_2.

- Hydrogen storage (the ideal technological aim of the research work this work thesis is built on)

- Transformation in usable energy (through fuel cells).

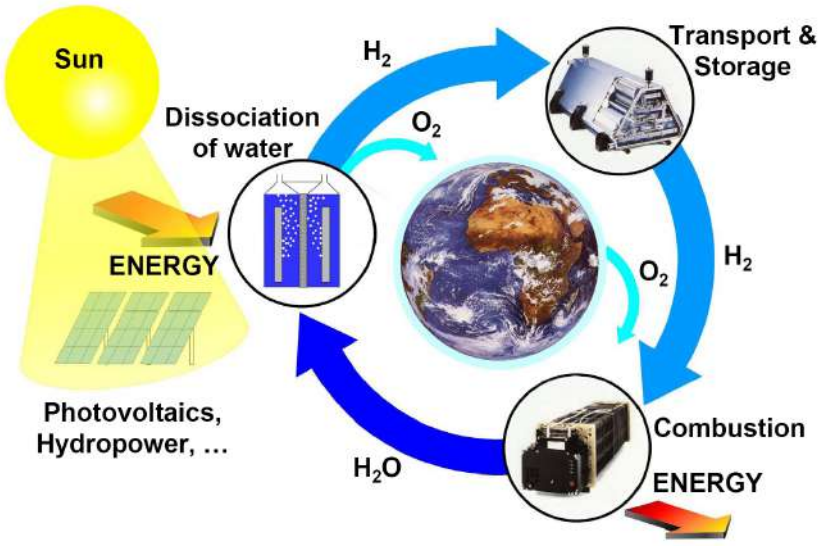

Figure 1.1: The ideal cycle of hydrogen, in a fully renewable-energy-based society

Starting from the end of the cycle, Fuel cells are open systems where the anode and cathode can be represented as ways to transfer charged matter. The main character is the redox reaction taking place within. The resources for such a reaction are provided from the outside, in mainly two ways (see Fig. 1.2): in a physical way, through highly pressurized tanks where hydrogen is stored in liquid or gas form, or in a chemical way, whose details will be described later on.
More generally speacking, a Fuel Cell is an electrochemical conversion device (see Fig. 1.2) that has a continuos supply of fuel such as hydrogen, natural gas, or methanol and an oxidant such as oxygen, air, or hydrogen peroxide.
Basically, the following reactions happen at Anode:

$$4H_3O^+ + 4e^- \rightarrow 2H_2 + 4H_2O \tag{1.2}$$

and Cathode:

$$4OH^- \rightarrow O_2 + 2H_2O + 4e^- \tag{1.3}$$

Collecting together eq. 1.2 and 1.3 we are led back to eq. 1.1.
Fuel cells can have auxiliary parts to feed the device with reactants or catalists to improve the kinetics of the reaction.[1]
Althought a few results were reached in the last years, the main problem remains the storing of hydrogen. For these projects to be technologically appliable,e.g. mounted on a hydrogen fuelled car, we need to reach the required performance of autonomy, supply

time, lasting and economic cost, without exceding the safety boundaries. In the next section we will invastigate the feature a storage system should display to be taken into account for long scale mass production.

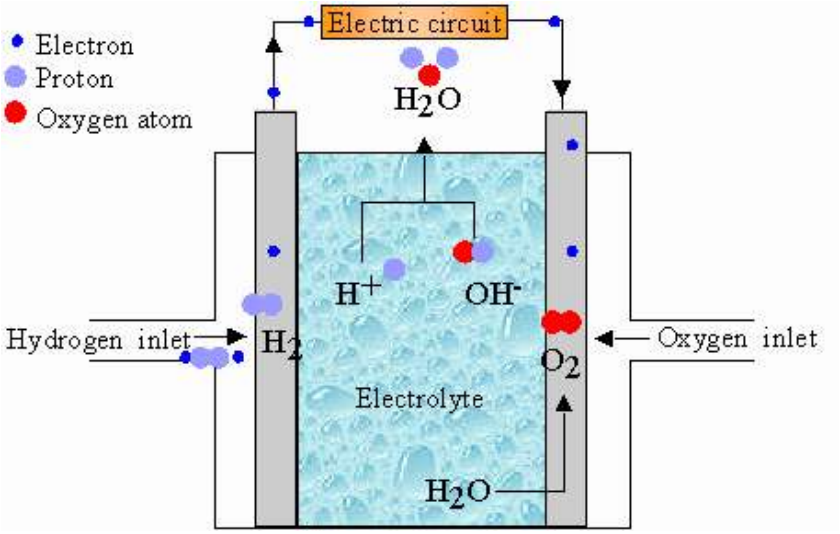

Figure 1.2: This skecth highlights the continuos supply of reactants and the redox reaction taking place within the cell itself.

Table 1.1: Goals for futures hydrogen storage systems according to [3]

	U.M.	2010	2015	Latest
Gravimetric Capacity	wt% di H_2 to be used	4.5	5.5	7.5
	kWh/kg	1.5	1.8	2.5
Volumetric Capacity	kg/m^3 of H_2 to be used	28	40	70
	kWh/m^3	900	1300	2300
Min/max temperature	°C	-30/50	-40/60	-40/60
Purity	$\%H_2$		99.97	
Supplying time (every 5kg of H_2)	Minutes	4.2	3.3	2.5

1.2 The ways to store hydrogen

Neglecting the problem of producing and consuming the required amount of hydrogen required for the new H-based society we would aim to live in, one must necessarily consider the issue of how to store it. A good storing allows the perfect conservation of Hydrogen in order to make use of it whenever we want. The perfect tank is supposed to be light enough for moving it in order to supply fuel in a fast way (like it happens with petrol pump). However, we need to consider the place needed for both production and consumption of H_2.
In table 1.1 we can see the main features a hydrogen storage system should have according to the USA Department of Energy.
[2] These data refer to ideally functioning storing systems. Up to now we can distinguish three main kind of storage systems:

- Physical containment (let it be a compressed gas or liquefaction)
- Fisiorption (Absoprtion of H_2 at the surface of porous materials)
- Chemisorption (Metal Hydrides, which we will discuss more in detail and classify later on).

Different ways of hydrogen storage and associated physical dimensions are portrayed in Fig.

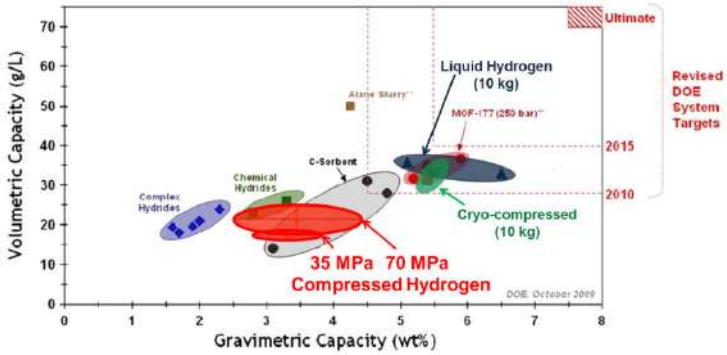

Figure 1.3: *Volumetric Capacity vs Gravimetric capacity of the existing ways for H storing.*

1.2.1 Physical containment

The challenge in hydrogen storage is the physic containment, i.e. storing hydrogen as compressed gas or liquid.A tank of compressed gas has two important advantages:

- Hydrogen is immediately available to be utilized
- The technology to build tanks up to a pression of 700 bar is now available
- The current tanks can store H_2 up to 700 bar owing to their multicomposite structure made by carbon fiber to grant containment, by inner walls made by metal or polimers that work as a barrier for the diffusion of the gas and from a third outer material, hence reaching a volumetric capacity of 36 kg/m^3.[4]

However there are some problems that makes gas hydrogen not ideal. Besides the composite tanks are much heavier and that entails a compromise between the gravimetric capacity and the volumetric one (the more capacity induces a huger weight).
Not even the confinement as liquid hydrogen seems to solve our problem since liquifying hydrogen requires a greater cost, as we need to reach temperatures up to 20K, so though it allows great volumetric capacities, it can't be a valuable method of storing hydrogen.[4]

1.3 Physorption

Physorption entails hydrogen to be adsorbed at the surface of a material by means of London's intermolecular forces, since no polar attraction could take place (molecular hydrogen shows no polarity).

These materials display a great density of H_2 for unity of surface and a great porosity in order to increase the specific surface ($\frac{m^2}{g}$). The most famous example of such a material is graphene that can reach a gravimetric capacity of 7 wt%.
Nevertheless, a huge flow of these materials is that they all need to work at high pressure or equivalently at low temperature ($\sim 77k$, hence cooled via liquid nitrogen).

1.3.1 Chemisorption

Chemisorption(chemical absorption of hydrongen from a surface) involves those materials that make a chemical bond with the hydrogen like metal hydrides. They usually are binary hydrides of the transition metals and the nature of the bond is mainly metallic, but also ternary compund such as $LaNi_5H$ and others more complicated structures have been reported in research.
Such compunds show a multiphase system whose nature will be described later on, where a high-concentrated "hydride phase is used for storage". From a structural point they usually display hidrogen atoms in interstitial sites.
Hence we also name them interstitial hydrides.No matter how fast the loading of hydrogen in such materials can be, the true problem is the release mechanism which is normally slower.
As hinted above, hydrides are the most promising materials, e.g. the Mg hydrides displays the most interesting feature for a future technological use (7.6 wt% of gravimetric density). Hence, the research was adressed so far to the modification of their thermodynamic properties, cinetic and morfologic and strucutrals in order for them to be used for technological uses. [5]

Chapter 2

Metal hydrides

2.1 What are they?

This sytem has been long known in the past since the experiments of T. Graham on Pd in 1868[41], but only recently research decided to give the due attention to the M-H system. Metal hydrides are now being widely investigated for successful hydrogen storage application.
Since a large amount of heat is stored in the chemical bonds of these materials, research also focused on non-hydrogen storage application of metal-hydrides. This means a wide ragne of technological devices such as heat pumps, air conditioner and so on that generally tends to use wasted heat and smart windows.
The hydrogen is by nature a very reactive element and can form bonds in several ways with metals, depending on several parameters (mainly electronegativity and electron affinity).
Without entering the details of the different atomic identities, metal hydrides can be classified according to the temperature of H-desorption (High,Average, Low Temperature Metal Hydrides) and according to the atomic structure originated[8].
We can mainly distinguish three kind of hydrides, Ionic,Complex and Interstitials. The latter will be the one investigated in this work thesis
Interstitials Hydrides exists within metal or alloy's bulk. Hydrogen occupies the tethraedical interstitial sites or octahedral, depending on the lattice we are actually considering (see Fig. 2.1). Such a M-H system is such that the hydrogen electrons form very delocalized bonds ,and can be treated with the model of electronic bands in metals. Many transition metals form interestitial binary hydrides which are highly non stekiometric when they are hydrogen-exposed, e.g. forms $TiH_{\leq 2}$.
Interstitial hydrides can be alloys of one or more solutes solved in a matrix element or intermetallic compounds of an easily hydrable element A and a less hydridable element B in order to have interemdiate thermodynamics'affinity. The standard classification of

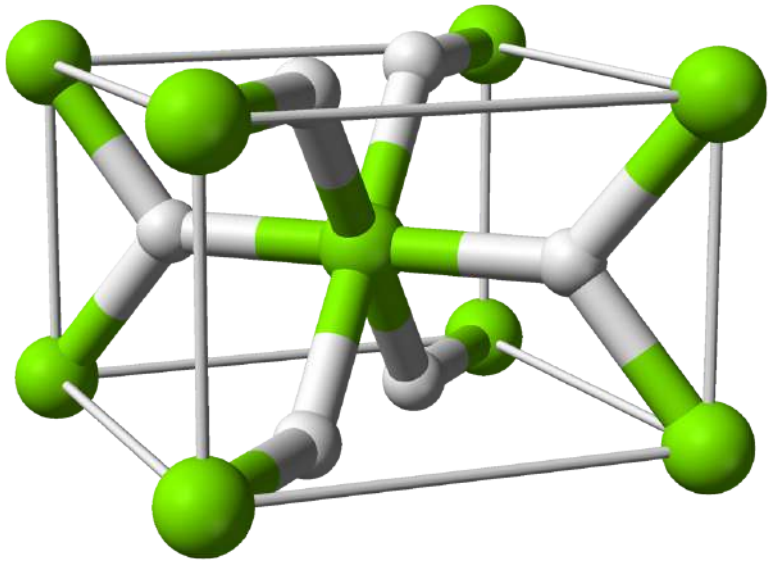

Figure 2.1: Typical crystal structure of a very important metal hydride such as MgH_2. The green balls correspond to the Mg atoms, while the grey ones identify hydrogen. As we can see they occupy the interstitial sites (white spheres) of the crystal

intermetallic compounds for hydrogen classificates them according to:
$AB_5, AB_2, AB, A_2B \rightarrow LaNi_5, TiCr_2, TiFe, Mg_2Ni$.
We are now going to analyze the behaviour of hydrogen in Bulk hydrides from both a thermodynamic and kinetic point of view.For Bulk Materials we mean materials with a lenght scales not smaller than 200 nm.

2.2 Energetic spectrum of metal hydrides

In Fig. 2.2 we can immediately notice important energies that are immediately displayed.[7]

- The energy is scaled with respect to the energy of molecular hydrogen (H_2) far away from the surface. In this condition H_2 is the stable form and the cost of atomic dissociation is provided by the dissociation energy $E_{H_2 \rightarrow 2H}$
- As we get close to and eventually within the surface, new energetic levels arise. We have the energy of physisorption of the molecules ($E_{H_2}^{phys}$) that can be split through dissociative chemisorption at the surface($\rightarrow E_H$). Then, the atom encounters the activation energy for hydrogen absorption H_{hydr}
- E_{diff}, the energy of desorption energy from a subsurface site.

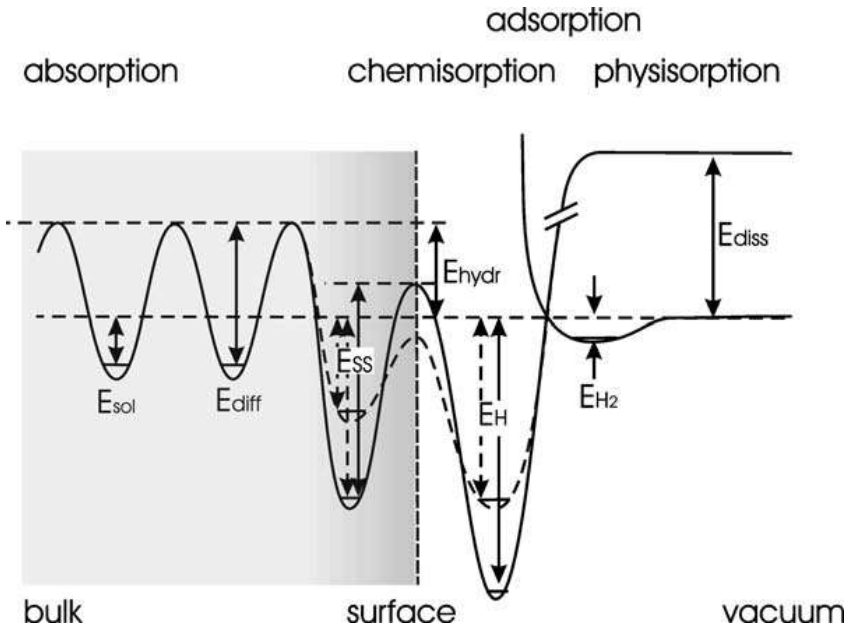

Figure 2.2: sketch of the potential energy of a hydrogen atom entering the material from the void, from right to left.

- E_H, the desoprtion energy from a chemisorbed site (E_M), both for the original and reconstructed surfaces.
- Then, E_{sol} which is the Heat of solution

2.3 Thermodynamics of bulk metal hydrides

The thermodynamics of a a generic M-H system is well described by a PCI graph (Pressure Composition Isotherms) in which the Pressure P_{H_2}(or equivalently the chemical potential) is plotted versus the H/M ratio in the solid phase. We can distinguish an α phase , i.e. an interstitial solution of Hydrogen and metal, and a β phase, i.e. the new formed hydrides. The transformation process occurs according to:

$$MH_{x_\alpha} + \frac{x_\beta - x_\alpha}{2} H_2 \rightarrow MH_{x_\alpha} \tag{2.1}$$

The decomposition of an interstitial solid solution based on a metal or intermetallic matrix results in a formation of 2 phases characterized by different concentrations of interstitial solute atoms. Since we are at equilibrium the transformation can only occur at constant chemical potential[1] (and hence at constant pressure), i.e. $\mu_\alpha = \mu_\beta = \mu_g$

[1]This is true for bulk system. Things change when dealing with films as we will discuss later on.

where μ_g is the chemical potential of the H_2 gas reservoir. Let's try to find an expression for the equilibrium chemical potential.
2.1 can be recast in terms of chemical potential.

$$2(\mu_\alpha^M + c_\alpha^H) + (c_\beta - c_\alpha) \rightarrow 2(\mu_\beta^M + c_\beta^H) \tag{2.2}$$

The chemical potential can be just interpreted as the molar partial Gibbs Free Energy:

$$\mu = \bar{G} = \left(\frac{\partial G}{\partial n}\right)_{p,T} = \left(\frac{\partial H}{\partial n}\right)_{p,T} - T\left(\frac{\partial S}{\partial n}\right)_{p,T} = \bar{H} - T\bar{S} \tag{2.3}$$

If we substitute 2.3 in 2.2 we get:

$$\Delta H_{\alpha\rightarrow\beta} = T\Delta S_{\alpha\rightarrow\beta} \tag{2.4}$$

where:

$$\begin{aligned} \Delta H_{\alpha\rightarrow\beta} &= 2\frac{H_\beta - H_\alpha}{c_\beta - c_\alpha} - \bar{H}_{H_2} \\ \Delta S_{\alpha\rightarrow\beta} &= 2\frac{S_\beta - S_\alpha}{c_\beta - c_\alpha} - \bar{S}_{H_2} \\ A_\nu &= \bar{A}_\nu^M + c_\nu \bar{H}_\nu^H \end{aligned} \tag{2.5}$$

with A = (H,S) and $\nu = (\alpha, \beta)$.

According to classical thermodynamics, the molar partial entropy depdens on the pressure as follows :

$$S_{H_2}^g as = -Rln\left(\frac{p}{p_0}\right) + S_{H_2}^0 \tag{2.6}$$

In 2.6 $S_{H_2}^0$ is the standard molar entropy (which means evalued in standard conditions).
If we substitute 2.6 in 2.4 we get:

$$ln\left(\frac{p}{p_0}\right) = \frac{\Delta H_{\alpha\rightarrow\beta}}{RT} - \frac{\Delta S_{\alpha\rightarrow\beta}}{R} \tag{2.7}$$

From an experimental point of view we are actually in fiting the plateau pressure displayed at different temperatures. In fact we can write:

$$\frac{\partial\left(ln(p)\right)}{\partial\left(\frac{1}{T}\right)} = \Delta H_{\alpha\rightarrow\beta} \tag{2.8}$$

So the angular coefficient of this fit will be given by our entropy of formation. This value is very important since it behaves as a sort of compass for our reaction.
For example, the hentalpy of formation of MgH_2 is thermodinamically favourable since it is an esothermic reaction liberating $\sim 74\frac{kJ}{mol_{H_2}}$ (this means $\Delta H_{Mg\rightarrow MgH_2} \sim -74\frac{kJ}{mol_{H_2}}$).

Such a value for δH entails that the inverse transformation will be thermodinamically sfavoured, hence making pure MgH_2 a difficult compound to destabilize in order to release hydrogen.
An ideal material that should serve as an hydrogen tank should have an hentalpy of formation close to zero, in order for the hydrogenation process to equally or almost equally occur in both senses.As we will see, that can be achieved through elastic constraints[30], or through working out several types of interfaces, depending on the system we are considering, e.g. layer layer interfaces in nanostacked geometries, grain boundaries interfaces, as well as planar defects interfaces.[10].
To understand which reactions could come in our help we need to focus on the kinetic.

2.4 Kinetics

Kinetics tells us how fast a reaction is happening and focuses on the driving forces for the reaction we are interested at. A well described kinetic phenomenon is the diffusion. Here we will mainly focus on the approximation of diffusion taking place as a series of discrete jumps. If we call G_1 and G_F the initial and final energies respectively, the driving force will be given by $\Delta G = G_F - G_1$ since a driving forse is generally always arisen from a difference in terms of Gibbs free energy.
However, according to this model,before reaching G_F, the atom must go through another state, namely the activation energy state G_A which corresponds to an *activated state*. The difference in energy ΔG_A is so called the thermic activation or diffusion energy through thermally activated jumps(see Fig. 2.3)
Kinetics analysis focus on the behaviour of the reaction as a function of time. The theoric

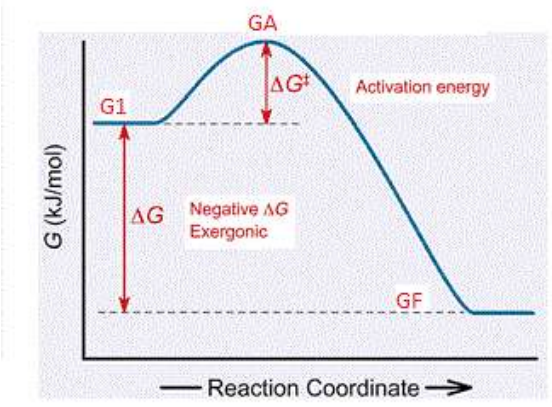

Figure 2.3: Gibbs Free energy behaviour according to the model of thermodinamically activated jumps.

field we usually refer to is the JMAK theory (Johnson-Mehl-Avrami-Kolmogorov)**??** theory which is in turn based on nucleation and growth phenomena.
Let α be the transformed fraction of α or for an hydride, the ab(de)sorbed hydrogen fraction at time t.From JMAK the following trend for that is derived:

$$\alpha = 1 - e^{(kt)^{\eta}} \tag{2.9}$$

where k is a kinetic parameter, while the exponent η is called *AVRAMI coefficient* or order of reaction. 2.9 can be rewritten as follows.

$$ln\left[-ln\left[1-\alpha\right]\right] = \eta ln\left(k\right) + \eta ln\left(t\right) \tag{2.10}$$

2.10 is very important since it allows us to harvest η by plotting α as a function of time. The Avrami coefficient is a key kinetic parameter since it contains many information regarding the reaction.
The kinetic parameter k is very important too, since it is related to the activation energy according to:

$$k = k_0\ e^{-\frac{\Delta G_A}{RT}} \tag{2.11}$$

(In this way we can also find k). While performing this fit we must pay attention at not including data coming from the tail of the transformation, since the above hypothesis cease to hold there.[10]

The Diffusion Constant

A key physical dimension characterizing kinetics is the Diffusion Constant **D**. It appears in the Fick's law for solutions displaying Henry's behaviour(very soluted solution):

$$J = -D\nabla c_1 \tag{2.12}$$

where D is given by the Nerst-Einstein's equation:

$$D = k_B T M \tag{2.13}$$

in which M is the mobility and k_B is the Boltzmann constant.
If we combine 2.12 with the continuty equation involving the flow of particles, assuming their total number to be conserved, namely : $\frac{\partial c}{\partial t} + \vec{\nabla} \cdot \vec{J} = 0$, we get the famous Diffusion equation:

$$\frac{\partial c}{\partial t} = -D\nabla^2 c \tag{2.14}$$

Depending on the boundary conditions, eq. 2.14 returns different solutions for the concentration as a function of both space and time, whose main shape is that of n+1-Dimensional Gaussian, where n is the dimensionality of our system and the term 1

displays the involvment of time.
To determine a valid expression of the diffusion coefficient **D** several models have been built. The most effective one in describing what actually happens is the diffusion through activated atomic jumps, as already stated above.2.4 This model returns the following expression for D:

$$D = Ae^{\frac{S_m}{k_B T}} e^{-\frac{H_m}{k_B T}} \tag{2.15}$$

where A is a set of parameters involving the inner structure of the material we are considering and the pedex "m" indicates the migration free energy of the atom (here splitted in its entropic and hentalpic part). We can use 2.15 to retrieve the behaviour of the diffusion coefficient in our case of interest, i.e. the interstitial diffusion. In particulary we find that:

$$D = D_0 e^{-\frac{E}{k_B T}} \tag{2.16}$$

Eq. 2.16 displays the Arrenhius behaviour, i.e. an exponential behaviour of the diffusion coefficient as a function of the temperature. That ceases to be true as we approach lower temperature. In fact, that being the case, the thermically activated jumps to overcome the activation energy is hindered, so the only way for diffusion to take place is through quantum tunneling. This effect is shown in Fig. 2.4[42]

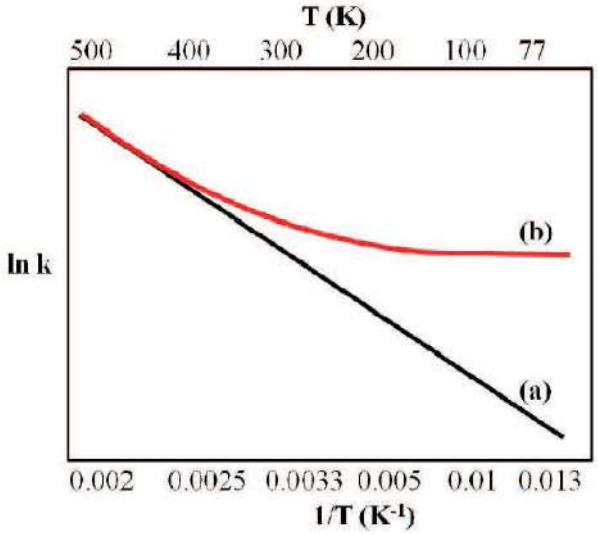

Figure 2.4: Typical example of an Arrhenius plot. The logarithm of the diffusion constant (k) should be a line when plotted against $\frac{1}{T}$. But at low temperatures the energetic barieer for activation gest overcome only through tunneling and that explains the deviation from the linear behavior at low temperatures.

2.5 Brief mention to the theory of elastic stress in metal hydrides

Many multicomponents solids can be represented by a continuousm model. On such basis a thermodynamic theory of multicomponent stress solids has been constructed. The equilibrium of a solid solution in which atoms diffuse through vacancy mechanism or through interstitial sites has been widely studied in literature [14][15]. The fundamental theoric basis is given by the continuum theory of solids according to which the physical properties of our system are continuous functions of position and that discontinituies occur mainly at interfaces, surfaces and dislocations.
The position of each continuous point x modifies as $x^{'} = x + u$ because of the strain that occurs. We can define the strain tensor as follows:[14]

$$E_{ij} = \frac{1}{2}\left(\frac{\partial u_i}{\partial x_j^{'}} + \frac{\partial u_j}{\partial x_i^{'}}\right) \tag{2.17}$$

Equation 2.17 indicates how the displacement u is affected along the main orthonormal directions.
We can now define the internal energy density $\varepsilon^{'}$ and the entropy density $s^{'}$ measured both measured per unit volume as follows:

$$\text{Ł} = \int_v s dv \tag{2.18a}$$

$$\varepsilon = \int_v \varepsilon dv \tag{2.18b}$$

$$\varepsilon = \varepsilon(E, s, \rho_I, ..., \rho_N) \tag{2.18c}$$

In **??** we can appreciate the dependence of ε. ρ_I is the moloar density of component I per unit volume in the reference state.
Coming back to our internstitial solid solution, that has one component which is free to move (mass constant, density ρ arbitrary). Now, the equilibrium condition we need, can be obtained by minimizing$\varepsilon = \int_v \varepsilon dv$ taking into account the constant entropy and the constant mass of the interstitial component.

$$\vec{\nabla}\left(\frac{\partial}{\partial E}\right) = 0 \tag{2.19a}$$

$$\theta = \frac{\partial \varepsilon}{\partial s} \tag{2.19b}$$

$$\mu = \frac{\partial \varepsilon}{\partial \rho} \tag{2.19c}$$

where 2.19b and 2.19b are the Lagrange multiplier for 2.18b and 2.18a.
According to this theory, the Stress Tensor T, whose effects we aim to analyse is simply given by:

$$T = \left(\frac{\partial \varepsilon}{\partial E}\right) \tag{2.20}$$

2.5.1 The Stress-Strain relation in interstitial solid solution

Coming back to the problem of finding a valid expression for the equation condition, we can write the differential of the energy ε, starting from 2.18c:[14]

$$\varepsilon = T_{ij} dE_{ij} + \theta ds + \rho_0 \mu dc \tag{2.21}$$

In 2.21 we can identify ρ_0 as the number of lattice per unit volumes, which means that the partial composition of the solute interstitial element is simply given by: $c = \frac{\rho_I}{\rho_0}$. From 2.21 we can harvest the core equation of this theory which reads like:

$$\left(\frac{\partial E_{ij}}{\partial c}\right) = -\rho \left(\frac{\partial \mu}{\partial T_{ij}}\right)_{c,\theta,T_{kl}\neq ij} \tag{2.22}$$

2.22 is a very important equation since in metal hydrogen systems the change of the axial strains $E_i i$ with H concentration c is a material constant $\rightarrow \frac{\partial E_{ii}}{\partial c} = \alpha$. That is no longer valid if defect formation is involved, but in the frame of pure elastic processes it holds true. Hence we can evaluate how the chemical potential and hence the pressure varies during ab(de)sorption processes.
For example, according to the Eschelby model[6], we consider a linear elastic body like a bulk metal hydrides undergoing stress, strain and displacement following the adding of an outer body (e.g. the adding of hydrogen in the case of interstitial solution).
Change of the shape and of the size of the main body is hindered. In the case of our interest, one finds the following equation for the strain energy :[14]

$$E_{el} = N v_0 G_s \frac{1+\sigma}{1-\sigma} \epsilon_0^2 \bar{c}(1-\bar{c}) = A\bar{c}(1-\bar{c}) \tag{2.23}$$

where the terms of A are so defined:

- **N** is the total number of interstitial sites
- $v_0 = \frac{V}{N}$
- G_s is the shear modulus
- σ is the Poisson ratio
- $\epsilon_0 = \frac{da}{ad\bar{c}}$ is the concentration dependence of the crystal lattice parameter **a** on the concentration

2.5.2 Hysteresis phenomena

The presence of an elastic energy, shaped according to 2.23 suggests that many things plays an incredibile role in the thermodynamic of our interstitial solid solution. As hinted in 2.3 an interstitial solid solution having a metal or intemetallic matrix results in a decomposition in two phases characteriyed by different concentrations of interstitial solute atoms, whose relative composition is given by the lever rule:

$$a_1 + a_2 = 1 \tag{2.24a}$$

$$a_1 x_B^1 + a_2 x_B^2 = x_B^0 \tag{2.24b}$$

Let $c^{\alpha(\beta)}$ be the concentration of interstitial atoms in the $\alpha(\beta)$ phase.Then our system, as highlighted from 2.24 splits into two phases α(in absence of mixture there are no interstitial sites occupied, i.e. $c_\alpha = 0$) and β (when mixture is present, the ordered phase presents a fully occupation of interstitial sites). Hence our transformation goes from a pure α phase, i.e. a solution between the interstitial element (the hydrogen in the case of our interest) and the metallic matrix to a pure β phase which corresponds to the formation of the hydrides.
According to the rules of equilibrium this trasformation can only occur while the chemical potential of both α and β phases are the same and remains constant throughout the transformation. Furthremore they must equal the chemical potential of the gas reservoir which the interstitial solution is plundged in ($\mu_g(P,T)$), i.e.:[9]

$$\mu_\alpha(c_\alpha) = \mu_\beta(c_\beta) = \mu_g(P,T) \tag{2.25}$$

The compass to evaluate the evolution of the transformation is of course the Gibbs free energy: we can write the free energy per lattice site for the αphase as follows:[9]

$$F_{\alpha(\beta)}(P,T,c) = f_{\alpha(\beta)}(P,T,c) + Ac(1-c) \tag{2.26}$$

where in 2.26 $f_\alpha(P,T,c)$ is just the Gibbs free energy of the $\alpha(\beta)$ phase "isolated". To make a more realistic picture we need to add the elastic contribution given by the strain produced by the interstitial atoms diffusion in the metal lattice. There is neat relationship between c_α, c_β and $\bar{c}$, expressed through a modulation of 2.24b. Once defined W as the volume fraction of the β phase, hence the relative fraction of interstitial sites occupied in β we can write :

$$W c_{beta} + (1-W)c_\alpha = \bar{c} \tag{2.27}$$

Then if we introduce the possibility of varying the concentration, we need to consider the chemical potential. The Gibbs free energy in 2.26 becomes then a thermodynamic function describing a Grancanonical system and via 2.27 we can rewrite it as follows:

$$G(T,P,\mu;c_\alpha,c_\beta,\bar{c},W) = W f_\beta(c_\beta) + (1-W) f_\alpha(c_\alpha) + A\bar{c}(1-\bar{c}) - \mu\bar{c} \tag{2.28}$$

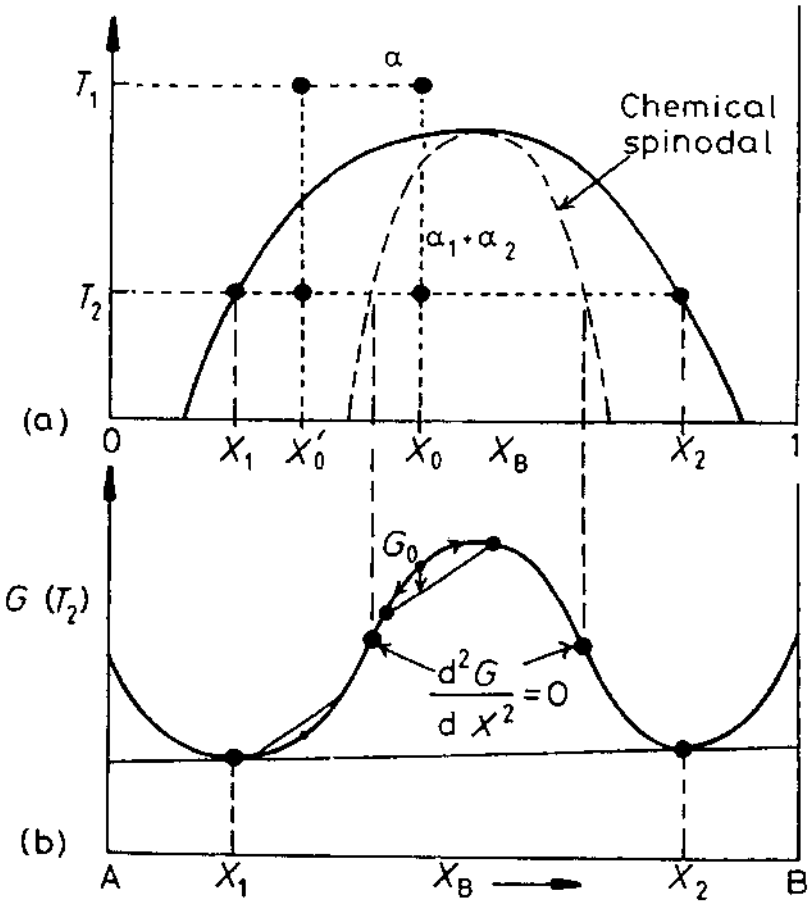

Figure 2

Figure 2.5: Sketch of the forementioned composition. In this special case, being the G-curve symmetric we refer to the decomposition of the system as **Spinodal decomposition** The term spinodal indicates the inflection points of δG. 2.24 refers to the general case of a non symmetric δG.[12]

In order to get an expression for the chemical potential reached at equilibrium we need to minimize 2.28. Without entering the detail of the calculations, we can harvest the following two conditions for equilibrium, that needs to be fullfilled simultaneously.[9]

$$\mu_\alpha(c_\alpha) = \frac{\partial F_\alpha}{\partial c}|_{c=c_\alpha} = \frac{\partial f_\alpha}{\partial c}|_{c=c_\alpha} + A(1-2c_\alpha) \tag{2.29a}$$

$$\frac{f_\beta(c_\beta) - f_\alpha(c_\alpha)}{c_\beta - c_\alpha} - \frac{\partial f_\alpha}{\partial c_\alpha} = 0 \tag{2.29b}$$

Now, the chemical potential $\mu_1(P,T)$ remains constant during the $\alpha \to \beta$ reaction. The starting composition will be obtained according to 2.29b, i.e. through a common tangent construct, as highlighted in Fig. 2.6 and it is equal to $c_{alpha}^{stationary}$. To that composition corresponds a certain chemical potential $\mu_g^{Abs}(c_\alpha^{stationary}, p_1, T)$ (and hence a pressure p_1[2]) shaped according to 2.29a.

Now, simply looking at Fig. 2.6 we can realize how the presence of the elastic energy term in 2.29a entails that $\mu_g^{Abs}(c_\alpha^{st}) \neq \mu_g^{Abs}(c_\beta^{st})$, so the reaction ends at once reached the final composition c_β^{final}. That means that β phase needs to absorb further interstitial atoms from the gas reservoir.

We can apply the same reasoning to the desorption process, i.e. the $\beta \to \alpha$ reaction which leads to a reaction occurring at chemical potential $\mu_g^{des}(c_\beta^{stationary}; p_2, T)$starting from the composition $c_\beta^{stationary}$ and ending with the final composition c_α^{final} which means the α phase has to desorb interstitial atoms during the desorption process. So what we are looking at is an *Hysteresis* phenomenon at the PCI (Pressure-Composition Isotherme), whose width is modulated by the elastic strain. So to summarize:[14]

$$\mu_g^{absorption}(p1,T) = \frac{\partial f_\alpha}{\partial c}|_{c=c_\alpha^{stationary}} + A(a - 2c_\alpha^{stationary}) \tag{2.30a}$$

$$\mu_g^{desorption}(p2,T) = \frac{\partial f_\beta}{\partial c}|c_{=}c_\beta^{stationary} + A(a - 2c_\beta^{stationary}) \tag{2.30b}$$

$$W_H = \mu_g^{absorption}(p1,T) - \mu_g^{desorption}(p2,T) = 2A(c_\beta^{stationary} - c_\alpha^{stationary})[9] \tag{2.30c}$$

In 2.30c we also made explicit the width of the hysteresis which as hinted above should be proportional to the elastic coefficient A.

Unfortunately, no experimental fit this model, since the true measured hysteresis widths are smaller than expected by 2.30c. So this model over-predicts the hysteresis and lacks of something that was not resolved up to now[3].

[2]we can explicit the dependence on the pressure by considering $p_1 = p_0 exp(\frac{\Delta\mu}{RT})$ where $\Delta\mu = \mu_1 - \mu_0$ with $p_0(\mu_0)$ is a standard value of pressure (chemical potential)

[3]Private communication with S. Wagner

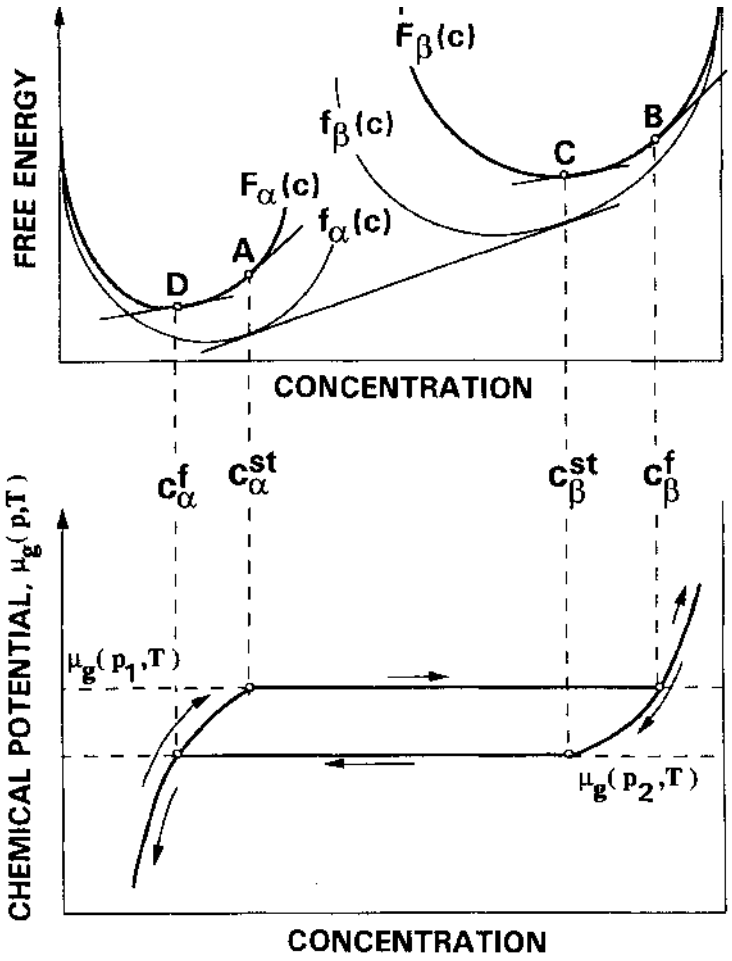

Figure 2.6: behaviour of the equations 2.29 as a function of the composition (above), and PCI graphic (Below).[9]

2.5.3 Modification of PCI isotherm due to inner structures

The presence of surfaces, grain boundaries, dislocations and vacancies affects the behaviour and the sites occupation of the hydrogen diffusing within the metal crystal. Let's see why:

- ***Grain boundaries***: a grain boundary is an interface between two crystals with same structure but different orientation. If the difference of the angle of orientation is larger than 10° we speak of High-angle grain boundaries, which are the most interesting in our treating. Of course when we deal with materials of the order of the nanoscale grain boundaries are something we have to consider, because depending on the growth conditions of the material every nano-domain will eventually develop its own orientation. Anyway, the GB fraction will be considerable in nanocrystalline materials.
  The different behaviour of the PCI plateau pressure for bulk Pd-H and nano Pd-H, in which the role played by high angle grain boundaries is preminent was studied in literature[18] [19]. It was developed a theoric model according to which a nanohydride can be divided into a grain boundary region that doesn't partecipate at the hydride formation and a bulk-like one.[19] That entails a narrowing of the PCI plateau as we can see in Fig. 2.7.
  That happens because at low concentrations grain boundaries sites offer low energy sites that are initially filled with hydrogen (hence plateau begins at higher concentration in Fig. 2.7), while at high H concentrations only bulk-like regions transform into hydride. That means that the plateau ends at a lower concentration than bulk-hydride. A quantitative formula to evaluate the schrinkage of the plateau line was provided:[18]

  $$\Delta c_n = (1 - f_{GB}) \cdot \Delta c_{bulk} \tag{2.31}$$

  Where in (2.31) f_{GB} is equal to the relative fractions of sites in grain boundaries and Δ_c is the width of the plateau in nanoparticle's case and in bulk-like's case.
  Grain Boundaries have also been found to affect the diffusion of hydrogen too. That explains why diffusion constant in n-Pd-H is dependent on the hydrogen composition (while the bulk-like material shows a constant behaviour), ranging from one order of magnitude lower than D_{bulk} at low concentrations to an order of magnitude higher than D_{bulk} at high concentrations. [7][19].

- **Dislocations**. Since dislocations (misfitting between lattice plains) are always present in materials, it is important to determine if and how they affect the hydrogenation process.
  In particular, edge dislocations are the most interesting ones: in FCC (Face Center Cubic) materials, stress fields are isotropic, so H will only interact with edge

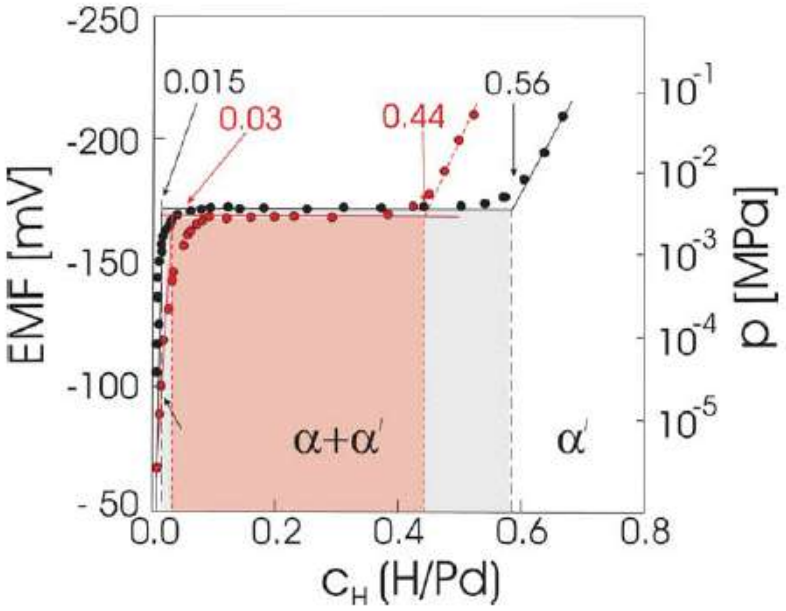

Figure 2.7: PCI's isotherm for bulk Pd-H and nano-Pd-H.

dislocations.
They occur when extra atoms are added to a lattice plane, hence making the material more keen to deformation. If we consider the diffusion of Hydrogen in bulk palladium, it was found that edge dislocations act as energy traps for H.[7].
In Fig. 2.8 we can see the improved solubility of hydrogen in Pd when its plastic deformation is increased.
The interpretation arose from numeric calculations and from neutron scattering experiments [7] is that an hydrogen-enriched cylinder develops at the core of an edge dislocation, whose radius is a function of the total hydrogen concentration c_{tot}.

- **Vacancies**: since vancancies are always present at any temperatures, their influss must be also taken into account. Normally, at room temperature, vacancies are neglectable since their concentration is very low($\sim 10^{-34}$). If we glance at this problem from the perspective of statistical thermodynamic, vacancies are expected to dramatically increase when the metal system approaches the melting temeprature (highly disordered phase).
  Now, the presence of hydrogen has been found out to dramatically increase the concentration of vacancies at equilibrium: For Pd-H system heated up to 1000 K and plundged in an hydrogen gas pressure of nearly 5 GPa, a 18% of vacancy concentration was found[13]. The vacancies discovered in this configuration carry

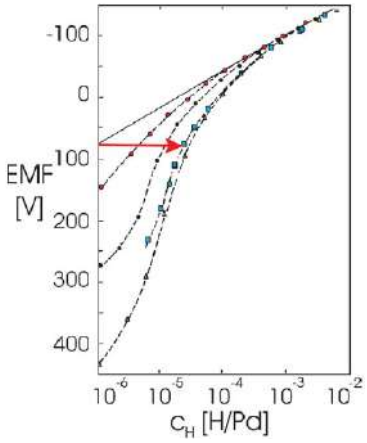

Figure 2.8: PCI's isotherm of Pd-H as a for different plastic deformation (from 0 to 73%). The straight line identifies the bulk-like behaviour. [7]

the name of **S**uper **A**bundant **V**acancies, since such a huge concentration is far larger than the concentration expected for the metals close to the melting point ($\sim 0.01\%$[7]).
When the concentration of vacancies is no longer neglactable, the interstitial mechanism of diffusion we have earlier described ceases to be energetically favourable because hydrogen is trapped into more convenient energetic sites at the vacancies. This means that (2.15) modifies in the following way:

$$D = Ae^{\frac{S_m+S_v}{k_BT}}e - \frac{H_m + H_v}{k_BT}[23] \tag{2.32}$$

where in (2.32) $S(H)_V$ is the Entropy (Hentalpy) of vacancy creation, since for diffusion to take place through vacancies we need to consider the energetic and entropic cost of introducing a vacancy in the crystal structure.
So, high vacancy concentration also means high hydrogen concentration, since H atoms are trapped at each vacancy site(up to a number of 5 hydrogen atoms per vacancy site). Hence, both gravimetric and volumetric capacity of these materials, called superabundant vacancies increase and so they have to be considered as a valuable candidate for hydrogen storage materials.
In fact, hydrogen being trapped by vacancies hugely affects the total hydrogen concentration. An estimation of huw much $c_{H,tot}$ is affected can be given by:

$$c_H, tot = f \cdot c_{vac} + c_{H,M} \tag{2.33}$$

where in Eq. 2.33 f is the trapping factor, i.e. the average number of hydrogen atoms per vacancy. So, Eq. 2.33 yields that in a solid solution, vacancies tend to increase the total concentration of hydrogen. [7]

2.6 Magnesium hydride

As suggested before, one of the most interessant material for hydrogen storage is MgH_2 because of its high gravimetric and volumetric capacity as it can be seen in eq. 2.34:

$$c_{MgH_2,g} = \frac{m_{H_2}}{m_{MgH_2}} = \frac{2m_H}{m_M g + 2m_H} = 7.66 wt\% \tag{2.34a}$$

$$c_{MgH_2,v} = \frac{m_{H_2}}{V_M gH_2} = c_{MgH_2,g} \cdot \rho MgH_2 = 9\frac{MJ}{kg_{Mg}} \tag{2.34b}$$

As clear from Eq. 2.34b, magnesium hydride shows the highest energy density for hydrogen storage and that's why it needs to be analyzed in detail.
We can take a glace at the Mg-H phase diagram in Fig. 2.9, in which the different phases which Mg-H undergoes to are shown. We can appreciate the existence of an

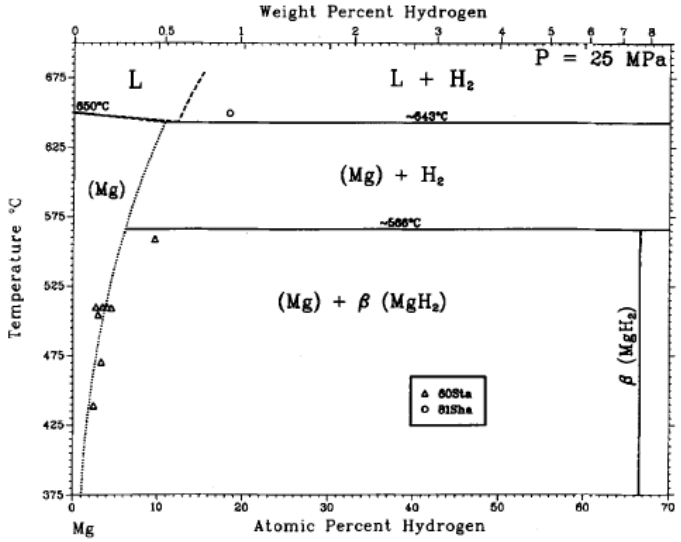

Figure 2.9: Phase diagram of Mg-H

hyride phase at equilibrium with Mg, namely the β-MgH_2 phase, to which we need to add also a further high pressure hydride phase, namely γ-MgH_2.
Nevertheless, though this particular kind of hydride seems to fullfil many requests from 1 normal bulk MgH_2 cannot be used for technological purposes. A huge obstacle is represented by the very high hentalpy of formation ($\sim 74\frac{kj}{mole}$) that needs to be lowered in order to make the hydrides less stable. Furthermore:

- the Kinetics of Hydrogen absorption and desoprtion reactions is too slow for pure Mg

- At standard condition of pressure, i.e. 1 bar, the release or the absorption of hydrogen can only take place at high temperatures, ($\sim$ 600 K).

There are many factors producing this undesired situation:the formation of oxide at the surface, which means we need to break it before the hydrogen can enter Magnesium, and the low dissociation rate of molecular hydrogen at Mg surface caused by an elevate dissociation energy.
Once the reaction has somehow taken place there is another huge obstacle, since the formation is further slowed by layers of hydride itself which hinders the diffusion of hydrogen within the Mg sample. These blocking layers entail that the diffusion coefficient D_{MgH_2} of Hydrogen inMgH_2 is far smaller($\sim 10^{-20}\frac{m^2}{s}$) than the diffusion coefficient of $D_{Mg}(\sim 10^{-11}\frac{m^2}{s})$[16]. Because of this blocking layers, nanosized Mg is highly suggested in order to overcome such hinderness.

2.6.1 The role of catalysts

An interesting way to lower the energy barieer at the Mg crystal surface that the H_2 molecule encounters before splitting ,is adding another element to Mg. This other element that will behave as an effective *catalyst* should also have the property to enhance the diffusion of the hydrogen atoms in MgH_2.
Hence a catalyst is able to lower the activation energy at the surface, making easier the chemisorption of hydrogen and modifying the cristalline structure of magnesium, in order to prompt a better diffusion of H within Mg hydride.
The best elements fulfilling this role are the transition metals, e.g. iPd,Fe,V,Zr,Ti,Mn as well as combinations of those metals. Their features related to their action as catalist of magnesium hydrogenation are listed in literature at [17], for example. The most important characteristics to look at are:

- *Lightness* Since a catalyst is not involved in the processes of hydrogen storage, it needs to be as light as possible in order not to weight too much the structure.

- *Velocity of the reaction* A good catalyst must ease the dissociation of the hydrogen, since its mixture with Mg reflects in a larger amount of dissociation sites.

- *cost.* A good catalyst should be not so expensive and should be available in decent quantities on the Earth'surface

For the last reason, the most fit candidates for catalyst is Titanium. In fact, excellent results were obtained by a Mg-Sc compound [20] which displayed hastened kinetics, but Scandium is a very rare and expensive element, so research focused on Titanium, which has similar features but it's much cheaper.
Yet, the integration of Titanium with Magnesium shows a huge problem. As we can see

from Fig. 2.10, these two materials are widely unmixable. In fact, because of the Ti fusion temperature (1668°C) being much higher than Mg's one(1090° C), it is impossible to create an alloy between these two elements by exploiting the usual metallurgic technique.
Therefore other technique need to be investigated, e.g. the ball milling, also known as "meccanical milling" which produces Ti-Mg bulk material or thin films created through PVC (Physical Vapor Deposition) methods, such as MBE deposition or sputtering deposition, the latter being the core of this paper.
These techniques rely on forcing Mg and Ti to coexist thermodinamically in nanostructures. Producing nanomaterials is a pleasent side effect since materials with spatial dimentions not larger than a few tens of nanometers further quenches the hindering of hydrogen diffusion through MgH_2.

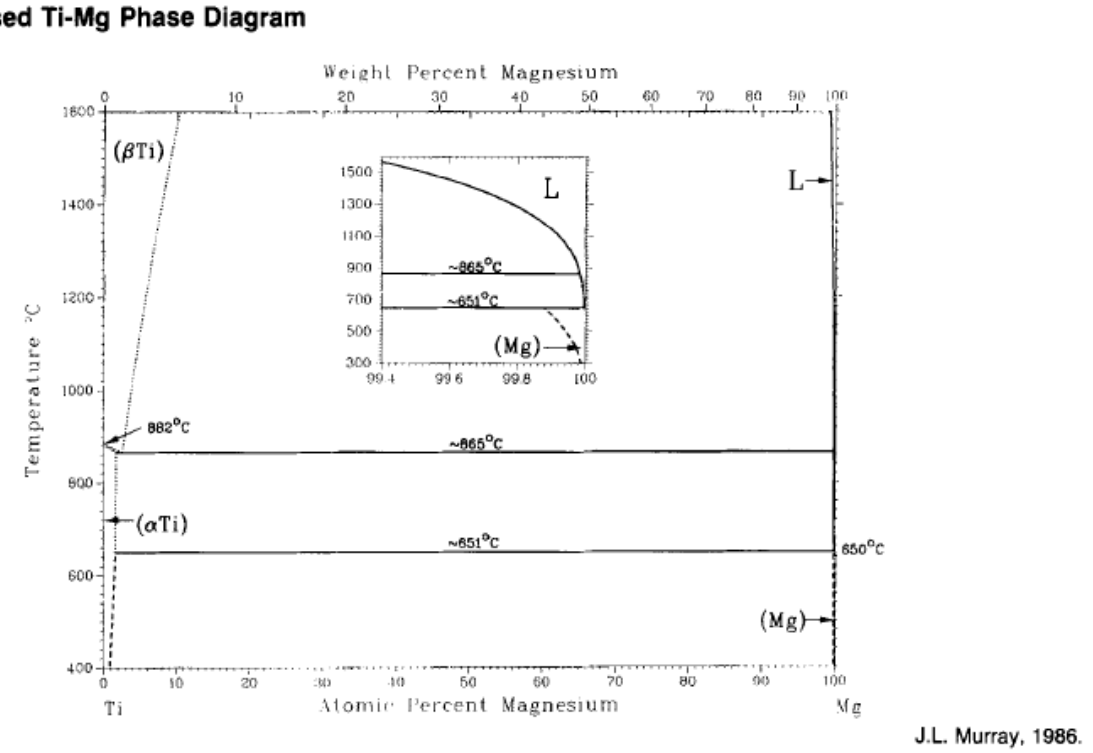

Figure 2.10: Phase diagram of Ti-Mg

Chapter 3

Metal hydrides thin films

In this chapter we will focus on how the kinetics of the reaction changes when dealing with nanostructures. First of all, Though they certainly make model systems for studying and better understanding the thermodynamics with elastic constraints, we have to foresay that nanostructures such as thin films are very unlikely to be used for hydrogen storage. Nevertheless they may also find an outlet in other fields of technology.
For examples, the M-H transformation can be embedded in a device that behaves as a switchable mirror. That's could be the first step to realize a fully operative "smart window".
[21]. In fact, in the M-H transition we can go from a reflective metallic state, namely the α phase to the hydrided and transparent β phase. This change in optical properties is exactly what we aim to witness in such a device.
Furthermore, thin films, or nanostructured hydride materials can also be used to build Hydrogen sensors. In fact, in an hydrogen fuelled vehicle, such sensors are essentials and should be as reliable as possible.In particular, the optical changes in metal hydrides allow the development of optical fiber sensors. Since we are currently dealing with just optical properties, the systems are potentially safe.[21]

3.1 The effects of nanostructure

As stated before, there are many reasons for the low kinetics of H_2 in forming Mg_{H_2}. One of the reasons was the high energy barrier the H_2 molecule ecounters when getting near to the Mg surface. One idea would be would be to increase the free surface of the sample.
Hence the idea of focusing on the realization of thin films, which of course display a great surface/volume ratio. Many compounds have been studied, but, for the reason discussed above, the Mg nanosystem was the main studied because of its storing properties. In Fig 3.1 we can take a glance at the enhanced kinetics induced by the nanoscale.

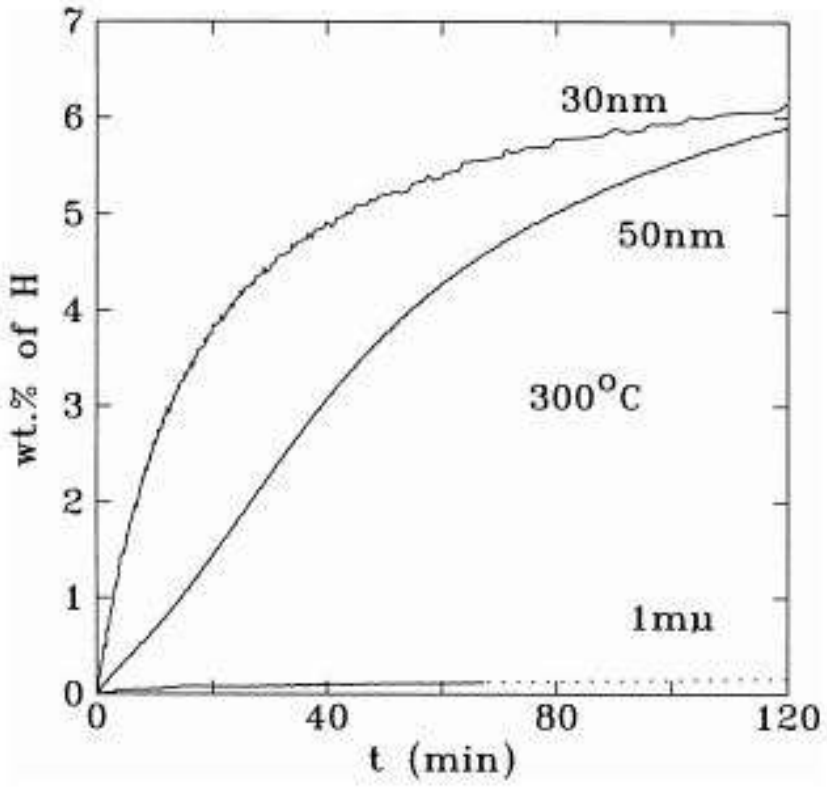

Figure 3.1: Absorption kinetics for different-sized Mg. The nanostructure considerably betters the materials kinetics [22]

3.1.1 The role of thermodynamics

The reduction of the scale highly affects the thermodynamics of the M-H system. In fact, in such systems we cannot neglect the contribution of the interface energy beetween the hydride and the metal phase. Let γ_i be the interfacial free energy of the i-th M-H-M interface.
When dealing with the difference in terms of free energy formation of the hydride transition between a bulk material and a nanostructure, we need to consider the bias that these interfaces induce in terms of free energy of formation:

$$\delta(\Delta G^0) = \Delta G^0_{nano} - \Delta G^0_{bulk} = \sum_i A_{MH,i}\gamma_{MH,i} - \sum_j A_{M_j}\gamma_{M_j} \tag{3.1}$$

where in 3.1 A and γ are the free energy per unity of surface and the sum can be extended all over the system surfaces.

In literature many researches about this argument can be found. For the purpose of this thesis we now report the results of [24] which is a sort of benchmark in this field.
For this experiment Mg thin films of different are deposited on a substrate and sorrounded by Titanium layers of fixed extentions to increase the kinetics, as stated before. The whole system is then capped with a Pd layer to prevent the oxidation.
When considering the hydrogenation of Mg, we can write an expression for the equilibrium constant which is somehow related to the plateau pressure through:

$$-lnK = ln\frac{p_{H_2,nano}}{p_0} = \frac{\Delta_r G^0_{nano}}{RT} = \frac{\Delta_f G^0_{MgH_2}}{RT} \tag{3.2}$$

but the free energy of formation for a nanomaterial is made of both a bulk term and the interface energy term of 3.1.
When considering the difference in terms of plateau pressure between a nanomaterial and a bulk material the two bulky terms will cancel out and only the interface term will remain. So we can write:[24]

$$ln\left(\frac{p_{nano}}{p_{bulk}}\right) = \frac{\gamma A_{MgH_2|TiH_2} - \gamma A_{Mg|TiH_2}}{RT} \tag{3.3}$$

where in 3.3 we considered isotropic materials, which means γ is independent on the orientation of the considered interface. We could further semplify 3.3 by assuming a constant Area of interface, notwithstanding the two different interface Area (Mg—TiH_2 and $MgH_2|TiH_2$). By setting $\gamma_{MgH_2|TiH_2} - \gamma_{Mg|TiH_2} = \Delta\gamma$ we can rewrite 3.1 as follows:[24]

$$\left(\frac{p_{nano}}{p_{bulk}}\right) = \frac{A}{RT}\Delta\gamma \tag{3.4}$$

From eq. 3.4 we can actually verify the dependence of the plateau pressure on the thickness d of each Mg layer, since the term A can be approximated by $A = \frac{2V}{d}$ (when neglecting the small contribution of the $Mg|MgH_2$).
In Fig. 3.2 one can easily see that the plateau pressure which the hydrogenation occurs at, gets higher as the layer shrinks.

3.1.2 The role of the elastic strain

Elastic strains also plays a role in destabilization of thin films; they develop when our films are clamped to a substrate and are not free to expand following H absorption (we remind that the hydride volume is larger than the single metal system).
Several model have been developed to describe such a contribution and they all predict an enthalpic destabilization proportional to the strain ϵ:

$$\delta\Delta H^0 = -2B\bar{V}_H\epsilon \tag{3.5}$$

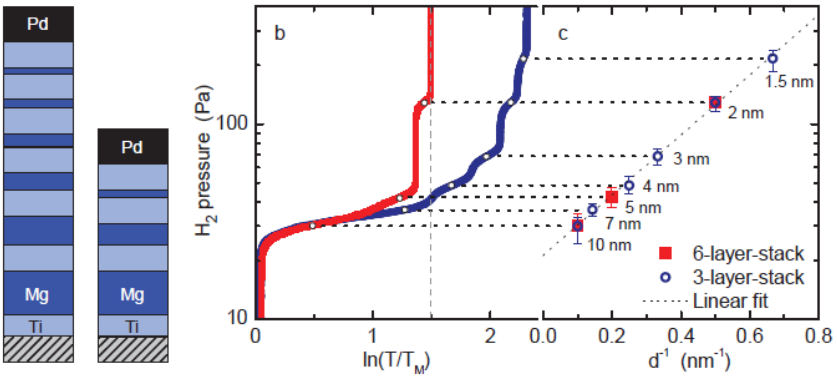

Figure 3.2: Brief sketch of the devised thin films system (left) and absorption relative PTI (Pressure, Transmittance Isotherm). The plateau pressures of each layer are then extrapolated and plotted as a function of the thickness in order to get a valid figure for $\Delta\gamma$[24]

where B is is the bulk elastic modulus of the metal, $\bar{V}_H$ is the partial molar volume of H in the hydride.
We can actually derive an expression for the change of the plateau pressure following an induced elastic strain in a thin film and experimentally verify it. That was made in [26]:

$$ln\left(\frac{p^*}{p^0}\right) = \frac{E_{Mg}}{\tilde{E}}\left[1 - \nu_{Mg} + (1 - \nu_{Cap})\frac{E_{Mg}}{E_{Cap}}\frac{d_{Mg}}{d_{Cap}}\right]^{-1} \tag{3.6}$$

where $\tilde{E}$ depends on the molar volume of both Mg and H_2, while E is the Young's modulus. According to 3.6 the plateau pressure of our Mg-capped hydride is dependent on the thickness of the Mg layer (the thicker the Mg layer, the lower the plateau prossure). In Fig. 3.3 the experimental results for Mg layers of different thickness seem to validate this model.
As widely reported in [27], the chemical potential of H in a Pd film dramatically changes as a function of the film thickness and mechanical stress; even the grain boundary size plays an essential role in the process.
While the grain size brings in a lateral and hence in plane microstructural constraint, the reduction of the film thickness imposes a vertical and hence out of plane geometrical constraint. The effect of film-substrate clamping stress *sigma* on the chemical potential is described through eq. 3.7 and directly comes from Eq. 2.22[27]:

$$\delta\mu_H(\sigma) = -2\bar{V}_H\alpha_H\sigma(x_H) \tag{3.7}$$

being x_H the H concentration in Pd, $\bar{V}_H$ the partial molar volume of interstitial H, and α_H the expansion factor defined as the relative change of the lattice parameter.

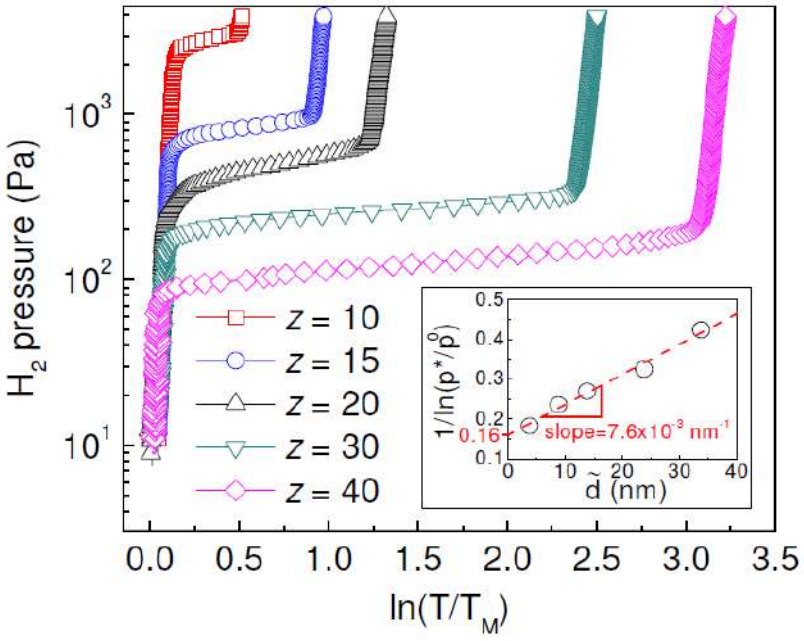

Figure 3.3: Behavior of the Plateau pressure as a function of the thickness of the Mg-layers clamped to a glass substrate and then eventually capped with a Pd layer. One must pay attention at the true thickness of the film which is lower than reported, since part of the film is "eaten" during a nano-alloying with the Pd layer.

In Fig. 3.3, taken from [27], one can actually understand the action of the substrate-induced stress on the shifting upwards of the chemical potential at which the hydride transformation occurs with respect to a bulk material.

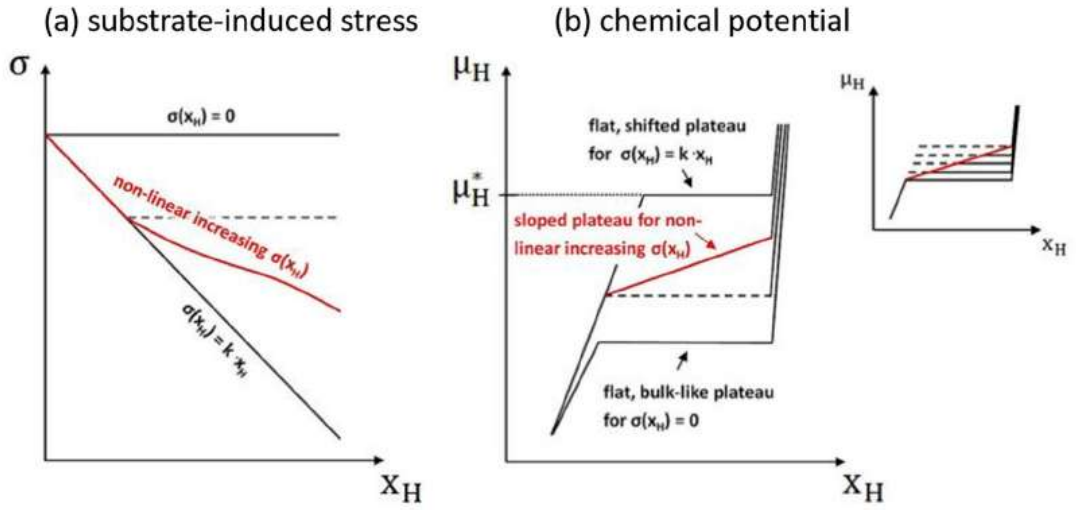

Figure 3.4: Results of the induced stress in the chemical potential-composition isotherm of a Pd thin films clamped to a substrate. We can see both linear and non linear behavior for the stress (left) and the relative consequences on the shifting of the chemical potential as a function of the composition graph (right)

The substrate-induced stress is supposed to be linear with the composition $\rightarrow \sigma = k \cdot x_H$ and that simply entails a shifted μ_H. Nevertheless, in a thin film it may happen that, as the H atoms enter the metal, the film might become to release dislocations, hence lowering the stress, which will in this case exhibit a non linear behavior. That will entail a sloped plateau pressure, the steepness of which will depend on the intensity of such dislocations.
However, as the film gets thinner and thinner, the emission of dislocations becomes energetically hindered and so we witness to a high plateau pressure.[10]
Notwithstanding this very interesting behavior, the focus of such a research should be on the desorption isotherm, the core of any future technological use. It was attempted to exploit the substrate induced strain to destabilize hydrides such as Mg. Unfortunately researches that analyzed a Mg thin film capped with Pd concluded that both clamping with the substrate and nanoalloying with Pd were actually responsible for the shift in the absorption plateau pressure for Mg, but clamping effects (see eq. 3.7) did not affect significantly the desorption isotherm. [10]

3.2 Methods of investigation

To analyze the physical dimensions involved in the hydride transformation, several experimental methods can be arranged. We will here discuss the two of them that were

actually used during my staying in Karlsruhe.

3.2.1 Electrochemical hydrogen loading

In this method an Oxygen-free electrolyte solution is poured into a loading cell. The electrolyte solution is such that it will provide the H^+ that will enter the thin film. Of course the thin film needs to be adjusted in order to be set duly in contact with the electrolyte solution.
Such a system is shown in Fig. 3.5. A Pt small slab is used as counter electrode and it is naturally plundged in the electrolyte solution. According to the Electrochemical hydrogen loading cell depicted in Fig. 3.5, the following reactions take place:

$$\textbf{Sample} \ : Pd + H_3O^+ + e^- \rightarrow PdH + H_2O \tag{3.8a}$$

$$\textbf{Counter electrode} : Pt + 6H_2O \rightarrow Pt + O_2 + 4H_3O^+ + 4e^- \tag{3.8b}$$

The system is connected to a tension generator.

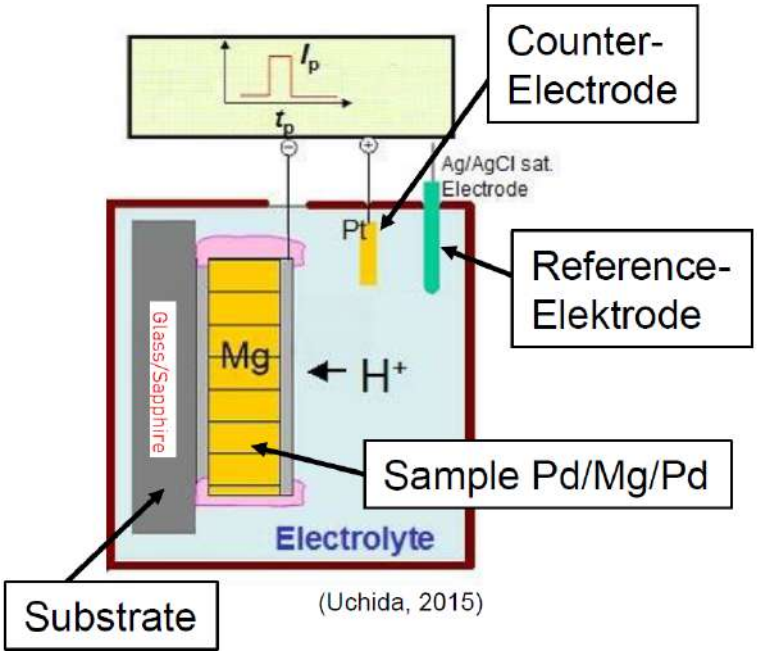

Figure 3.5: Sketch of an electrochemical Loading cell[11]

A current pulses will induce the electrolyte solution to release the hydrogen in the solution, depending on the solution we are considering. Through Faraday law we can

adjust the mean hydrogen concentration released after the current pulse, by setting the current intensity I and the time pulse t:

$$c_H = \frac{\eta_H}{\eta_M} = \frac{I \cdot t \cdot V_M}{F \cdot V} \tag{3.9}$$

where F is the Faraday's constant and V the sample volume and V_M the molar volume of the metal.
The idea is to make many H concentration steps and measure every time the value of Electromotiv force of the sample against a counter-electrode. This value of tension can be easily linked to the chemical potential of hydrogen (and hence to its pressure) as follows.
According to Faraday's law,

$$\mu - \mu_0 = -F(U - U^0) \tag{3.10}$$

and considering very diluted solution:

$$\mu = \mu_0 + RTln(c) \rightarrow c = exp(\left(\frac{\Delta\mu}{RT}\right)) \tag{3.11}$$

where in 3.11 and 3.10 μ_0 indicates the variation of the chemical potential with respect to a reference stato μ_0, while in 3.10 U^0 represents the value of the reference electrode.
We can eventually link the chemical potential to the pressure of hydrogen. Let's take a glance at Fig. 3.6:

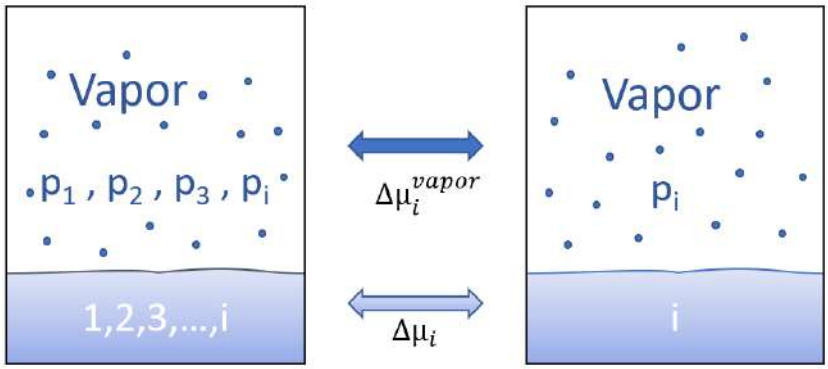

Figure 3.6: *Solution with the i-th elements in equilibrium with the mixed vapour and solution of pure i in equilibrium with pure i vapor. For the scope of this work thesis of course the Vapor will be considering will be H_2!*

According to the equilibrium rule, the two systems are in equilibrium if the i-th element

of a solution is in equilibrium with its vapour, namely:

$$\mu_i = \mu_i^{vap} \tag{3.12a}$$
$$\mu_i^0 = \mu_i^{vap,0} \tag{3.12b}$$
$$\Delta\mu_i = \Delta\mu_i^{vap} = \Delta\bar{G}_i \tag{3.12c}$$

According to 3.12, we can immediately write an expression for the partial pressure of the i-th element (it is a similar situation with our hydrogen in the interstitial solution at equilibrium with the H_2 gas reservoir). By considering the inphinitesimal variation of the Gibbs Free Energy as $dG = -SdT + VdP = VdP$ since we are working at constant temperature, and by applying the perfect gas law for a mole $\rightarrow$ PV = RT, we get:

$$\Delta\mu_i = \Delta\mu_i^{vap} = \Delta\bar{G}_i = \int_{P_i^0}^{P_i} VdP = ln\left(\frac{P_i}{P_0}\right) \rightarrow \tag{3.13a}$$
$$P_i = P_0 exp\left(\frac{\Delta\mu_i}{RT}\right) \tag{3.13b}$$

where in 3.13b P_0 is 1 bar.
Combining eq. 3.13 and 3.10, we achieve the following expression for the Pressure :

$$P_i = P_0 exp(\tfrac{F(U-U_0)}{RT}) \tag{3.14}$$

We can now show some examples of how these data look like and how they should be read. In Fig. 3.7, we can harvest the concentration at which the hydride is being formed in a Pd thin film, by looking at the points in which the loading curve begins to flatten (though since we are dealing with).

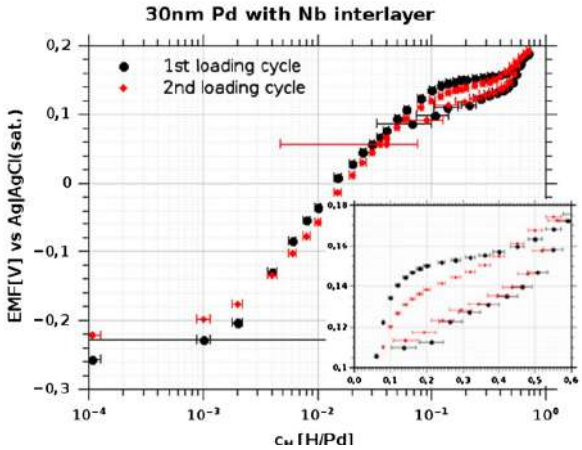

Figure 3.7: *Curve of EMF loading curve of a 30 nm Pd thin film with an ultra-thin Nb layer to improve adhesion, vs Hydrogen concentration loading steps. A first and next second load, with relative unload is shown in the graph.[28]*

3.2.2 Absorption and Sievert's Law

The above calculations and description of electrochemical loading are an ideal opportunity to take a glance at the mathematical models describing the absorption oh hydrogen in a metal. In particular we are going to discuss more in detail about the Sievert's law, named after Prof. A. Sieverts who first noticed in 1929[31] a linear relationship between the square root of the hydrogen pressure and the hydrogen concentration:

$$\sqrt{P_H} = K \cdot c_H \tag{3.15}$$

.
where K is a constant. The goal of this section will be to provide a mathematical model able to retrieve a valid estimation for K.
Let's consider the chemical potential of H in metal starting from Gibbs free energy:

$$G = H - TS = H - TS(S_c + S_n) \tag{3.16}$$

where S_n is the contribution of nanointeraction that can be described by other detailed models. Let's now focus on determining S_c, i.e. the configurational entropy of the system:

$$S_C = k_B ln\left(\frac{n_s!}{n_H!(n_S - n_H)!}\right) \tag{3.17}$$

where n_s is the number of sites available for interstitial diffusion of hydrogen and n_h is the number of hydrogen atoms. In particular the configurational entropy is given by the Boltzman formula $S = k_B lnW$ where W in this is case is nothing else the binomial

coefficient $\binom{n_s}{n_h}$, i.e. the many different ways of disposing n_h elements in n_s sites.
Since we are dealing with very huge number, we can make use of the Stirling's approximation (lnN! = NlnN - N), which transforms eq. 3.17 into:

$$S_C = k_B n_S \left(\frac{n_S}{n_S - n_H} \right) - k_B n_H ln \left(\frac{n_H}{n_S - n_H} \right) \tag{3.18}$$

Now we will derive 3.18 with respect to n_H in order to eventually harvest an expression for the chemical potential of Hydrogen.

$$\frac{\partial S_C}{\partial n_H} = k_B ln \left(\frac{n_S - n_H}{n_H} \right) \tag{3.19}$$

Now, imaging our diffusion sites follow a Fermi-Dirac distribution, the following equation for the configurational entropy contribution to the chemical potential of hydrogen in metal can be achieved:

$$\mu_S^{Hinmetal} = \varepsilon_0 + k_B T ln \left(\frac{c}{r - c} \right) \tag{3.20}$$

being ε_0 the energy of the interstitial diffusion site. Collecting the previous equations with 3.16 we can write an expression for μ_H^{metal}:

$$\frac{\partial G}{\partial n} = \mu_H^{metal} \sim h_\alpha - T s_n + k_B T \cdot ln \left(\frac{c}{r - c} \right) \tag{3.21}$$

where in eq. 3.21 h_α is the partial molar hentalpy, while s_n is the partial molar entropy due to other nanoscopic models (both derived with respect to the number of moles).
Assuming $\mu_H \sim \frac{1}{2}\mu_{H_2}$ and combining that with eq.3.21 and 3.20 we eventually get

$$\sqrt{\frac{P_{H_2}}{P_0}} \cdot exp \left(\frac{h_\alpha - T s_{nc} - \frac{1}{2}\mu_{H_2}^0}{k_B T} \right) = \frac{c}{r - c} \tag{3.22}$$

which is exactly the Sievert's law, where the parameter K in eq. 3.15 is given by:

$$k_S = exp \left(\frac{h_\alpha - T s_{nc} - \frac{1}{2}\mu_{H_2}^0}{k_B T} \right) = exp \left(\frac{\Delta G_\alpha(T)}{k_B T} \right) \tag{3.23}$$

We could actually expand our theory by including all the entropic contributions foreshadowed by the term S_{nc} in eq. 3.16, such as the protonic and elastic perturbation term ($\Delta\mu_{H^+}$), along with the electronic term ($\Delta\mu_{e^-}$). But that does matter for this work thesis is the behavior entailed by the simple Sievert's law, which describes the behavior of pressure, and hence of the Electromotoric force during the loading in the device depicted in Fig. 3.5 , before reaching the plateau. That is well described in Fig. 3.8

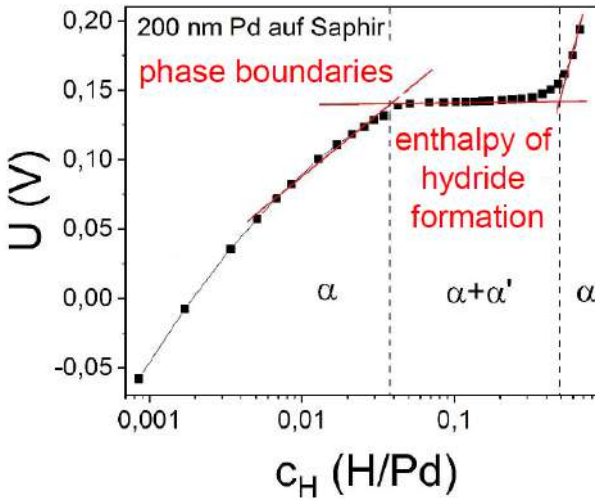

Figure 3.8: Loading curve (EMF vs Hydrogen concentration) of a 200 nm Pd thin film deposited on Zapphire substrate.[32]

3.2.3 Estimation of the diffusion constant

When loading the sample in an electrochemical loading cell, we can always monitor the EMF of our sample, as a function of time.
In Fig. 3.9 we can see an example of such a plot. We can harvest lots of information about how the hydrogen has been diffusing through the thin film layer. In particular, we can roughly estimate the loading time, i.e. the time elapsed between the beginning of the tension peak and the end of the exponential decay. That is the time the hydrogen needed to diffuse through the thin film.
That is very important because a simple model ,linking the loading time with the diffusion constant D_x of an x material, can be elaborated. According to [16], when trying to electrochemically load a Mg thin film, capped with a Pd thin film (this is the frame conditions I have been working on during my staying at KIT), D_{Mg} can be derived from the following equation:[16]

$$t_{load} = \frac{1}{2}\frac{\left(a^{Pd}\right)^2}{D_H^{Pd}} + \frac{1}{2}\frac{\left(a^{Mg}\right)^2}{D_H^{Mg}} + \frac{a^{Pd}}{k}\frac{a^{Mg}}{D_H^{Mg}} \tag{3.24}$$

where in eq. 3.24 $a^{Mg(Pd)}$ is the thickness of the Mg(Pg) layer and k is defined as follows:

$$k = \frac{C_{H,Mg}}{C_{H,Pd}} \tag{3.25}$$

Of course this method only provides a very rough estimation of the order of magnitude of D and it entails a huge error. Of course the higher the reliability on the recorded

hydrogen concentration, the lower will be the error.

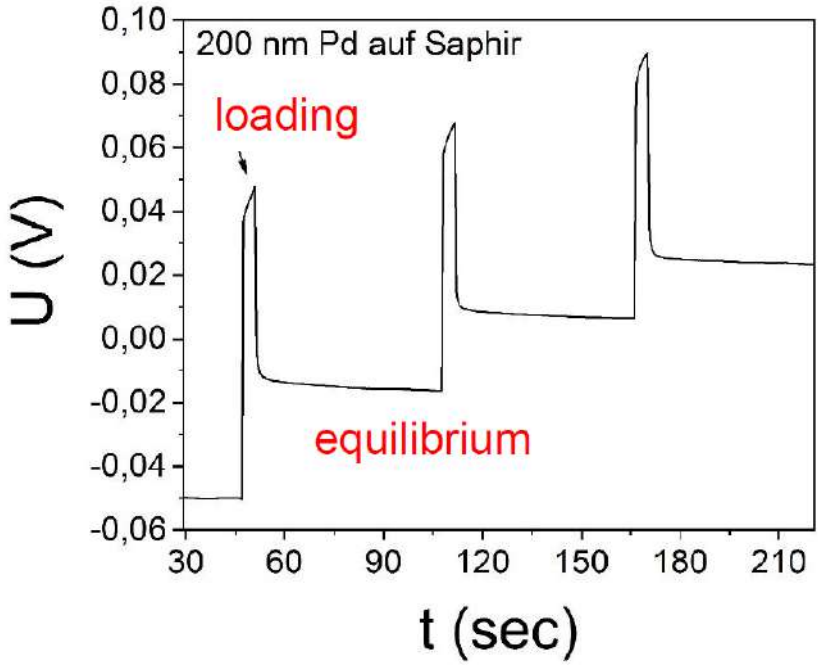

Figure 3.9: Trend of the measured EMF of a 200 nm Pd thin film vs time.[32]

3.3 Relative transmittance

Hydride nucleation and growth in thin films can be monitored in situ through optical ways, e.g. by evaluating the change of the trasmittance measured through a microscope aimed at the thin film.
In fact, for most metals, the transmittance increases with the hydrogen content, as a function of the used wavelenght. That becomes clear through the Lamert's Beer law:

$$c_H = -\frac{1}{\epsilon \cdot d} ln\left(\frac{T}{T_0}\right) \tag{3.26}$$

Where T_0 is the first measured transmittance and ϵ and d are respectively the "exctinction facto", and the thickness of the film.
The term $ln\left(\frac{T}{T_0}\right)$ implies that we are substracting every recorded value of T with the starting value T_0, in order to eliminate possible systematic errors, due to surface contaminations of films or problems with the microscope's lenses. [28] Eq. 3.26 is the solution

for the very easy differential equation describing the behavior of the intensity of beam crossing a slab of thickness d (differential dl), with ϵ defined as an extinction factor:

$$dI = -I\epsilon dl \tag{3.27}$$

A very important result of 3.26 is that the Relative Transmittance depends on the hydrogen concentration, so we could actually evaluate the PCI in terms of this new physical dimension. Nevertheless, when plotted against the hydrogen concentration we have to make a few considerations.
In fact, the Relative Transmittance remains more or less constant while the system remains in the α phase, with hydrogen entering the metal, while it will begin to increase as the system becomes the phase transition towards the hydride phase. So in this case, the shift from α to β phase is not characterized by a plateau but it is severly sloped.
In particular, In a PTI (Pressure, Transmittance Isotherms) the extension of the pressure plateau, indicating the width of the optical change the film undergoes upon hydrogen absorption, is actually directly proportional to the film's thickness through 3.26.
It is then an optical technique in which the light transmitted through a thin film is recorded from time to time while duly increasing the hydrogen concentration. The whole process is called "**Hydrogenography**"[36].[1]

3.3.1 Evaluation of desorption through unloading

The goal of hydrogenography is not only to evaluate the load of a thin film, but also its unload. Once hydride has been completely formed and the film has become transparent, we can go backwards through the loading steps, hence realizing a full unloading cycle, which will have a final result the thin film being without hydrogen, as it was before starting the first load. At this point further cycles of loading and unloading could follow to test the behavior of the film.
Comparison between EMF plateau's values for both loading and unloading cycles can be used to evaluate the phenomenon of hysteresis, taking place when a metal absorbs and then desorbs a certain amount of hydrogen (see 2.5.2)

[1]Hydrogenography is particularly interesting within the frame of electrochemical loading since we can theoretically have a value for the hydrogen concentration. Gas phase loading, which is mostly used, does not provide that.

Chapter 4

Experimental procedures

The first ingredient to perform decent hydrogen loading of thin films is of course producing thin films. For this work thesis two methods have been exploited for thin films manifacturing in cooperation with T. Reisinger et al. and S.Wagner et al. at Kit: film deposition through cathode beam sputtering machine and through a molecular beam evaporator.
In the next section we will explore these two methods.

4.1 Sputtering

Sputter deposition is a widely used technique to deposit thin films on substrates (let them be SiO_2 and glasses). Roughly speaking, this technique requires an ion bombardment of a source material, namely the target. That entails the creation of target's vapour molecules that will eventually condensate on the substrate.
So it is a physical vapor deposition technique.[33] It is highly found in nature, expecially in outer space (e.g. the solar wind impinging a space-body).
A very interesting physical dimension describing sputtering is the sputter field Y, defined as the ratio between the number of sputter ejected atoms and the number of incident projectiles, i.e. the ions impinging the target. Several expression have been derived in order to retrieve a fancy expression for Y. According to [34], the most general model for Y is simply given by:

$$Y = \frac{3}{4\pi^2}\alpha\frac{4M_1M_2}{(M_1+M_2)^2}\frac{E}{U_s} \tag{4.1}$$

where E is the energy of the projectile that is trasferred through momentum transfer to the target, M_1 and M_2 are the masses of the ions and of the target atom and U_s is the surface binding energy.
The explanation to 4.1 is rather intuitive. In fact, the term $\frac{4M_1M_2}{(M_1+M_2)^2}$ entails the transfer of momentum from the ions to the substrate' surface. Hence, momentum's transfer must

be large enough to overcome the surface binding energy term U_s. The larger the mass of the ions plasma, the larger will be the momentum transferred and hence Y.
There is also a probabilistic way to define Y, based on qualitative-probabilistic interpretations. In fact, in this simplified model, the numbers of target' vapour molecules created per incindent ion (R_{pr}), multiplied by the probability that the alleged vapour gas is created close enough to the surface to escape(R_{pp}) and by the probability that such recoil atoms could travel towards through the surface (this last term is $\sim \frac{1}{4}$ in the simplest geometry) and multiplied by the ratio between the projectile energy and the average energy of the recoils ($\frac{E}{E_{avg}}$), Y is given, according to eq. 4.2 by: [33]

$$Y = \frac{E}{E_{avg}} \frac{R_{pr}}{R_{pp}} \frac{1}{4} \tag{4.2}$$

A very important physical dimension characterizing sputtering is the deposition rate $\dot{n} = \frac{dn}{dt}$,i.e. the rate at which the atoms of the target will deposit on the substrate. It will be considerably improved as the anode-cathode intensity current is increased.
Of course before starting any sputtering procedure we need to know in advance the sputter-rate for the specific materials we want to deposit.
There are actually two ways to provide the ion projectiles necessary for the sputtering of the target.

- **Ion gun**: in this way we use an ion source which points at the target and the sputter process goes on as described above. But Ion guns are more widely used for other experimental techniques such as the secondary ion mass spectrometry.[34]

- **Plasma**. Ions can also very commonly stem out of plasma.If the target is the cathode, then positively charged ions are attracted from the "plasma cloud" to the target. The electric field in which the ions are plundged in, bestows momentum to the particles, hence enhancing their probability of sputtering. The plasma's way was of course the one used in Karlsruhe and we are now going to discuss about that more in detail.

4.1.1 Sputtering protocol

We will now describe more in detail the machine I worked with at KIT campus South in the group of S. Wagner at IAM-WK, Chemistry building. A picture of the machine can be seen at Fig. 4.1.
Had the machine stayed still for more than 1 week, the argon flux would have needed to be purged, and that could be performed by duly tampering with the Ar valves. That not being the case, we can start the sputtering process which consists in three main "acts":

- **Source ignition**Source ignition. The anode-cathode difference of potential driving the Ar+ ion sputtering is established. When sputtering a Mg target, the machine

needs to stay running for hours (this process is called **Pre-sputtering** and allows the removal of Mg-oxide that formes on the surface of the Mg slab.)

- **Mounting the substrate**. Once the source is running , we can place the substrates within the main chamber of sputtering, playing with the different vacuum pumps generating the HV conditions. The substrates(glass-like materials and Sapphire mainly), need to stay as clamped as possible to the sample holder (see Fig. (a picture of the sample holder)).

- **Sputtering deposition**: Knowing the sputter rate for each element (the machine allows sputter deposition of four elements: Pd, Mg, Ti, Nb), we need now to wait the time required to deposit a layer of the needed width, (e.g. 30 nm Mg $\sim$ 20 min.).

Once these stages are completed, we can retrieve the thin films if they need to be immediately loaded, or let them stay in the H-V pre-chamber in order not to be oxidated.

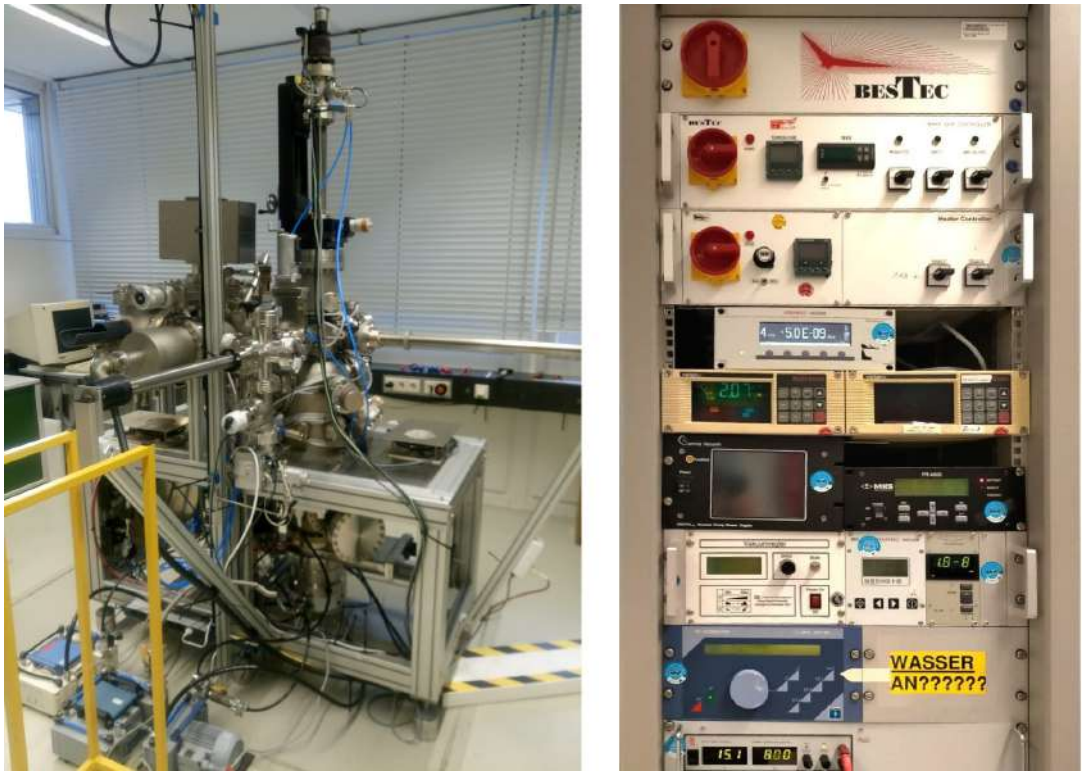

Figure 4.1: Picture of the sputter machine (left) and its electronic controls at KIT, Campus South, Chemistry building

.

4.2 Molecular Beam Epitaxy

Cuncurrently to sputtered-thin films, we attempted to load samples prepared in an other way, i.e. through Molecular Beam Epitaxy (MBE), in the group of T. Reisinger in INT. MBE is a material growth technique for thin film deposition of single crystals. Though widely used in the industry of semiconductors manifacturing, it can of course be used as well to create thin films.
It exploits physical vapor deposition, allowing a huge control over the purity of materials, the alloying composition and the interface formation.
This quality directly comes from the extremely Ultra High Vacuum environment in which the epitaxial growth takes place ($< 10^{-12}$Tor).
A brief sketch of the working principle is portraid in Fig. 4.2. The substrate is heated

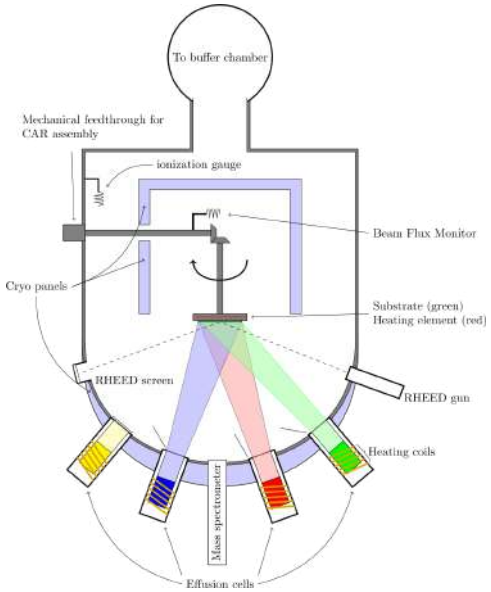

Figure 4.2: *Sketch of a Molecular Beam Epitaxy Evaporator chamber. The heating coils sorrounding the effucion guns allow the sublimation of the elements within, while a shutter in front of them can stop at any moment the beam. Lateral RHEED device allow for a control of the deposition up to the atomic layer.*

[38]

up to many hundreds of degrees. Then we bring to sublimation the materials in the effusion cells (e.g. Mg or Pd or Ti in our study). The beam of particles starting from there will eventually condense on the substrate, since because of the UHV conditions in the chamber, the mean free path of the molecules is rather high.
Once the molecules have landed on the surface of the substrate, the growing of the film begins, one atomic layer at the time. The effucion cells are endowed with shutter,

enabling a fast closure of the beam if needed.
The forementioned level of precision directly comes from the UHV conditions, since no dirt particles or gas molecules can tamper with the crystal growth[37]. While the system is running, we can monitor the depositions through RHEED (Reflection High-Energy Electron Diffraction) which is represented in Fig. 4.2. It is made of an electron gun, which sends electrons onto the surface of the substrate and evaluates the diffraction figure in order to precisely estimate the width of the growing thin films by means of the measurable diffraction angle θ as can be seen in Fig. 4.3

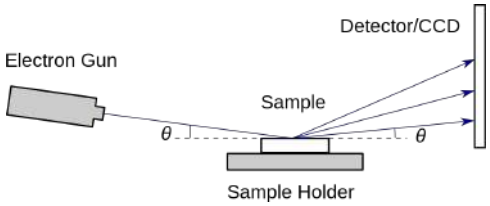

Figure 4.3: Brief Sketch of how a RHEED system is supposed to work

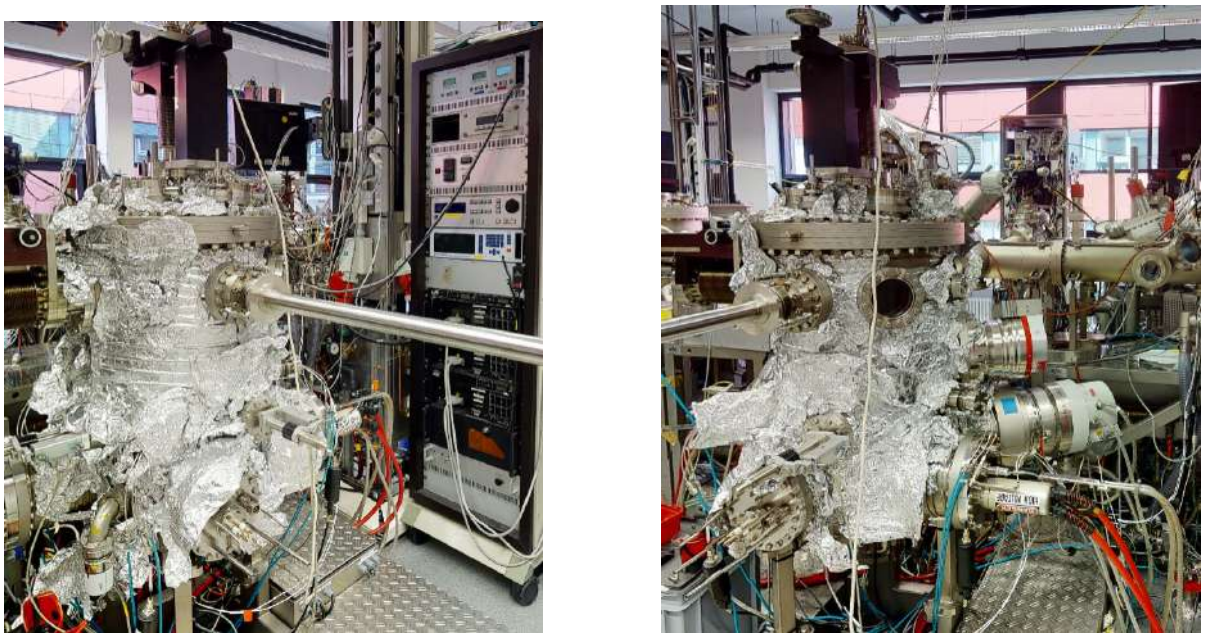

Figure 4.4: Front and lateral view of the EMB evaporator at KIT, Campus North, T. Reisinger group, INT

4.3 Hydrogen loading setup

Let's now describe the Hydrogen loading measurements; how they were performed and what tools were exploited.
The sample, let it be bulk Pd or a thin film containing Mg, was duly inserted in a loading cell like that in Fig. 4.5

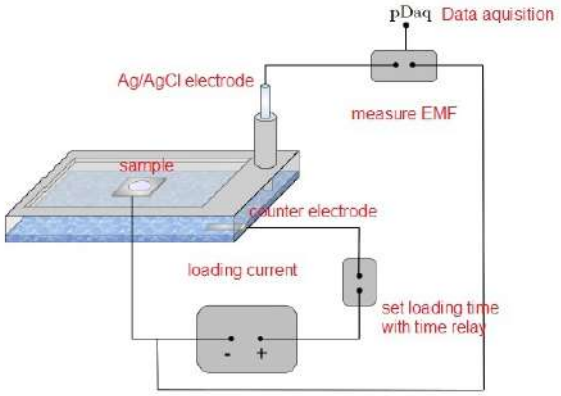

Figure 4.5: *Sketch of the loading cell using for hydride formation. Both the reference-electrode Ag-Cl and the electrolyte solution were eventually changed during the experiments.[40]*

So our sample is in contact with the electrolyte solution that will provide the Hydrogen for its loading. The sample is connected through a copper wire both to a current generator, and to a Digital to analog converter, in order for us to record the value of tension.
The Pt counter electrode, plundged in the electrolyte solution, is connected in turn to the current generator through a time relais, which allows to set the exact duration of the pulse (up to a precision of ms).
A picture of the electronic experimental setup I worked with can be seen in Fig. 4.6. It was very important to check every time for the stability of the contacts among the cables, otherwise the instruments would have reported false data.

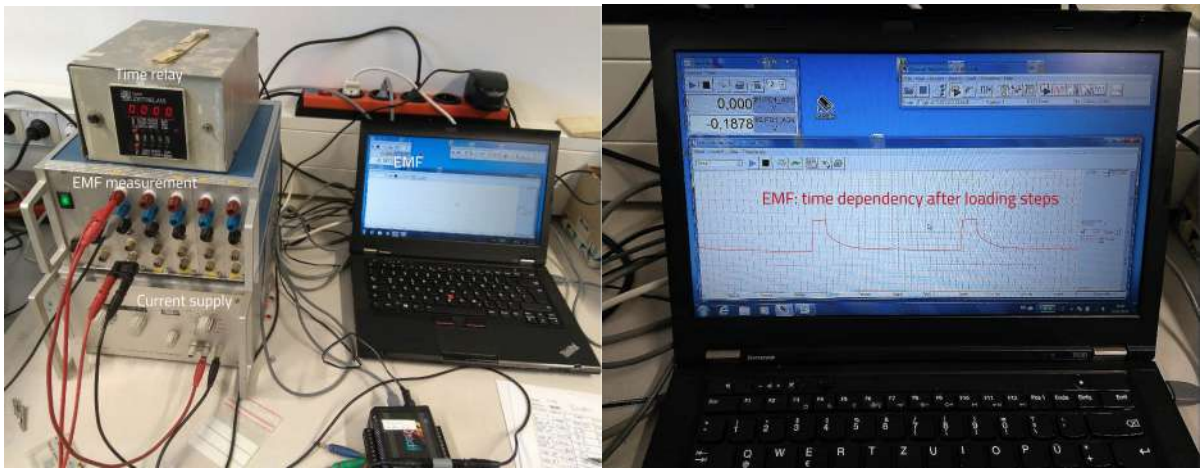

Figure 4.6: *Picture of the Data acquisition (right) program in which we can analyze the EMF dependency on time. on the left we can have look at the current generator with time relais on top and the devices able to perform the EMF measurements (left.)*

4.3.1 Evaluating hydrogenography

The true core of my work thesis was to evaluate by means of an optical microscope the transformation of the metal thin films into an hydride. At first we needed to place the loading cell under the focal plane of the microscope, trying to center the objective of the microscope on the thin film. The microscope was endowed with an RGB camera that was connected to a computer, in order for the images to be displayed and eventually saved and analysed. Analyzes were carried out through the program ImageJ, which made possible an evaluation of the average intensity of the picture we were considering. The idea behind is that the "brightness" of the picture should undergo small changes as we remain far from the plateau. But as we enter the plateau's region in terms of Hydrogen concentration, we should be able to see a considerable increase in the brightness of the picture we record, due to formation of the high concentrated hydride phase. In fact, the material is turning from metallic (and hence totally reflective) into a transparent hydride (that explains the increased brightness).
As anticipated, there is a strong bond between the measured transmittance and the hydrogen concentration, i.e. eq. 3.26.
Two pictures of both microscope and the camera's program on the attached computer can be seen in Fig. 4.7

Figure 4.7: *Picture of the loading cell mounted on the microscope in order to evaluate step by step the in-situ hydrogenation(right) and the microscope screened from an insulating capote to prevent images to be affected by the environment light(left)[40].*

4.3.2 The role of electrolyte solution

During my staying in Karlsruhe, two different kinds of electrolyte were used for the loading cell. At first we tried to load films with a mixture of Phosphoric acid (H_3PO_4) and glycerine ($C_3H_8O_3$). This configuration revealed to be a failure for Mg's film loading because this electrolyte was too aggressive and "attacked" laterally,in terms of corrosion, the Mg layer, hence entailing the self-loading of the film and the subsequential detachment of the film itself.
For that reason it was chosen to use the electrolyte KOH which prooved to be far less aggressive than the previous one (the film didn't self load). Nevertheless it was a 5M KOH solution, which means a PH larger than 14. For that reason it was necessary to take several precautions and to work in a safe environment. When remaining too long (more than 1 day) in the loading cell, KOH began to damage the screws holding the sample and started interacting with the copper wire of the counter electrode, making it no more conductive. These effects can be seen in Fig. 4.8

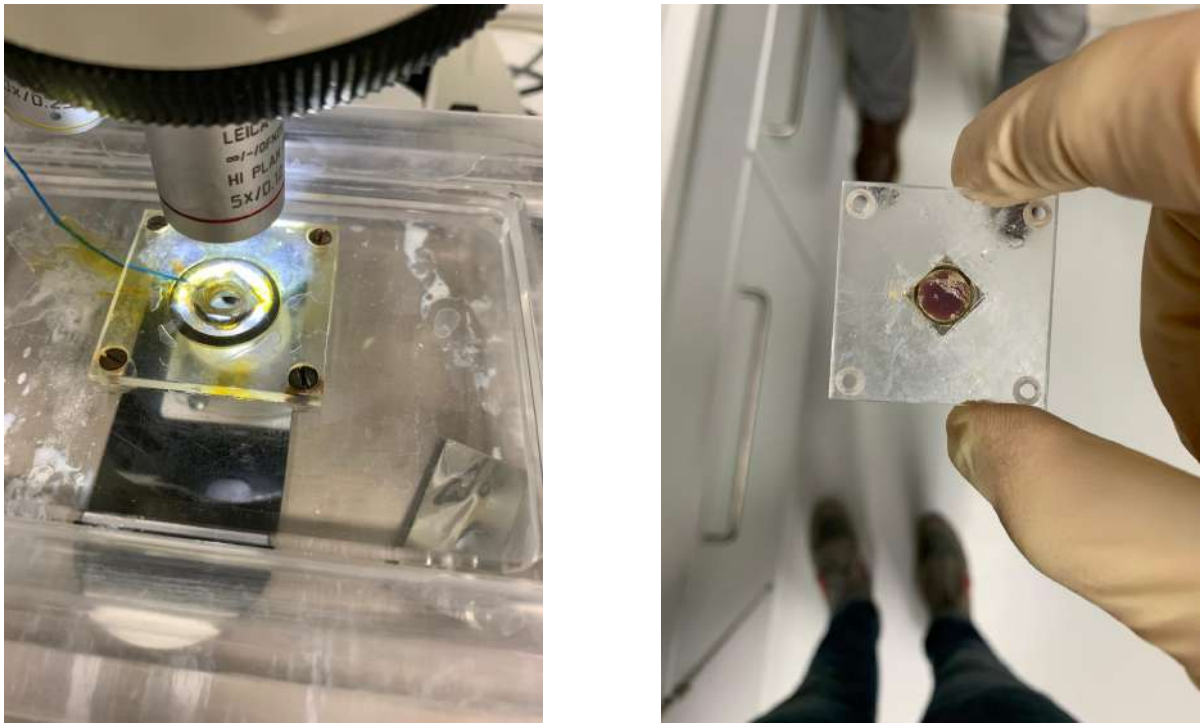

Figure 4.8: *Picture of the loading cell, left still for 3 days under the action of KOH inside. The yellow flow is rust coming from the screws(left). At the picture on the right we can see a layer of rust deposited over the film.*

The configuration with KOH as electrolyte will be analized in detail in the next chapter.

Chapter 5

Data Analysis

5.1 Calibration of bulk Pd

As first thing, we began the so called calibration of Pd, in order to be acquainted with the experimental apparatus. Its goal is to determine the electrode reference potential from the known plateau of Pd hydride. We mounted a bulk palladium squared block(150 μm of thickness and 56 mm^2 of area) in the loading cell reported in 4.5 and started loading it with hydrogen with the usual mixture of glycerine and phosphoric acid as electrolyte solution and an Ag/AgCl reference electrode (+0.176 V of reference tension). The loading curve is reported in Fig. 5.1.
We couldn't record many points because each step took a great amount of time. In fact, the thickness of the Pd block hindered and slowed the diffusion of Hydrogen within, hence entailing enormous loading time, see 3.9. The whole process took indeed more than 5 days to be completed, from the first concentration step of 0.00001 H/Pd that took 20 seconds up to the final concentration step of 0.1 H/Pd that took 3 days to be performed.

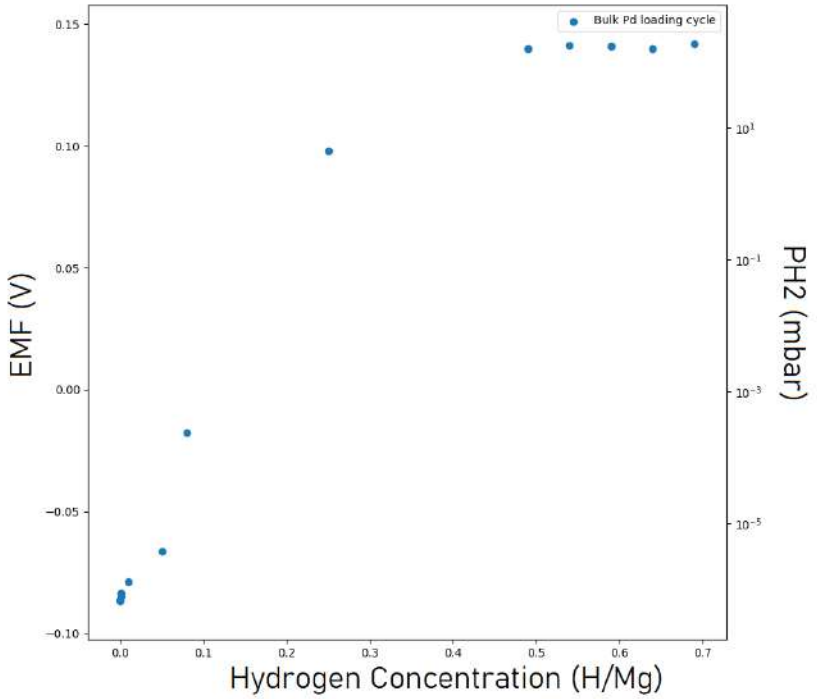

Figure 5.1: *Loading curve of bulk Pd (150 μm of thickness). Plateau EMF's value $\sim$ 0.14 V*

The idea behind the calibration process is rather simple. Basically we know that the plateau for Pd-H occurs at approximately 18mbar. In Fig. 5.1 a value of 0.14 V is reported as EMF plateau's value. That means that through 3.13 we can actually retrieve the value of the reference electrode standard potential (the Ag/AgCl electrode) that will be used to get the values of pressure when loading thin films. By means of 3.13 we get a value of $\sim$ 0.176 V.
Furthermore,when we will load a Mg thin film capped with Pd to prevent oxidation, we will obtain ideally a Pd's plateau, beside the Mg's one that allows us confrontations with the bulk Pd.

5.2 Loading of Mg thin films.

Once concluded the part concerning the calibration of the bulk material, we sputtered two thin films using sapphire Al_2O_3 as a substrate. The films were arranged in this way (starting from the substrate): 10nm Ti layer, 30 nm Mg layer, 10 nm Ti layer. The whole system was then capped with a 30 nm Pd layer to hinder oxydation. As stated before, the two Titanium layers both prevent the Mg alloying with Pd and improve the diffusion of hydrogen within Mg. Furthermore, they set the boundary conditions for the clamped Mg film.
We went on loading the two samples, but as soon as we started the measurement we realized that the samples were already loaded, because the electrolyte had "attacked" Mg layer laterally, hence self-loading without control. Once looking at the optic microscope we could actually see buckling forming and eventually we witnessed the full detachment of the film following a buckling growth that got huger and huger as time elapsed.
Buckling evolution can be seen in deatail in Fig.5.2.

In order to avoid the detachment of the film, one needs to improve the adhesion of

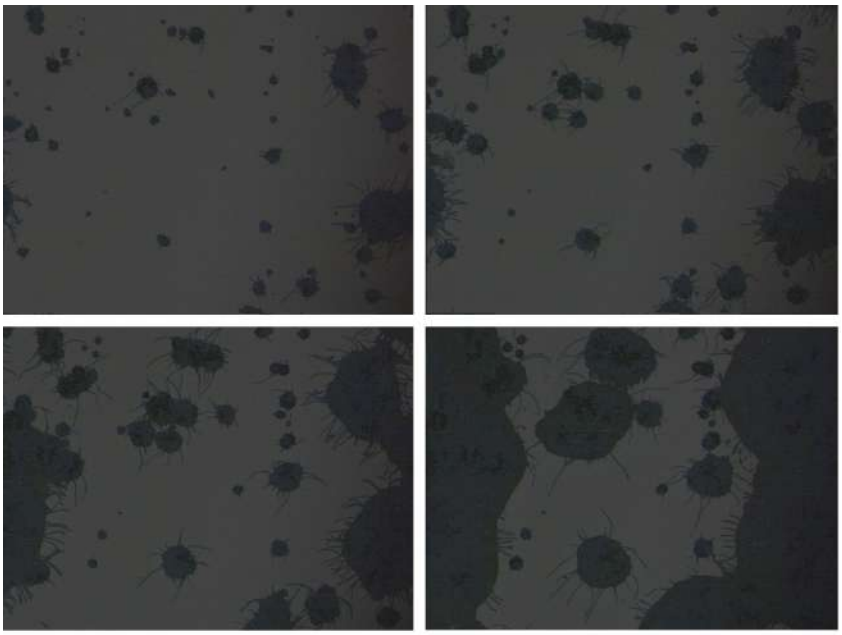

Figure 5.2: Time evolution of buckling in the 10nm Ti 30 nm Mg 10 nm Ti 30 nm Pd supttered thin films prepared at KIT campus South. In the last picture we can easily state that the film is completely detached.

the film to the substrate. That can be done by adding a very thin layer ($\sim$ 1nm) of Nb immediately after the substrate. Niobium's properties enhance indeed the adhesion of the film to the substrate [28]. Unfortunately, we obtained the same results, as showh in

Fig. 5.3

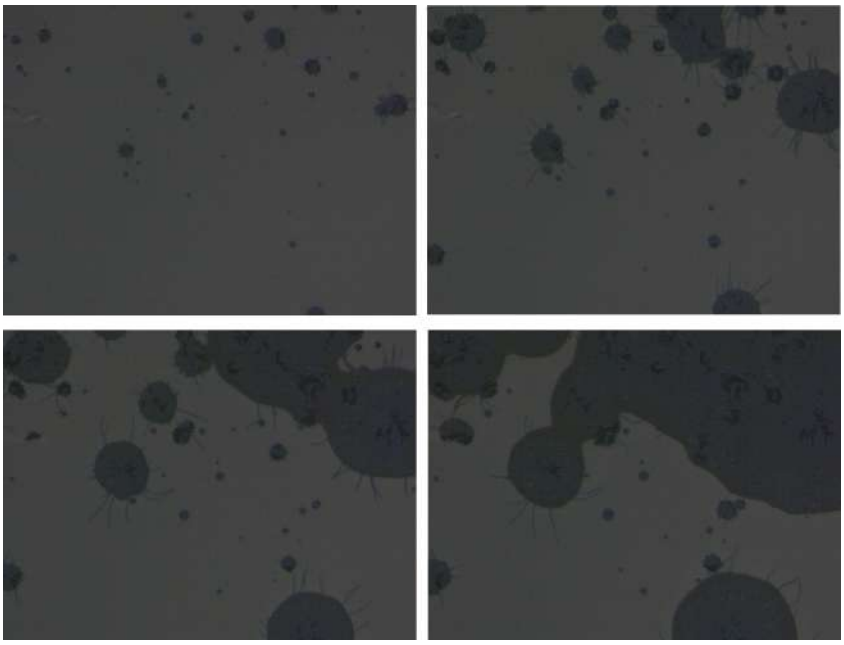

Figure 5.3: *Time evolution of buckling in a 1nm Nb 10 nm Ti ,30 nm Mg, 10 nm Ti, 30 nm Pd thin film in contact with phosphoric acid eletrolyte.*

Nevertheless, though producing no results, Fig. 5.2 and Fig. 5.3 confirms the results of [28]. In fact, in the poorly adhesive thin film, a large amount of buckling site can be seen, while in the high-adhesive one, there are less buckling island. Nevertheless, since both films have eventually ended up detaching, the problem was clearly not the adhesion to the substrate but the "aggressiveness" of the electrolyte solution and its corrosion on lateral Mg film.
So the biggest problem when dealing with loading of a Mg thin films with a phosphoric acid-glycerine solution is the uncontrolled self-loading of the film itself, which is not prevented by the Pd-cap layer. That entails of course that no further analysis can be carried out with this kind of electrolyte.

5.3 Loading of Molecular Beam Epitaxy deposited Thin film

In order for the causes of the self-loading to be led only to the electrolyte solutions, we contacted KIT Campus North, where a EBM evaporator was available for film deposition. In cooperation with M. Sc. Gleb Iankevich 4 thin films (engineered like the

sputtered ones) were produced. The samples were kept in a nitrogen-atmosphere to prevent oxydation.
Without connecting the electronic and monitoring the EMF values of loading, we placed the sample under the microscope and covered with a droplet of two different electrolyte solutions. The $C_3H_8O_3 - H_3PO_4$ solution and the KOH one. The idea was to minotor the brightness of the pictures recorded every minute in order to establish wether a self-loading process and subsequential film detachment was being carryng on or not.
The results of this very simple experiment are shown in Fig. 5.4.

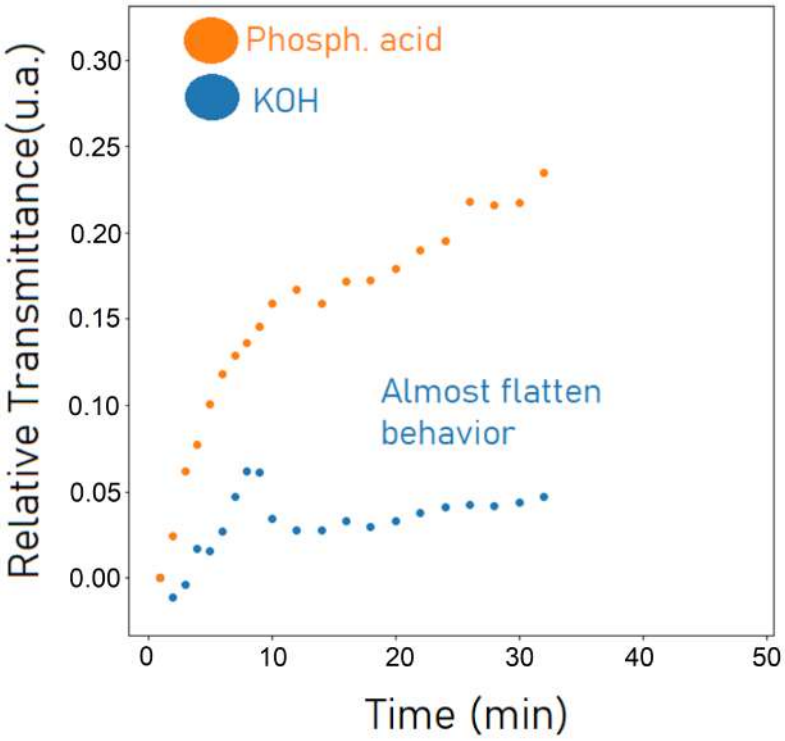

Figure 5.4: *Relative transmittance of the 10 nm Ti, 30 nm Mg, 10 nm Ti, 30 nm Pd thin film, deposited with MBE method when being in contact with standard glycerine-phosphoric acid electrolyte solution (orange) and a KOH solution (blue). We can appreciate a slight, yet not significative increase of the relative transmittance for the KOH solution, while a clear self-loading for the glycerine-Phosphoric acid solution.*

It is then clear from 5.4 that the film is self-loading, under the action of the glicerine-phosphoric acid solution. In particular, we can directly see, through the steepest change in relative transmittance, the moment in which Mg-H and Pd-H are being formed.
Because of these results, we could now move on with the loading experiments by making

use of KOH as electrolyte solution, since it appeared to be stable, or at least, the less unstable, since the behavior of 5.4 is not completely "flat". As forementioned in sec. 4.3.2, that entailed moving up the experimental apparatus into a safer enviroment because of the dangerousness of KOH.

5.4 Loading with KOH

As we have begun loading with KOH thin films from Campus North, we struggled to understand which configuration the sample and the counter-electrode should have been set on. Two loading ways are possible, both sinthetically sketched in Fig. 5.5 with the relative reactions going on.
The "Anodic" configuration, in which the sample is our anode seemed the most logical

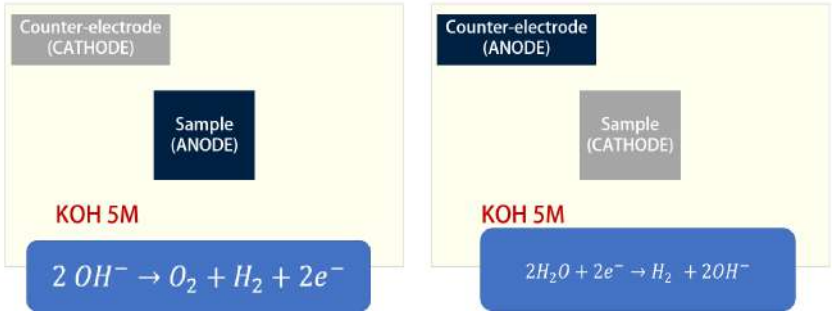

Figure 5.5: Brief sketch of the two possible configuration of loading: the anodic (left) and the cathodic(right), depending on the point of view of the sample.

one. In fact, the main characters of the reaction are the OH^- ions which the high ionization rate of KOH makes hugely available.
Unfortunately as depicted in Fig. 5.7, when trying to load the MBE deposited thin films prepared at Campus North, we witnessed no loading of the films. They did not hydride when the system was set in the anodic configuration, hence making the hydrogenation process useless.
Since the anodic configuration proved to be uneffective, we thought to test the cathodic configuration. This configuration would not be the intuitive configuration to be chosen, since the main role is played by water. KOH would just quench the possibility for water to oxidize the Mg layer, hence hindering the loading of the film.

5.4.1 Calibration with KOH

Once individuated the correct configuration, we went on with the calibration, as mentioned in sec. 5.1, in order to determine the value of the new HgO reference electrode.

The previous Ag / AgCl reference electrode didn't suit for KOH loading since it would have been soon spoiled by it.
Fig. 5.6 shows the calibration curve. A value of approximately 0.46V was estimated for the 18mbar plateau pressure of Pd, which leads to a value of 0.605V for Hg reference electrode, according to 3.13.

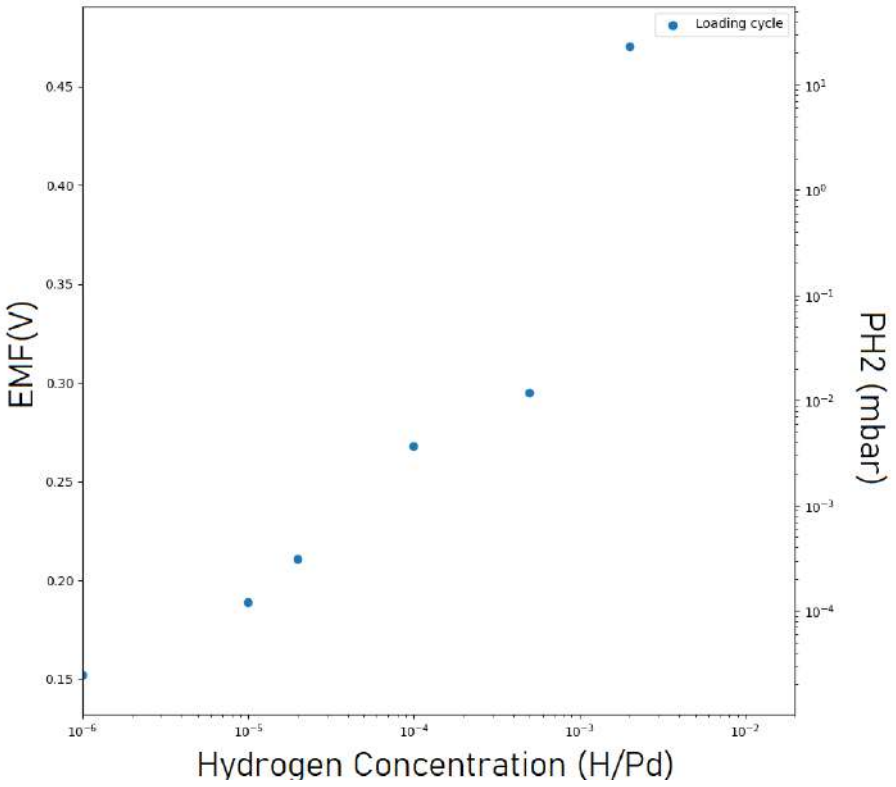

Figure 5.6: Calibration curve for a 150 μm thick bulk Pd. There are not so many points in it, because of the huge loading time required. Anyway a value of approximately 0.46V could be estimated for Bulk Pd EMF plateau value, to confronted with the reference 18mbar in order to get the value of the Hg reference electrode.

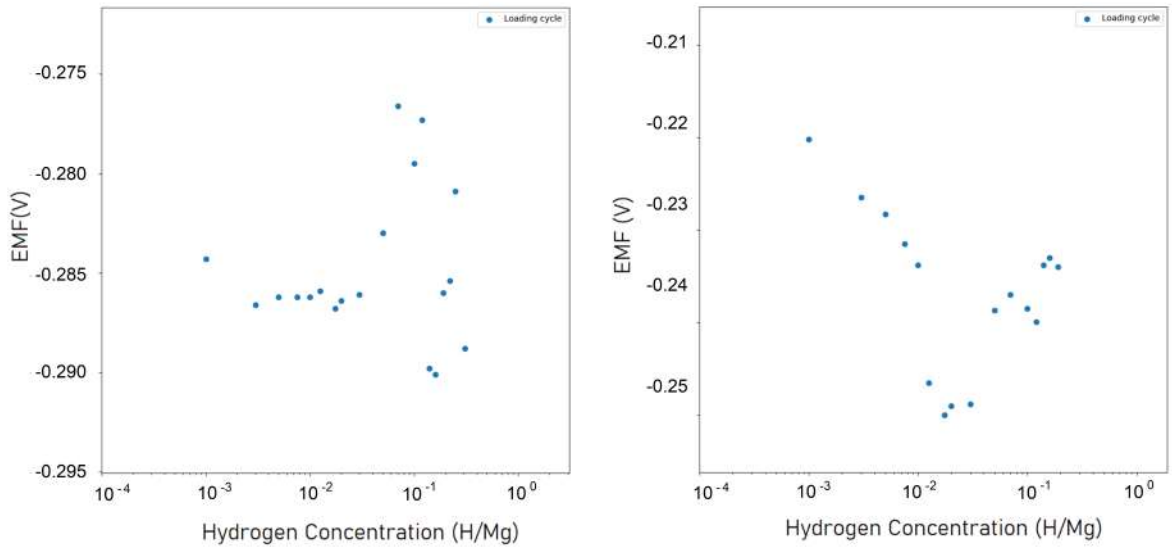

Figure 5.7: EMF loading curves for two aforementioned samples prepared with MBE deposition in the aforementioned anodic configuration (in which the sample acts as anode). The EMF curve, hence the chemical potential does not change, which means the samples are not loading.

The biggest problem we had to face with the calibration of a Pd thin film in a KOH environment was the highly increased loading time. In fact, 3 weeks were required to reach the plateau value of Palladium. That happened because a too large waiting time was required for equilibrium to be reached at every loading step, not even comparable with the calibration of a bulk Pd with phosph acid-glycerine electrolyte. Since the loading time for each recorded step were the same, a deeper analysis was required. To do that we analyzed the recorded EMF's value each second all over the calibration period, i.e. 19 days. The EMF trend as a funciton of time is depicted in Fig. 5.8.
In both graphs, many anomalies from what should be the ideal exponential decay after the loading step, depicted in Fig.3.9, can be seen.The linear-like decay we witness both in the initial steps and in the final ones, depends on the hydrogen concentration, as its width enlargres with that.
This unexpected behavior can be tracked down to many phenomena. At first it was thought to an activation energy required for water splitting, described by the reaction taking place in the "cathodic" configuration, in Fig. 5.5.
Another hypothesis, much more consistent with the available data, was that the hydrogen ecountered some sort of surface barieer, due to KOH environment, when trying to enter the sample. So basically the weird and unexpected loading time profile would be a consequence of surface effects going on at the surface of bulk palladium. That would explain the linear behavior before equilibrium was reached for each point recorded in

5.6. So the calibration took a long time to be performed but it actually foreshadowed deviations from the expected behavior, that we could also encounter while loading thin films.

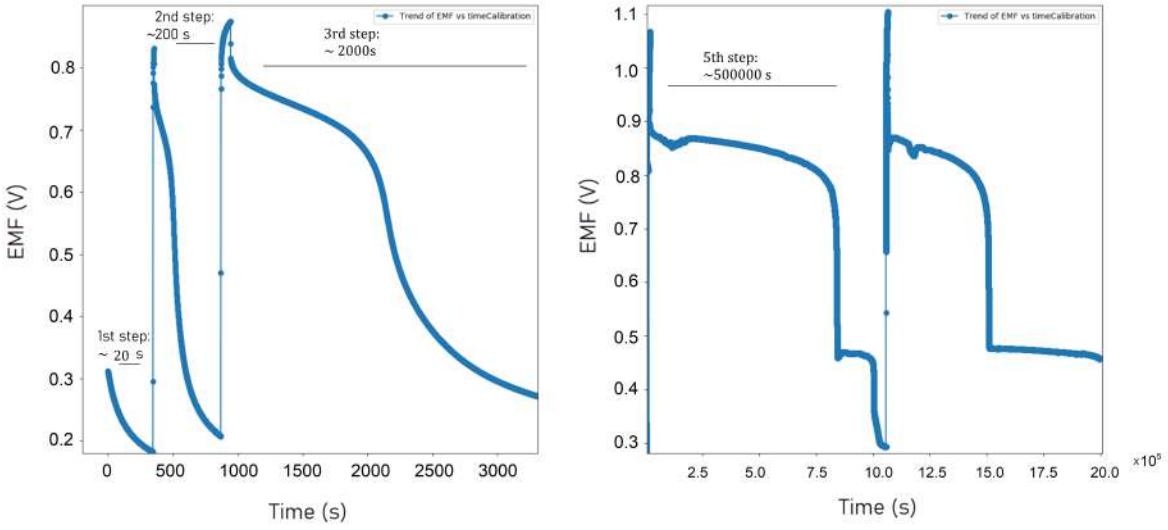

Figure 5.8: EMF recorded value every second during the 19 days of loading time for calibration of Bulk Palladium. The graph was split into two subgraphs, otherwise it would have not been possible to appreciate the deviations from the ideal behavior we are witnessing at every loading step. On the left we have the first 4 recorded points, while on the right graph we have the last two recorded points. The linear "plateau", before reaching equilibrium increases its extension as we increase the hydrogen concentration step. Furthermore in the right graph, we can see H-loss for the first recorded loading step, since the plateau EMF of 0.46 V was indeed reached before Hydrogen started diffusing back. So a further loading step was necessary to verify wether we were in the plateau region or not. The waiting time due to surface effects for each loading step are reported in the graph. We start from 20 seconds for the first step to reach a waiting time of almost 6 days (500000 s) for the final steps.

5.5 Loading of thin films with KOH

Since now more informations about the loading system were gathered, it was possible to start loading thin films. The two remaining films coming from Campus North MBE evaporator were no longer usable, since they were oxidated, as their nitrogen atmpshpere was long expired.
So two test films were sputtered, 30 nm Mg deposited on Sapphire and capped with 30 nm Pd, just to see if this time the loading process would have happened.
Now, from 3.9, another parameter we could act on during our experiments is the current intensity I. All over the previous experiments I = 50 μA[1], since higher currents were supposed to spoil and eventually to prompt buckling in the film, ending eventually in its detachment from the substrate.
Unfortunately, the attempt to load at 50μA didn't resolve in film loading,as can be seen in Fig. 5.9.

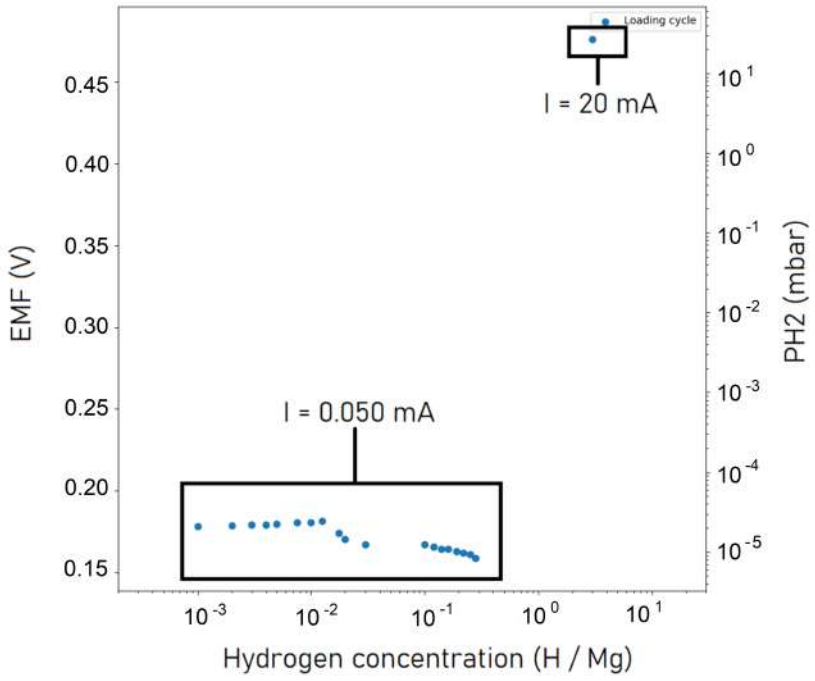

Figure 5.9: Loading curve (EMF vs concentration) of a 30 nm Mg thin film capped with a 30 nm Pd layer deposited on Sapphire substrate. No variation of the chemical potential can be observed until we se the current to its highest possible value

[1]This value corresponds to calibration experiments in Glycerin + Phosphoric acid for Pd films, in which it was showh that at such a current intensity, all hydrogen can be absorbed by the film. That entails a better concentration determination.

Hence, the idea to increase the current intensity, which is indeed the driving force of hydrogen incorporation into the film. Of course, the loading time would have drastically reduced, and the risk of breaking the film would have dramatically increased. Furthermore, with such a huge current intensity we could deal with the problem of highly probable hydrogen losses, which would yield unreliable and imprecise values for the recorded H-concentration in the film.

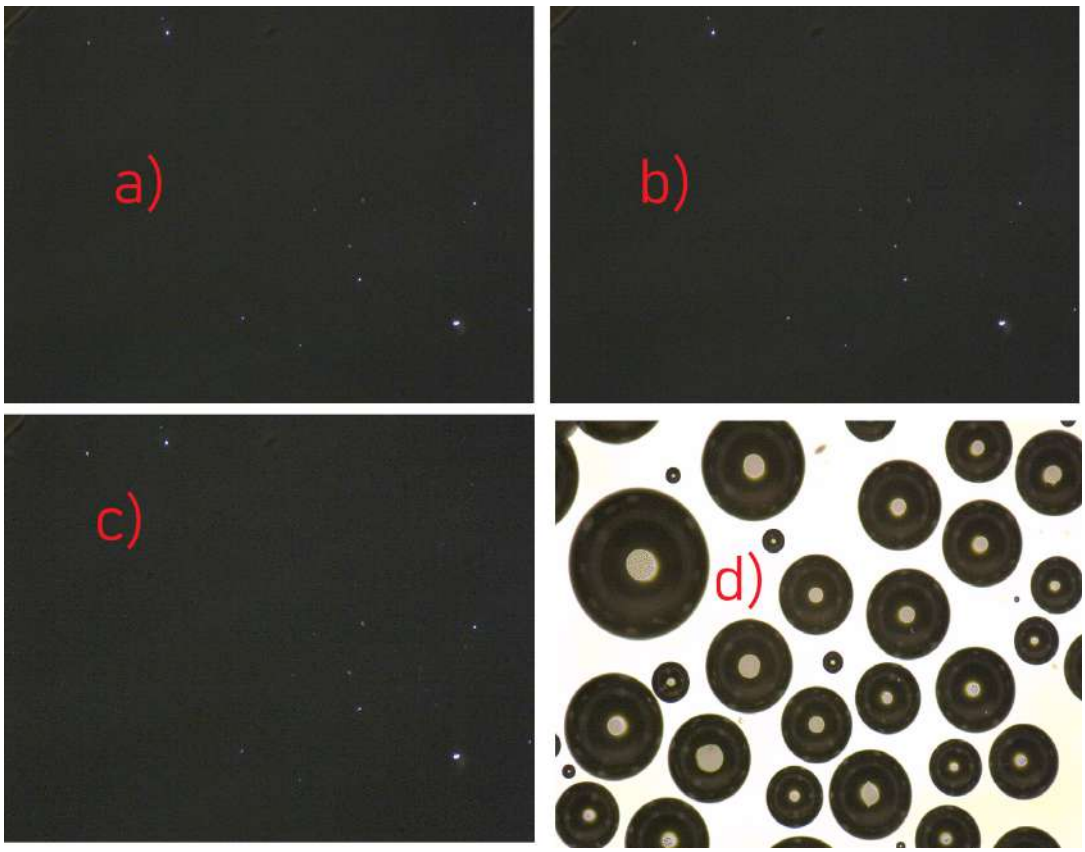

Figure 5.10: Sequence of loading of a 30 nm Mg layer capped with a 30 nm Pd layer deposited on Sapphire substrate. As long as the current remains at 50μA (a,b,c), the film doesn't load. Once the current is pushed to its instrumental limit value of 20 mA the sample does load, with an excess of hydrogen depositing on the surface on the newly-formed hydride as bubbles (d). In particular, in (d), the white background is actually the thin film being turned into a completely transparent state.

Unexpectedly, once performed a unique loading step of 10 seconds at the maximum value of current the current generator could provide, i.e. 20 mA, the film didn't break and became completely a hydride, as the recorded EMF reached the plateau's value for PD,

as observed in the calibration with KOH. That can be clearly be seen in Fig. 5.9. So, both Mg-hydride and Pd-hydride were formed. Because of the formation of Mg-hydride the film became completely transparent as clear in Fig. 5.10d, in which the white background represents the new transparent state the film turned into upon hydride formation. Even though the film was actually loaded, having neatly become transparent, lots of hydrogen bubbles were formed at its surface. That happened because such a high current pulse generated an excess of hydrogen which can result in huge H-loss, as mentioned above.
So the idea was to tamper with the loading time and the current intensity in order to get a clear and more gradual loading curve.

5.5.1 High-current Mg thin film loading in KOH

To that purpose, two new thin films were sputtered, like the previous ones, so 30 nm Mg layer capped with a 30 nm Pd layer, deposited on Sapphire substrate. This time a 2 nm Nb layer was inserted before Mg, in order to improve the adhesion to the substrate. In fact, due to the increased current intensity, the film should have faced unconventional stresses, that could resolve in the film detachment from the substrate.
This time a loading trends could have been harvested, though the nicest results occured for the first film loaded, since the second one had probably already begun to suffer oxydation. We start presenting the results of the second film.
Due to the alleged oxydation (the sample remained at open air for a day and a half and even the protecting Pd couldn't prevent it.), it was very difficult to play with the current to obtain a slow and gradual hydrogenation. Nevertheless the sample did load , as we can see from the pictures sequence in 5.11, but no interesting informations could have been harvested from the Pressure-Composition-Isotherm (Fig. 5.13) and from the analysis of the behavior of the relative transmittance as a function of the H composition (Fig. 5.13).
In particular, no unloading process (3.3.1) was possible, since the sample fully unloaded without intermediate stages.

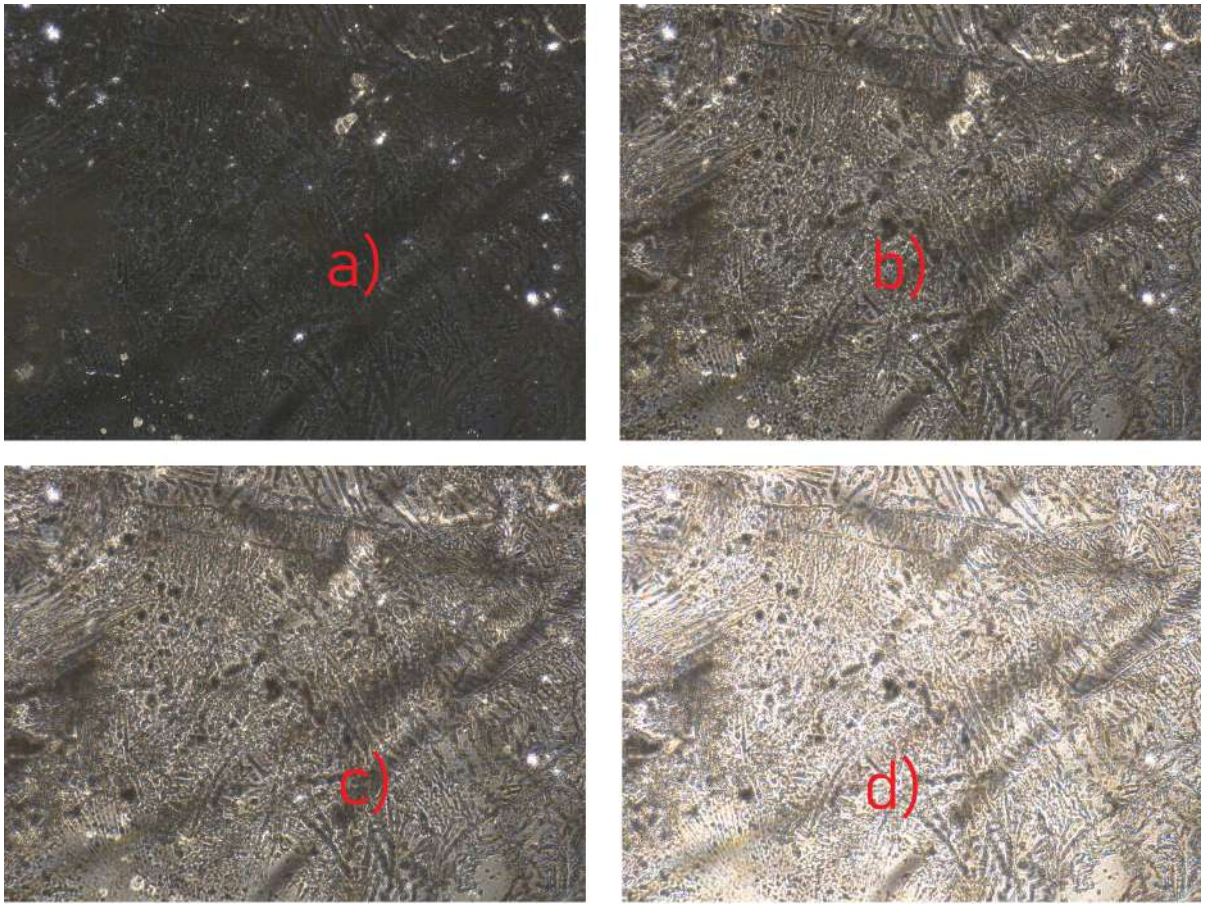

Figure 5.11: Microscope-recorded loading sequence for the second film.As hydride is being formed, slight hydrogen bubbles appear in (b), (c) and (d) respectively, but they did not damage the film. The star-like white points in (a) are scretches of the film that can be seen through the substrate. They become less evident as the film itself increases its brightness upon hydride formation. Eventually in (d) the thin film is fully hydrided.

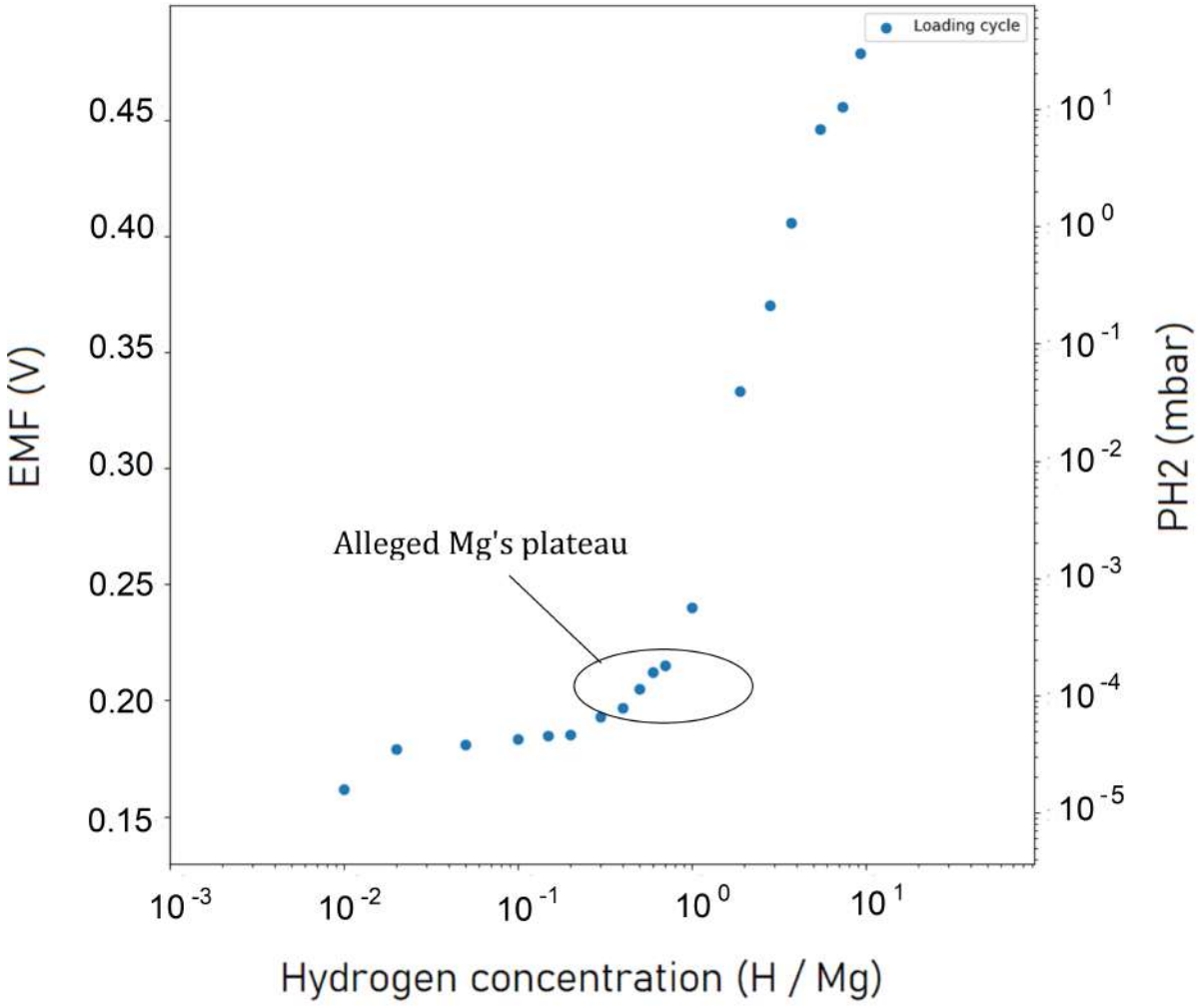

Figure 5.12: PCI of the second film. A small a highly tilted could be indiduated plateau, for Mg at the range of EMF [0.19V,0.22V], though in order to establish its existence, we need to check the Transmittance's graph. That can be compared with the values recorded for the PCI of the first film.

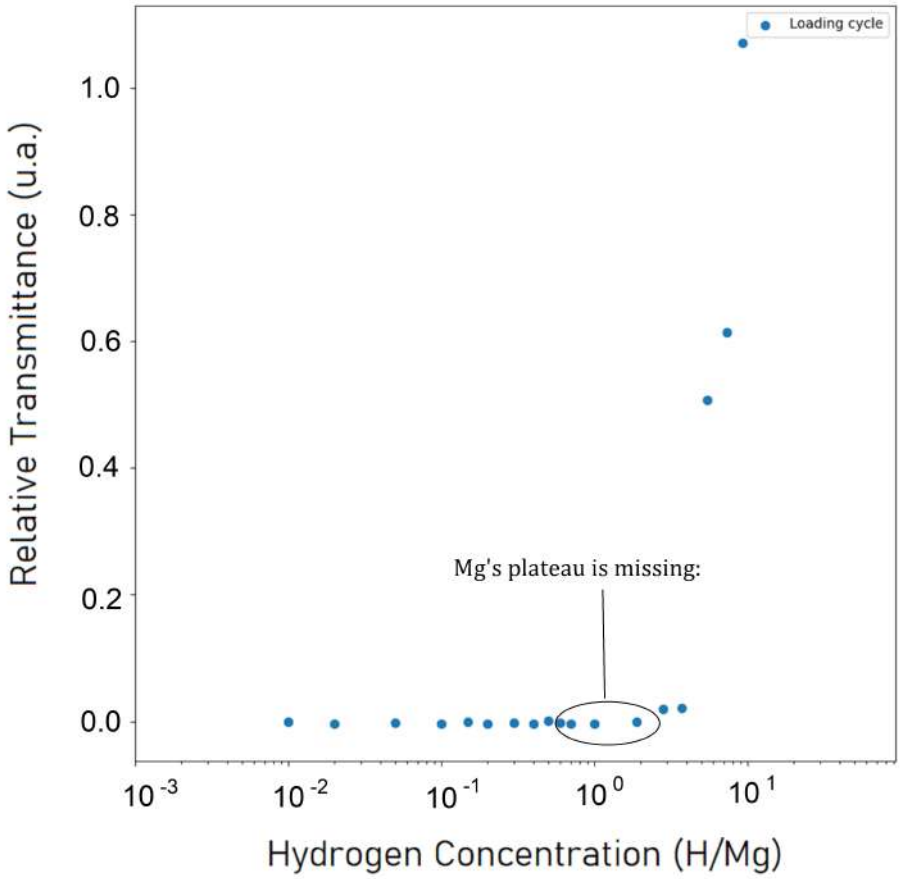

Figure 5.13: Relative Transmittance of the second film. The film alleged oxydation doesn't allow a gradual loading of the film, hence producing a rough and steep increase of the brightness. That doesn't allow a quantitative analysis of the second film. No steep increase in the film's brightness at the value of concentration of corresponding to the alleged Mg's plateau spotted in Fig. 5.12 can be witnessed. That entails that in 5.12no Mg's plateau was actually detected.

Things went far better with the first of the two 30 nm Mg-30 nm Pd sputtered on Sapphire-samples. The loading process unfolded decently: the film's brightness gradually increased as can be seen in Fig. 5.14. This time an unloading process (see 3.3.1) was partially possible. The Pressure-Composition-Isotherm and the behavior of the Relative Transmittance as a function of the H composition are displayed in Fig. 5.15 and 5.16 for both loading and unloading cycles.
The data doesn't allow to quantify the phenomenon of hysteresis, forementioned in chapter 2, sec. 2.6. In fact, we cannot establish which element (Mg or Pd)'s plateau is affected by hysteresis and at which extent.That's because no trend for the unloading cycle could have been harvested, since the film immediately filled with hydrogen bubble, see Fig. 5.18,, hence making hydrogenography impossible be performed.
Nevertheless Hysteresis could somehow be qualitatively appreciated in the PTI 5.16.

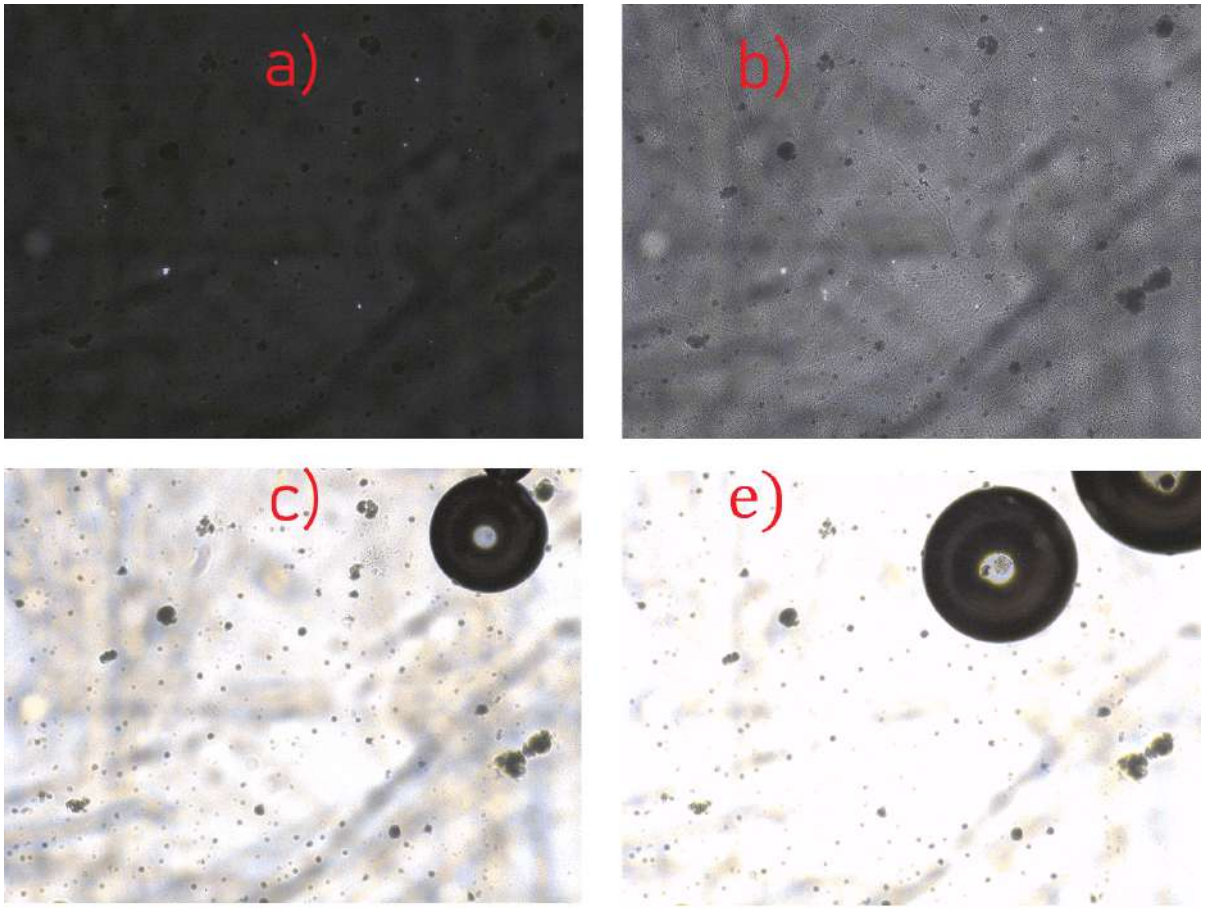

Figure 5.14: Microscope-recorded loading sequence for the first film. The film appears to be loading decently as its brightness increases from (a) to (d). Large H_2 bubbles formed in (c) and (d) do not seem to affect the hydrogenation or the film's quality. In (d) the sample is completely in the hydride state.

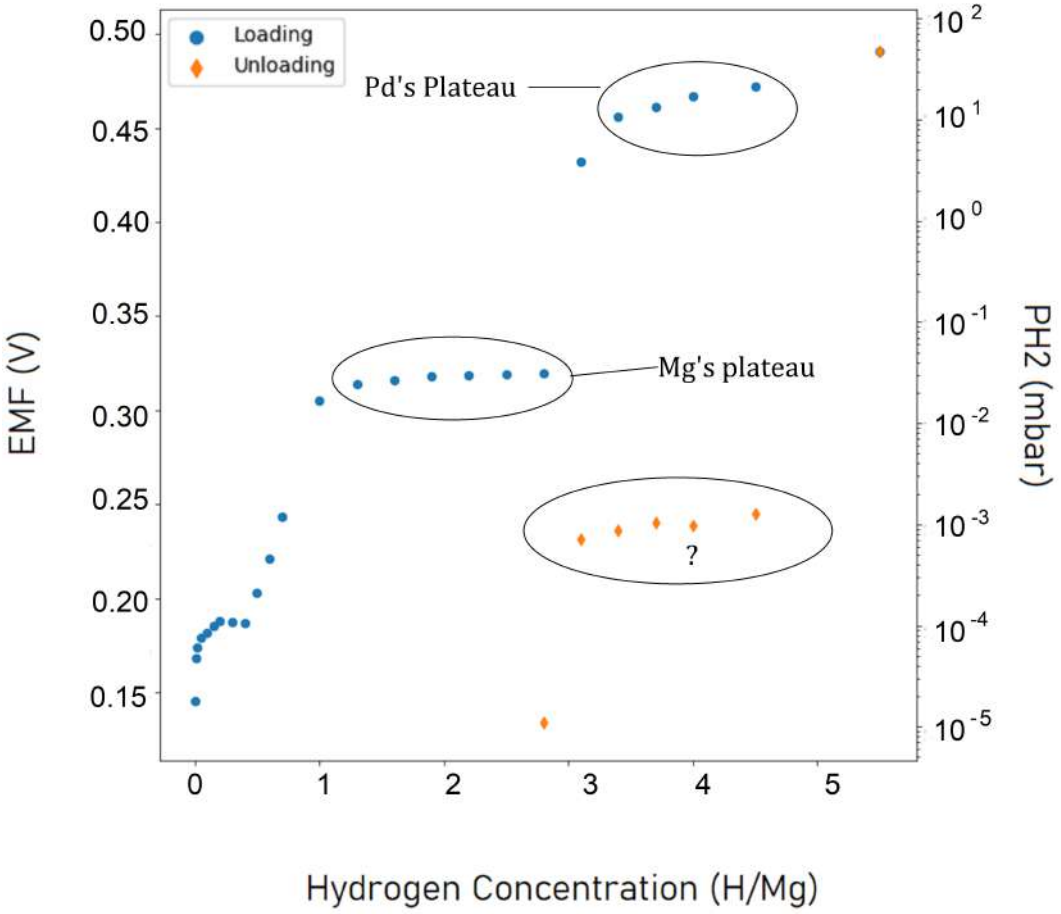

Figure 5.15: PCI of the first film. Unloading was partially possible and an alleged hysteresis is highlighted in the graph. The concentration axis is a nominal one since it cannot be relied because of the forementioned H-loss.

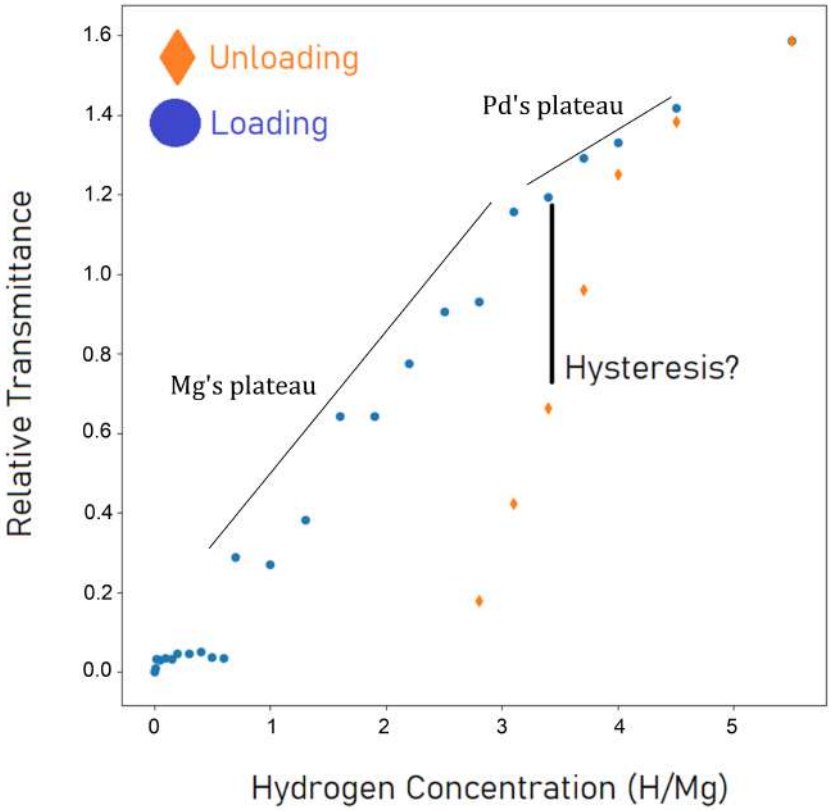

Figure 5.16: Relative transmittance as a function of the alleged composition. This time we can actually see the trend deducible from Lambert-Beer's law 3.26. In particular we witness a larger brightness during Mg hydride formation with respect to Pd hydride formation. That can be seen by looking at the slope of the Relative Transmittance value for the concentration range corresponding to the Mg-hydride formation in 5.15. Of course, even here the concentration axis is just an effective one.

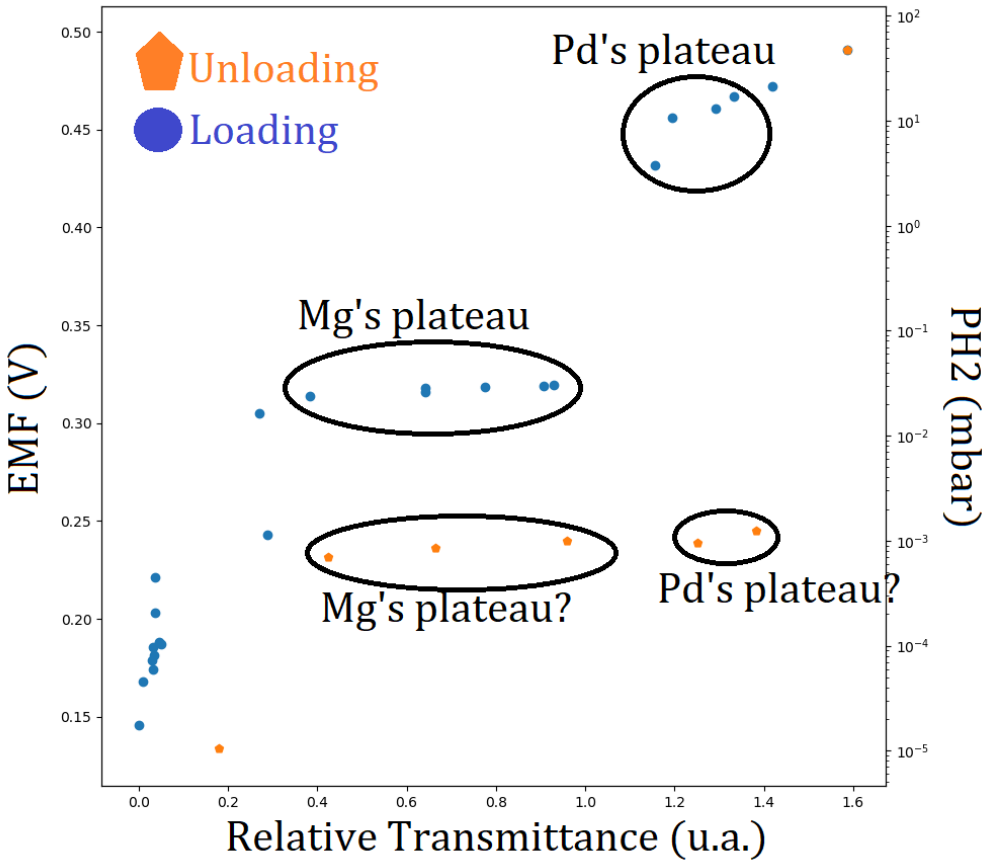

Figure 5.17: PTI (Pressure Transmittance Isotherme) of the first film. In this case, the thin film's chemical potential is evaluated as a function of the relative transmittance (RT). That can be done because RT is connected to the H-concentration through 3.26. We can see that the Mg's plateau is wider in terms of RT with respect to Pd's ones because brightness is supposed to increase mainly upon Mg-hydride formation. Basing on the width in terms of Rt of each plateau in the loading cycle we can actually individuate alleged plateaus for the unloading cycle too.

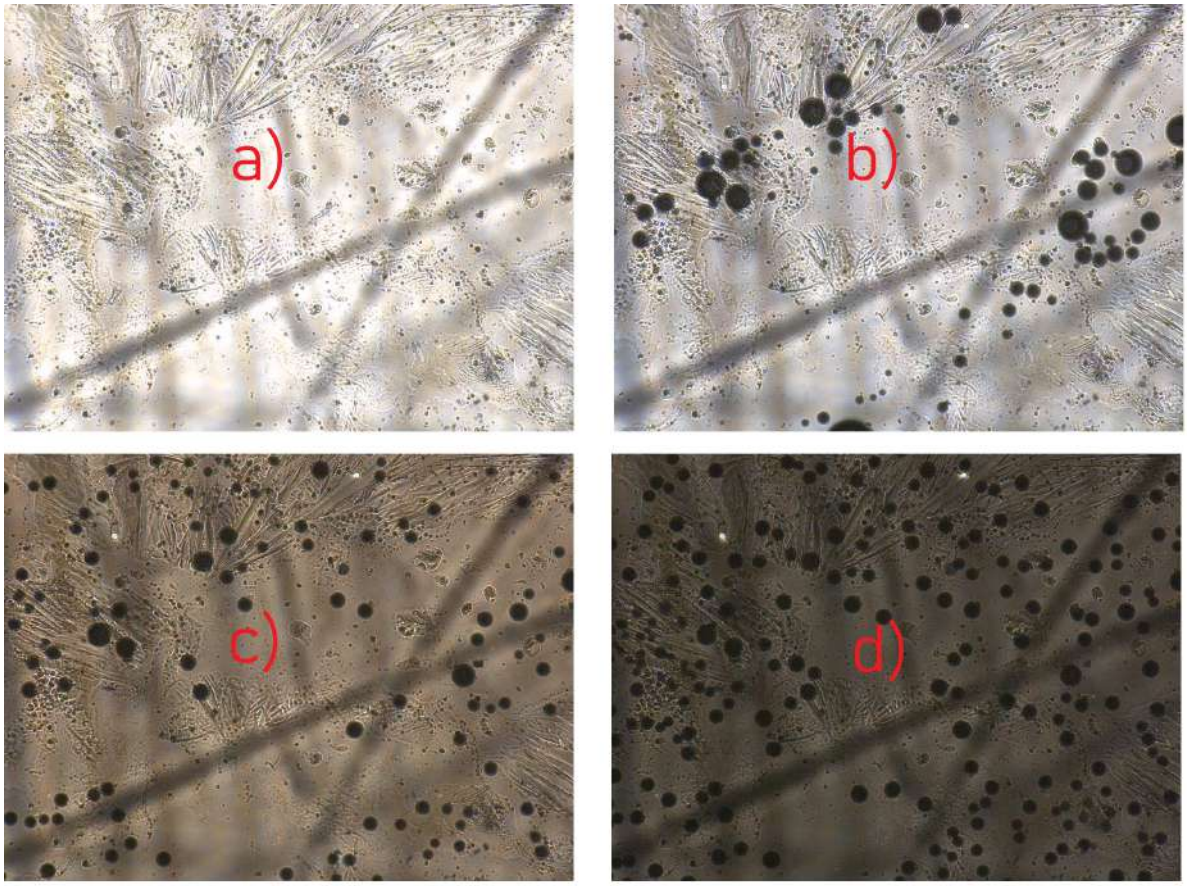

Figure 5.18: Unloading film for the first 30 nm Mg capped with 30 nm Pd, deposited on Sapphire substrate. The unloading process did took place, but there are lots of H_2 bubbles being formed, hence making impossible to go on with further loading and unloading cycles.

5.5.2 Loading of Ti-embedded Mg thin film in KOH

In light of the previous results, 4 more thin films were sputtered. The films were designed as follows: a 2 nm Nb layer to improve the adhesion to the substrate, a 30 nm Mg layer embedded between two 10 nm Ti layer and capped with a 30 nm Pd layer to hinder Oxidation.
Unfortunately, due to Covid-19 restrictions I could only perform the loading of just one of the four films, whose results will be now shown.
The film loading proceeded gradually as can be seen by the progressive increase in the film brightness as displayed in Fig. 5.19.

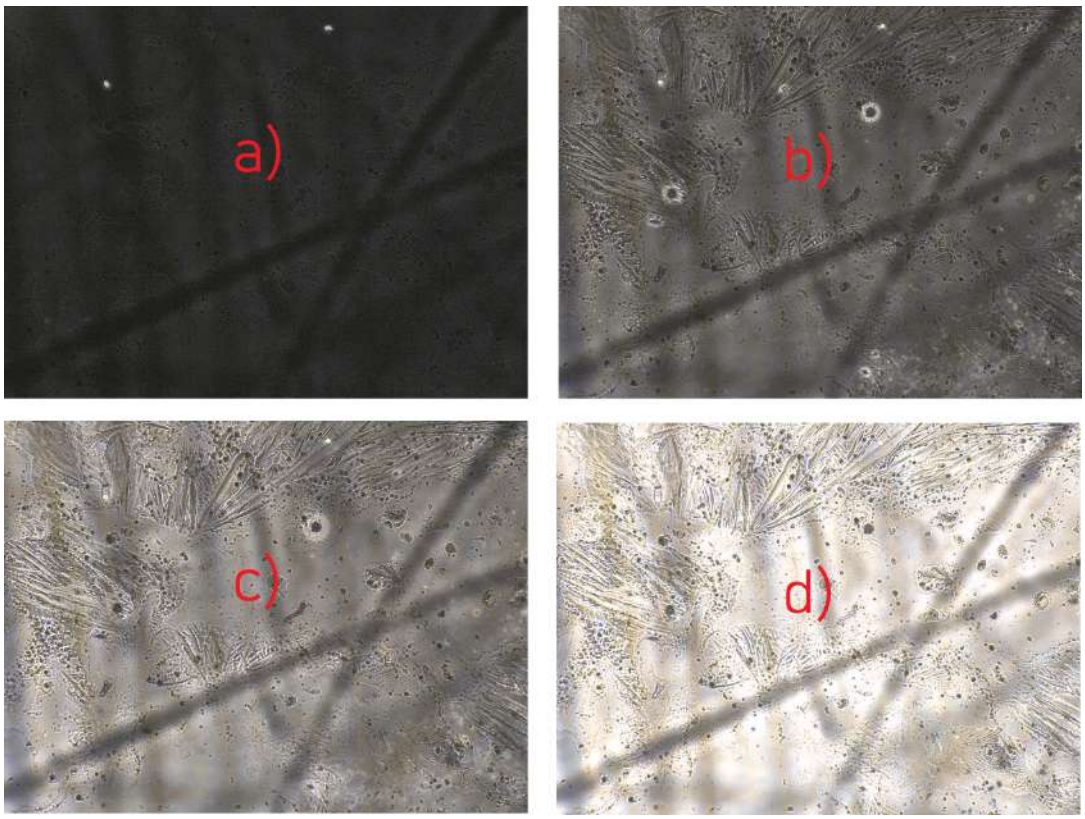

Figure 5.19: Microscope-recorded loading sequence of the first of the newly sputtered 2nm Nb-10nm Ti-30nm Mg-10 nm Ti, 30 nm Pd.

In this case a clear unloading of the film could be performed. Both loading and unloading cycles are displayed in Fig. 5.20(PCI). Here the hysteresis phenomenon can be observed and numerically evaluated for both Mg and Pd's plateau. In particular we can estimate a drop of an order of magnitude in terms of Pressure for what concerns the hysteresis of both Pd and Mg plateau pressure. That is pretty much in agreement with [43], at least for what concerns Pd at room temperature.

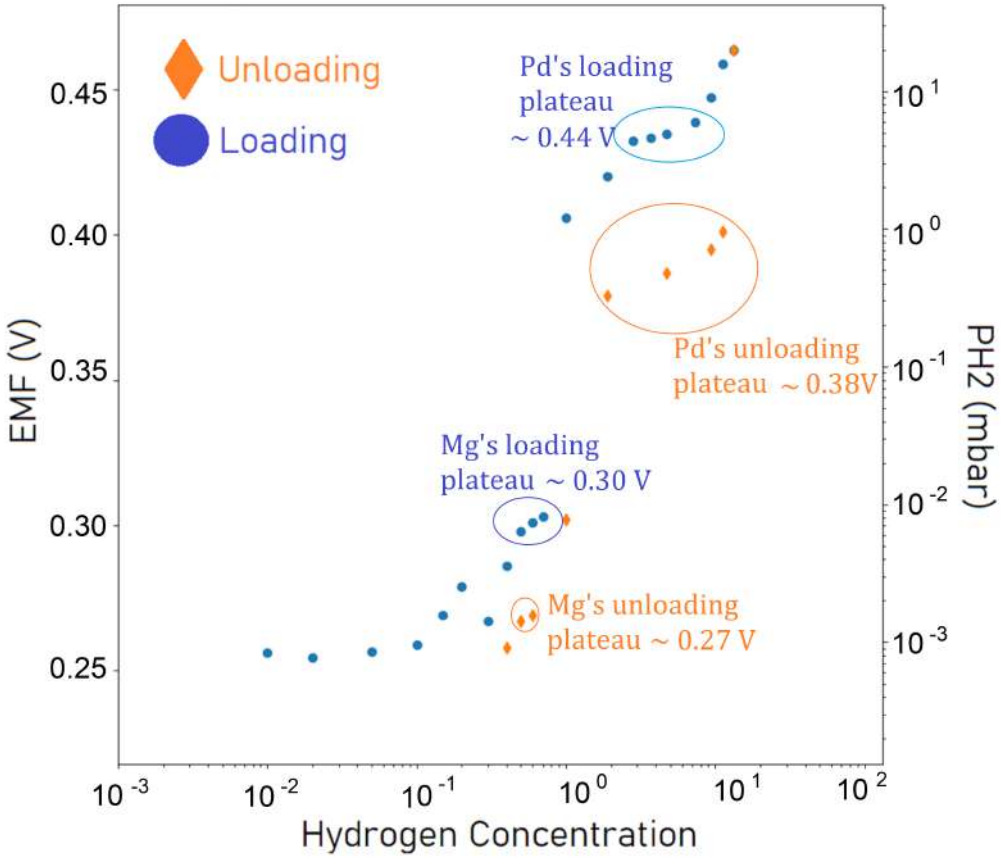

Figure 5.20: EMF loading (blu) and unloading (orange) curva as a function of the alleged Hydrogen composition of a 2nm Nb-10nm Ti-30nm Mg-10 nm Ti, 30 nm Pd thin film sputtered on sapphire substrate. The highlighted Mg and Pd plateaus are slowly tilted as they should be for thin films 3.22. Pd's EMF plateau's value is approximately $\sim$ 0.44 which is compatible with the value reported for the calibration. A clear hysteresis phenomenon is taking place affecting the absorption and the desorption plateau pressure.

Three load and unload cycles could be performed and recorded, though the second and the third unloading cycle were not possible to be controlled (H_2 bubbles formation, see Fig. 5.21). The comparison between the three consecutive loading cycles is shown in Fig. 5.22.

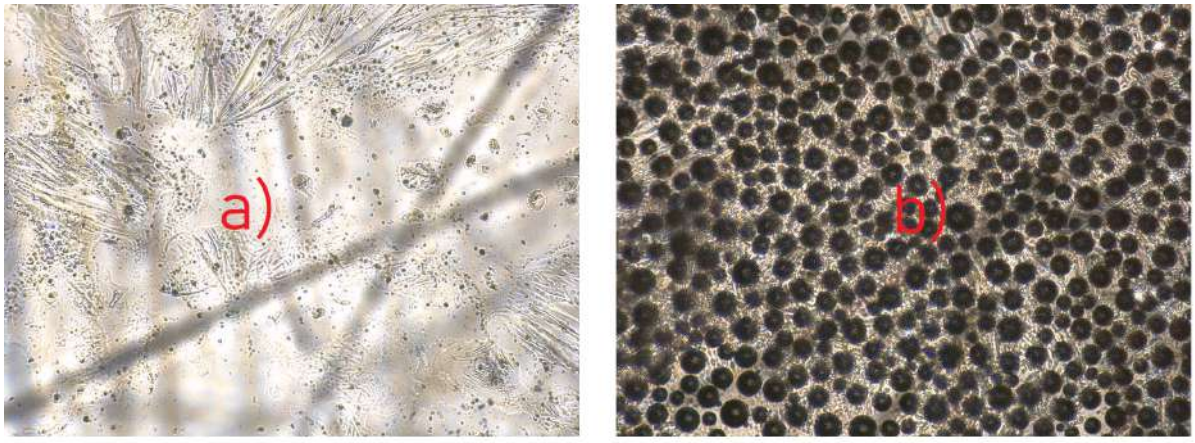

Figure 5.21: Microscope-recorded second unloading sequence of the first of the newly sputtered 2nm Nb-10nm Ti-30nm Mg-10 nm Ti, 30 nm Pd. Only two "states" are possible, since it is impossible to control the formation of H_2 bubbles. That is particularly clear in (b) where one can see how the sample is covered by hydrogen bubbles (the dark circular black spots).

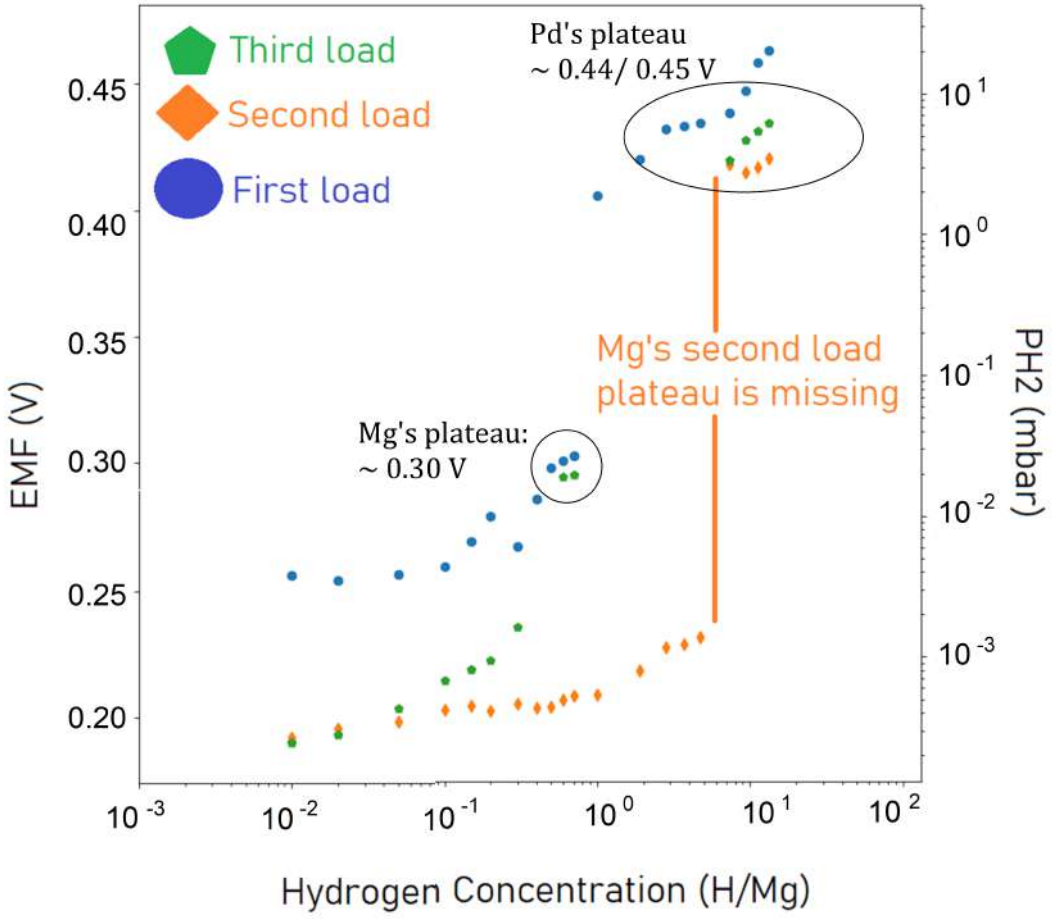

Figure 5.22: First three consecutives loading cycle of the newly sputtered 2nm Nb-10nm Ti-30nm Mg-10 nm Ti, 30 nm Pd. The Pd plateaus occur at approximately ~ 0.44 V for all three cycles, a result compatible with 5.6 and 5.22. Nevertheless, the Mg plateau values miss for the second load, without any possible clear explaination for that

We were then able to confront the PCI of the thin film containing Ti (Nb-Ti-Mg-Ti-Pd), with the PCI of the previously analyzed one, which did not contain Ti (Nb-Mg-Pd). That brings us to Fig. 5.23 that seems to confirm [29] according to which the plateau pressure-EMF-chemical potential of Mg is lower for Ti-Mg-Ti-Pd-designed thin films, with respect to Mg-Pd designed ones.

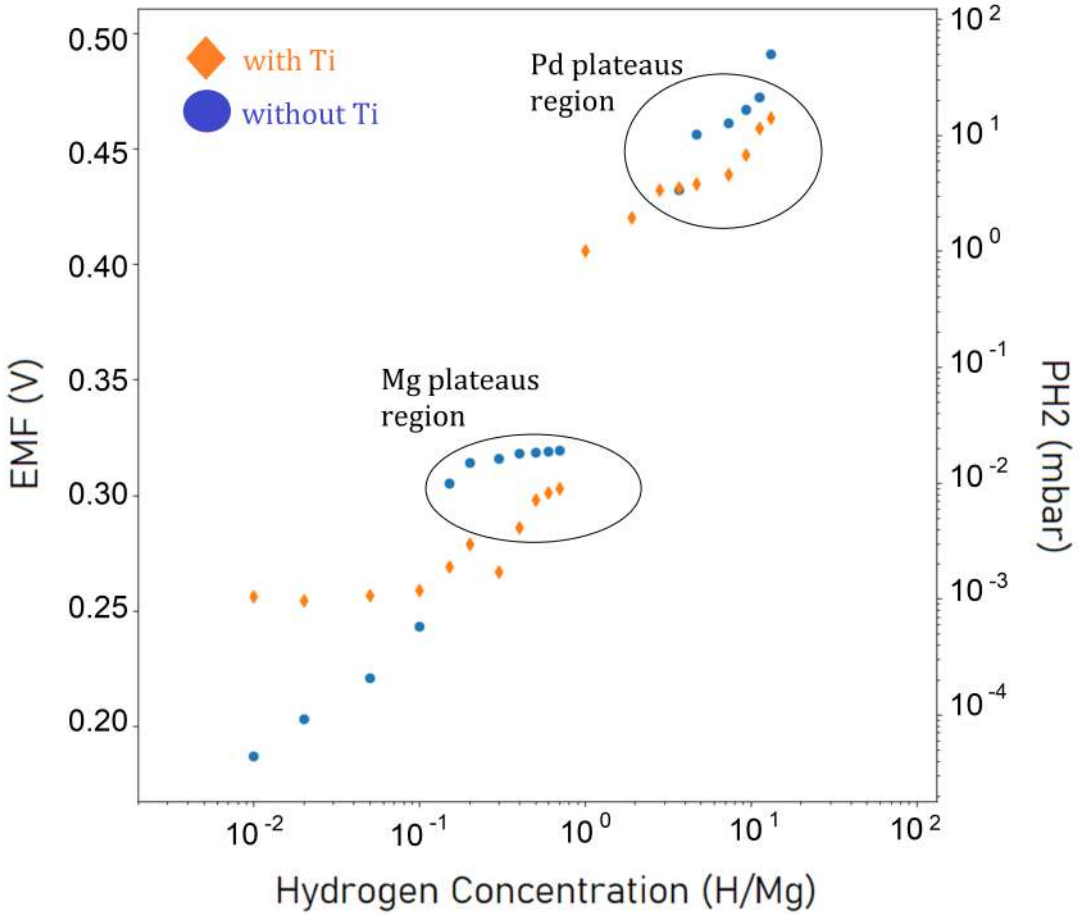

Figure 5.23: COnfrontation of the PCIs for the Mg-Pd thin film in Fig. 5.15(Blu) and for the Ti-Mg-Ti-Pd we have just considered

To conlcude this chapter, it would sound interesting to verify the presence of the surface effects foreshadowed in the calibration of bulk Pd in KOH 5.8. Basically the behavior of EMF as a function of time was recorded for each experiment, but we will focus on the latest analyzed thin film, since it is the one that provided us the best results. Fig. 5.24 and 5.25 show the behavior of EMF as a function of time in corrispondence of the plateau of Mg and Pd respectively. It seems pretty clear that the Mg's plateau loading

is hugely affected by some kind of surface effects, while the Pd one is not.

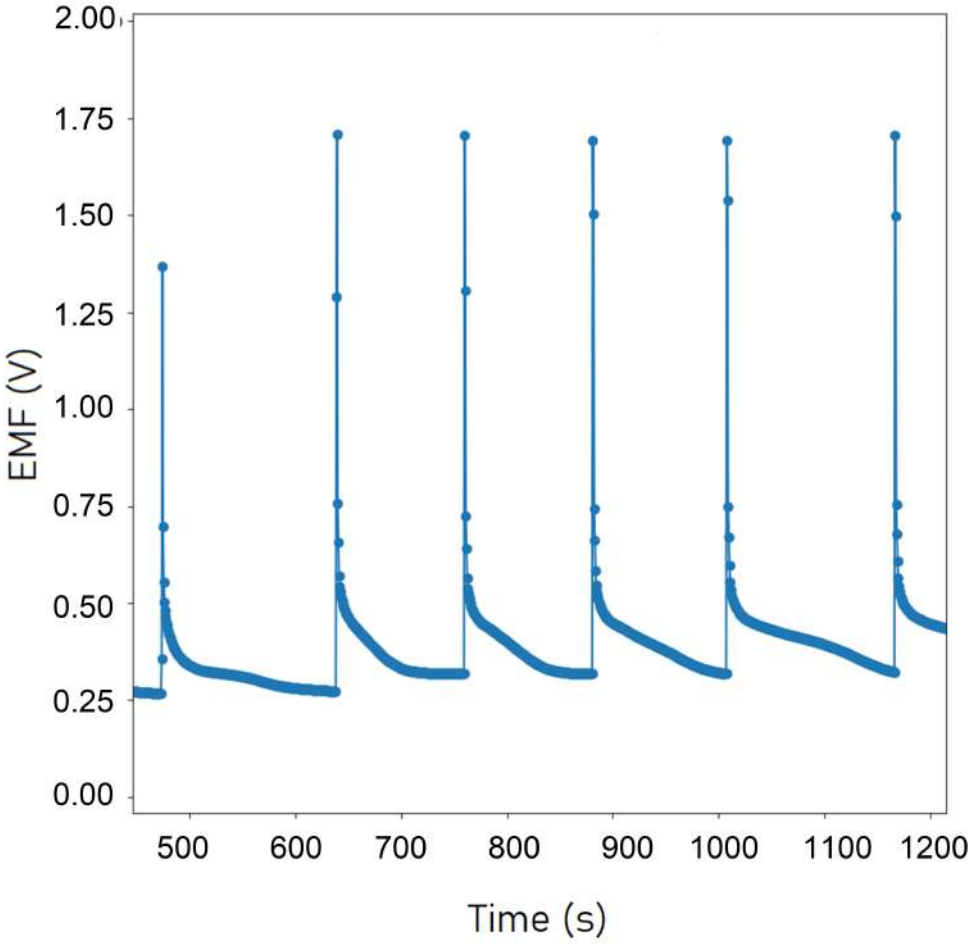

Figure 5.24: EMF loading curve as a function of the elapsed time (seconds) for the region of Mg's plateau of the first loading cycle.Alleged surface effects, i.e. deviation from the ideal exponential decay, comparable with those of 5.8 can be retrieved.

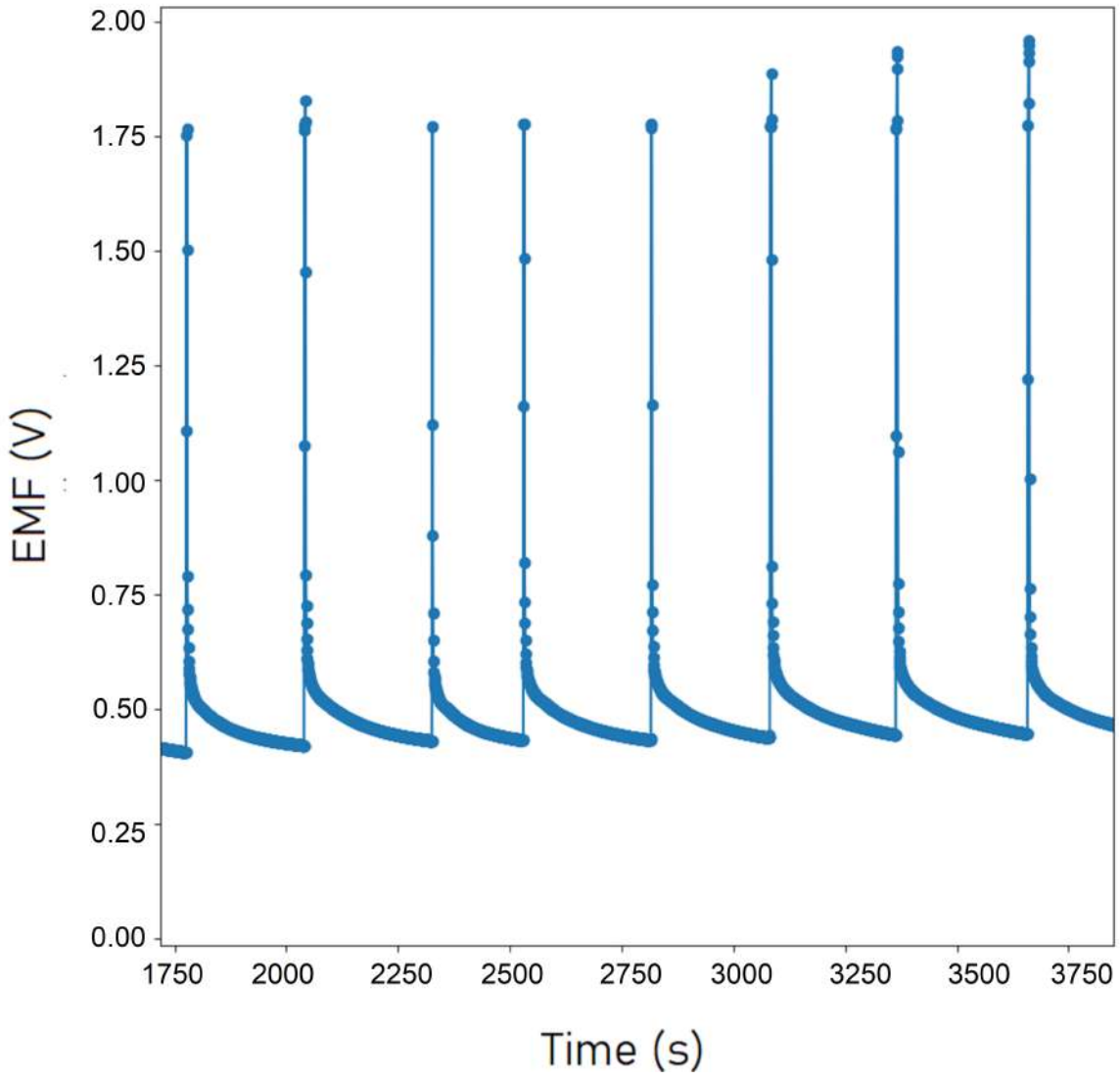

Figure 5.25: EMF loading curve as a function of the elapsed time (seconds) for the region of Pd's plateau of the first loading cycle. The trends for each loading step seems to be decent.

Chapter 6

Discussion of the experimental results

Through physical vapor deposition methods, namely Molecular Beam Epitaxy and Sputter deposition, several Mg thin films were produced and loaded.
At first, loading was attempted with a glycerine-phosphoric acid solution , but no results were achieved, because of the corrosion effects the Mg layers underwent due to the action of the electrolyte solution itself.
Things changed when the electrolyte solution was switched, from the accustomed gylcerine / Phosphoric acid solution to a 5M KOH solution (pH>14). However, not all the films produced were loaded succesfully. At first we needed to get acquainted with the new electrolyte solution in order to understand the mst effective polarity of the sample in order to induce hydrogen loading. Once concluded that the cathodic configuration with the sample as the cathode turned out to be the only possible way to load hydrogen in the films when using KOH electrolyte, results have begun to arrive. Nevertheless KOH was very difficult to work with, because of its dangerousness as a strong basis.
The calibration of bulk Pd 5.6 and 5.8 suggested the presence of surface effects linked to possible activation barriers that one needs to pay attention at. The idea we got to overcome these hindering effects was to increase the driving force of the reaction, i.e. to increase the current intensity, which yielded an increased release of hydrogen for each loading.This proved to be a winning strategy, since the films started loading as we wanted. So, though it has provided many problems that we are now going to discuss about, this method, applied to this specific configuration and electrolyte solution, proved to be effective in loading Mg thin films.
That allowed us to perform hydrogenation as the results in 5.4 show, and to confirm a couple of well-known experimental results of the past [29] and [43], at the cost of losing any information about the recorded hydrogen concentration, because of the hydrogen waste following the highly enhanced current pulse. It needs to be remarked that in all the graphs shown in 5.4, the concentration axis was totally arbitrary because it is as-

sumed that all electrons giving rise to the measured current partecipate in the chemical reaction at the cathode, which is a large overestimation.
For what concerns the surface effects, the chemical side of the matter needs to be better elaborated. However from fig. 5.25 and 5.24 it is suggested that in thin films mainly Mg is affected by such surface effects, while thin Pd seems to be "immune". That's counter-intuitive, since only Pd is in contact with the electrolye solution and should be the more sensible to any surface effect.
The presented results suggest that, through experience, a better control of hydride reaction is needed as the next step. In particular it was very difficult to manage the unloading cycles, which proved to be much more affected by H_2 bubbles formation than the loading's ones.
Had I had the chance to continue with the experiments, we could have tried combinations of current intensity and loading time for each loading step, in order to achieve a better and more gradual hydrogenation.
The problem of an unreliable hydrogen concentration is that it doesn't allow to estimate the diffusion constant of H, through the analysis of the EMF profile vs time (see eq. 3.24). A way to overcome this problem could have been to perform X-Ray diffraction measurements in order to retrieve the H-composition of a hydrided thin film in KOH environment. That would have allowed us to set a valuable scale for the hydrogen concentration.
Unfortunately, one should design a new in-situ loading cell mounted on an X-Ray diffractometer, to monitor every loading step: that would be a technical challenge, expecially considering the high corrosion power of KOH.
At last, it is worth mentioning, the problem of oxydation. As previously mentioned, many batches of thin films were produced. Nevertheless it was possible to obtain some results, only with the first of each batch that were loaded. That revealed to be particularly true for MBE deposited thin films produced at Campus North. At the end, it was really necessary to keep the films under inert atmosphere until the start of hydrogen loading experimentsas long as we could the newest thin films from air, e.g. by leaving them in an High - Vacuum environment and only extracting them if immediate loading would have been possible.

Conclusions

The goal of this work thesis was to perform hydrogenography, i.e. in situ monitoring of hydride formation in a thin film, on Mg thin films, capped with a Pd layer working both as catalyst and as a protection layer for oxydation.
Many experimental setups were arranged. Electrochemical loading using a mixture of phosphoric acid - glycerine as a electrolyte solution proved to impossible, because of the corrosion that such an electrolyte induced on the Mg layer, prompting the self and uncontrolled load of the film itself.
By changing the electrolyte solution,i.e. by using a 5M KOH solution, hydrogenation of several films could be carried out, hence fulfilling the goal of the thesis.
Nevertheless the protocol developed to load the film in KOH environment presents many shortcoming, that need to be overcome, if future loadings in this configuration are to be performed.
Many results showed the presence of surface effects that hinder the absorption of hydrogen. The idea to improve the current intensity for the loading and unloading steps proved to be necessary for the succes of the experiments, though due to the high H-loss all the informations about Hydrogen composition within the thin films were lost. So the recorded Hydrogen composition was no longer a reliable variable.
A way to overcome this issue would have been to perform X-Ray diffractrometry experiments, though the technical challenges would have been a challenge difficult to win.

Thanksgivings

Ich möchte mich bei Dr. Stefan Wagner und Professorin Astrid Pundt bedanken für ihre verfügbarkeit und geduld, die sie mir gegenuber immer gezeigt haben.
Ich möchte auch danken Dr. Philip Klose and Fabian Fink, ohne deren wertvolle Teknische Arbeit, dieser Abschlussarbeit night möglich gewesen wäre.
Endlich möchte ich mich bei Enrico bedanken, denn er mir geholfen hat, mich in Deutschland weniger allein zu fühlen.

Ritorno infine alla mia lingua madre, per ultimare i ringraziamenti.
Ringrazio il mio relatore, Luca Pasquini per la gentilezza e la compresione che ha mostrato nei miei riguardi in un periodo così difficile per quanto riguarda la logistica e l'organizzazione di spostamenti.
Il sentiero che sto per concludere è stato costellato di ostacoli e difficoltà che sarebbe stato impossibile superare senza le giuste persone al mio fianco.
Avessi prestato più attenzione ai miei genitori, avrei potuto evitare molti problemi che mi sono occorsi in questi miei anni di università.
Usero' il margine molto stretto di questo foglio per ringraziare mio padre per il tempo trascorso insieme e per l'eredità che mi ha trasmesso.
Voglio poi sentitamente ringraziare mia mamma, per avermi trasmesso gli stimoli scientifici e culturali che mi hanno consentito di poter scegliere Fisica. Sono stati anni difficili, ma li abbiamo trascorsi insieme.
A Flavia, mia sorella, probabilmente la persona più distante da me per valori politici e sociali, vanno i più sentiti ringraziamenti per aver modellato la mia cultura, senza la quale sarei più povero e cieco, e per essere stata un parafulmine delle mie ansie e paranoie. Tra l'altro se non avessi iniziato a vedere Lost nel 2004 con lei, il mio inglese non sarebbe stato all'altezza della situazione, quindi grazie Flavia.
Ringrazio Arianna per aver varcato la soglia della porta della I E, quel lontano giorno del settembre 2009 e per avermi fatto scoprire che non vi è nulla di più confortante nell'andare a dormire pensando a qualcuno sapendo che quel qualcuno ricambia a sua volta il pensiero.
Vorrei ringraziare ogni cugin* e ogni zi* e descriverne la diversa sfumatura di affetto che

provo nei suoi riguardi, ma ancora una volta, ciò non può essere contenuto nel margine così stretto di queste pagine.
Ringrazio nonna Pipa per avermi insegnato cosa sia davvero la lotta di classe, e nonna Mima per avermi dimostrato sempre come l'eleganza dell'eloquio non abbia età.
Nei miei anni a Bologna e ad Ascoli sono stato tante cose, ma non sono mai stato solo.
Ringrazio Inti e Matteo, per la serenitá, la spensieratezza e la deresponsabilizzazione che solo le serate condotte a ritmo di prosecco da Ken parlando di geopolitica mediorientale e centroasiatica mi hanno saputo regalare.
Ringrazio ogni serata trascorsa al Caldaie o in un qualsiasi bar con sottofondo di lingue non indoeuropee, con la Grande Cordata Allargata.
Ringrazio Lucrezia, Martina e Valentina per essere state delle vere amiche nei miei momenti del bisogno.
Ultimi ma non ultimi sono i ringraziamenti per le mura di Via San Carlo 20. Loro, e il Popolo che lì ha dimorato, hanno contribuito a rendere questi anni più lievi e spensierati.

Bibliography

[1] *What are Batteries,Fuel Cells and Supercapacitors?*M. Winter, R.J. Brodd, Chemical Reviews 104 (2004), 4245-4269

[2] *Targets for onboard hydrogen storage systems for light-duty vehicles*U. D. of Energy - 2009

[3] *http://www1.eere.energy.gov/hydrogenandfuelcells/storage/pdfs/targets_onboard_hydro_storage_explanation.pdf*

[4] *Materials for Hydrogen storage* Andreas Züttel ISSN:1369 7021 (2003)

[5] *Size effects on the hydrogen storage properties of nanostructured metal hydrides: A review.*,V. Berube, Gregg Radtke, Mildred Drasselhaul, Ganh Chen, International Journal of Energy Research (2007), 31:637-663

[6] https://thesis.library.caltech.edu/11040/1/Official%20Senior%20Thesis.pdf

[7] *Hydrogen in Metals: Microstructural Aspects*, A. Pundt and R. Kirchheim, Annu. Rev. Maters. (2006), 36:555-608

[8] *Metal hydrides for energy applications-classification, PCI characterization and simulation* Vinod,Kumor, Sharma

[9] *Thermodynamics of Open Two-Phase Systems with Coherent Interfaces* R.B. Schwartz and A.G. Khachaturyan.

[10] *Design of Nanomaterials for Hydrogen Storage* Luca Pasquini , 2020

[11] *Lessons "Hydrogen in metal", held by Prof. Pundt at KIT.*

[12] *Composition dependent non-ideality in aqueous binary mixtures as a signature of avoided spinodal decomposition*, Sarmistha Sarkar, Saikat Banerjee, Susmita Roy, January 2015Journal of Chemical Sciences 127:49-59.

[13] *Evidence of copious vacancy formation in Ni and Pd under a high hydrogen pressure*, Fukai Y, Ōkuma N. 1993, Jpn. J. Appl. Phys. 32:L 1256-59

[14] *A linear theory of thermochemical equilibrium of solids under stress* F. Larchè and J.W. Kahn , 1973

[15] *The theory of Structural Transformations in Solids* A.G. Khachaturyan , 1983

[16] *Absorption kinetics and hydride formation in magnesium films: Effect of driving force revisited*: H.T. Uchida, S.Wagner,M.Harmm,J:Kürschner,R.Kirchheim,B.Hjövarsson and A.Pundt - 2014

[17] *A reviewofcatalyst-enhancedmagnesiumhydrideasahydrogen storagematerial*C.J. Webb - 2014

[18] *Segregation and diffusion of hydrogen in grain boundaries of palladium.* Müschele and Kirchheim , 1987

[19] *Hydrogen as a probe for the average thickness of a grain boundary.*Müschele and Kirchheim , 1987

[20] *Hydrogen storage in thin film magnesium?scandium alloys* R.A.H Nielsen, P.H.L.Notten

[21] K. Yoshimura , C. Langhammer , and B. Dam, *Metal hydrides for smart window and sensor applications*, Mrs Bulletin, June 2013, 495-503.

[22] A. Zaluska, L. Zaluski, and J. StromOlsen, *Nanocrystalline magnesium for hydrogen storage* Journal of Alloys and Compounds, vol. 288, no. 1, pp. 217-225,1999.

[23] *Kinetics of materials* Robert W. Balluffi - Samuel M. Allen - W. Craig. Carter, 2005: Chapter 8, p. 164.

[24] Lennard P.A. Mooji, Andrea Baldi, Christiaan Boelsma, Kun Shen, Marnix Wagemaker, Yevheniy Pivak, Herman Schreuders, Ronald Griessen, and Bernard Dam *Interface Energy Controlled Thermodynamics of Nanoscale Metal Hydrides*, Adv. Energy Mater 2011. T, 754-758.

[25] *Complex hydrides for solid state hydrogen storage: A thermodynamic and structural approach (English with French summary)*, Thesis for PhD from Abdel El Kharbachi, Advisor: Dr Ioana Nuta, Prof Chirstian Chatillon and Prof. Reza, March 2011

[26] Andrea Baldi, V. Palmisano, Marta Gonzales-Silveira, Bernard Dam *Destabilization of the MgH System through Elastic Constraints*, Physical Review Letters, June 2009.

[27] Stefan Wagner, Astrid Pundt *Quasi-thermodynamic model on hydride formation in palladium?hydrogen thin films: Impact of elastic and microstructural constraints*, 30 January 2016.

[28] J. Kuerschner, Stefan Wagner, Astrid Pundt *Delamination-supported growth of hydrides in Pd thin films studied by electrochemical hydrogenography*, Journal of Alloys and Compounds 593 (2014) 87?92

[29] A. Baldi, V. Palmisano, M. Gonzalez-Silveira, Y. Pivak, M. Slaman, H. Schreuders,B. Dam, and R. Griessen

[30] A. Baldi, M. Gonzalez-Silveira, V. Palmisano, B. Dam, R. Griesen *Destabilization of the Mg-H system through elastic constraints*, Phys Rev Lett. 2009 Jun 5;102(22):226102.

[31] *die Aufnahme von Gasen durch Metal* Dr. Prof. A. Sievert, Zeitschrift für Metallkunde, February 1929

[32] *Dünne Palladium-Wasserstoff-Schichten als Modellsystem, Dissertation thesis*,S. Wagner, Göttingen, 2014.

[33] D.Depla, S.Mathieu, J.E. Greene *Sputter deposition Processes*

[34] P.Sigmund *Theory of Sputtering I. Sputter yield of Amorphous and Polycrystalline targets*, Physical Review

[35] Aaron J.Ptak *Principles of molecular beam epitaxy*Handbook of Crystal Growth 2015, Pages 161-192

[36] *An optical Combinatorial Method to find new Light-Weight Hydrogen-Storage Materials.*, R. Gremaud, C.P. Broedersz, D.M. Borsa, A. Borgschulte, P. Mauron, H. Schreuders, J.H. Rector, B. Dam, R. Griessen.

[37] https://www.explainthatstuff.com/molecular-beam-epitaxy-introduction.html

[38] https://en.wikipedia.org/wiki/Molecular-beam_epitaxy#/media/File:MBE.svg

[39] https://en.wikipedia.org/wiki/Reflection_high-energy_electron_diffraction#/media /File:RHEED.svg

[40] *J.L. Schommartz, Bachelor Thesis* University of Göttingen, (2014)

[41] *On the relation of Hydrogen to Palladium*, T. Graham, Proceedings of the Royal Society, 212 - 1868.

[42] *"Tunneling Effects in Chemistry-Molecules in the Strange Quantum World"* Sharmistha Karmakar, Deepthi Jose and Ayan Datta

[43] *Thermodynamics, stress release and hysteresis behavior in highly adhesive Pd?H films*, Y.Pivaka H.Schreuders, M.Slaman R.Griessen, B.Dam.Volume 36, Issue 6, March 2011, Pages 4056-4067